CONTROL METHODS FOR A CONTINUOUSLY VARIABLE TRANSMISSION WIND TURBINE

By

Chad Phillip Glinsky

A THESIS

Submitted to
Michigan State University
in partial fulfillment of the requirements
for the degree of

MASTER OF SCIENCE

Mechanical Engineering

2011

ABSTRACT

CONTROL METHODS FOR A CONTINUOUSLY VARIABLE TRANSMISSION WIND TURBINE

By

Chad Phillip Glinsky

Continuously variable transmission (CVT) control, for a grid-connected wind turbine, is studied beyond the proof-of-concept by analytically and systematically designing and tuning controllers using various methods. Three different approaches are used for CVT controller design. These include typical torque (TT) control, classical proportional-integral-derivative controls, and modern control theory for disturbance tracking control and realizable drivetrain dampers. Entire control systems ranging from wind turbine start-up through rated conditions are designed, implemented, and simulated with nonlinear plant models using full-field turbulent wind inputs.

Various controller designs, based on rigid and rotationally-flexible drivetrain models, are compared for turbulent flow simulations of the nonlinear model with rotor rotation, drivetrain twist, and system load twist degrees of freedom. For the rigid drivetrain, the TT controller has less control action and better energy capture than the proportional controller. For the flexible drivetrain model, the proportional controller proves to be infeasible for practical implementation due to excessive drivetrain torque fluctuations. The TT controller with a realizable drivetrain damper proves to have the best damping characteristics, lowest CVT workload, and best power regulation. For the flexible system load model, the TT controller with a realizable damper has the best results again, with the exception of generator shaft loading conditions. The thorough comparison of CVT controllers leads to identification of controller feasibility, actuator workload, and achievement of objectives.

To my Opa.
His kindness, humbleness, and ingenuity will forever be remembered and inspiring.

ACKNOWLEDGMENT

I would like to thank Dr. Farhang Pourboghrat for opening his door to me in my pursuit for research in wind energy. His support and patience has been appreciated during this learning process. I would also like to give thanks to Drs. Brian Feeny and Ranjan Mukherjee for being part of my committee. Furthermore, I would like to thank professors, friends, and family who knowingly or unknowingly have influenced my work. Lastly, but most importantly, I thank my wife, Lauren, and dad, George, for their relentless support and encouragement. Without these relationships and others, there is little left in life that is without materialism, and for this I am grateful.

TABLE OF CONTENTS

LIST OF TABLES

LIST OF FIGURES

Chapter 1

Introduction

Around 80 percent of Earth's energy needs are fueled by coal, oil, and natural gas. Most of the carbon dioxide and other greenhouse-gas emissions are produced by the excessive usage of these fossil fuels. Their present abundance, present affordability, and well established facilities often make them the preferable choice for utility companies. Unlike wind and solar energy, fossil fuels exist with finite quantities which makes them susceptible to volatile pricing. In the United States (US), this leads to economic susceptibilities in the form of national security since the majority of the oil is purchased outside the country. In 2009, 63% of oil consumed in the US was imported. In 2008, $475 billion of US money was sent to foreign countries in exchange for oil. The US makes up 4.5% of the world's population yet consumes 25% of the worldwide production of oil. These facts clearly illustrate the excessive dependence the US has on oil and that it's an economic deterrent. [1]

Nuclear power was used for 9% of the US total energy consumption in 2009. Advantages of nuclear power include low carbon dioxide emissions and high energy density. However, disadvantages include high water usage, catastrophic consequences if system failures are en-

countered, and radioactive waste by-product that poses a threat to human health. Wind turbines do not produce carbon dioxide, consume no water, and do not pose a threat to human health. The 2011 disaster in Japan, caused by an earthquake and tsunami, led to serious damage to the Fukushima Daiichi nuclear power plant. The radioactivity became widespread throughout Japan, and scientists even reported increased radioactive levels in the US. The nuclear disaster in Japan is currently considered the second largest in history, only behind the Chernobyl disaster of 1986. The estimated cost of recovery due to the earthquake, tsunami, and nuclear disaster is as much as $308 billion. In the event of catastrophe, wind turbines do not pose near the threat to mankind nor rebuilding costs as nuclear power. [1, 2]

With the advent of large utility-scale wind turbines commonly seen in the news in recent years, it can easily be forgotten that utilization of wind energy is a practice dating back to around the 1st century B.C. for the first historically known windmill [3]. Some of the first well known devices used to obtain power from the wind include sail boats, grinding mills, saw mills, and hydraulic pumps. In present day, what is known as a modern wind turbine is most often used for the conversion of wind to electricity. In any case, modern or centuries old, the concept always involves the conversion of wind power to mechanical power. This mechanical power is then used to perform a certain task, or in the case of modern wind turbines, is then converted to electrical power via a generator. The continued development of wind turbines will lead to lower cost of energy (COE), solidifying wind power as an attractive and affordable commodity.

As part of the continued development in wind turbine technology, this thesis considers the design of a wind turbine that utilizes a continuously variable transmission (CVT), with

focus on the control system design. Various research studies have been conducted on the use of CVTs in wind turbines [4, 5, 6, 7, 8, 9, 10]. Many studies have been proof-of-concepts or focused on a particular type of CVT. In this thesis, focus is placed on advancements beyond the proof-of-concept by implementing various control models, including modern control theory, and comparing controllers on simulation models with varying degrees of fidelity.

Most wind turbines currently being developed have variable-speed rotors through the use of expensive power electronics (PE), meaning the aerodynamic rotor is capable of rotating at variable speeds dependent on wind conditions. This is opposed to fixed-speed wind turbines which must operate at nearly constant rotational speed regardless of wind speed, but little-to-no PE is required. A variable-speed rotor is aerodynamically more efficient over a range of wind speeds, and hence captures more energy making the PE costs viable.

The appeal of a CVT in a wind turbine is it enables variable-speed operation but with limited usage of PE as found in fixed-speed designs. Furthermore, a CVT could allow for a greater range of variable speed compared to technology often used on modern wind turbines, allowing further gains in energy capture [6]. Lastly, couple this with techniques used in this thesis for controlling the CVT, and the increased energy capture can be joined by reduced drivetrain fatigue loading. Overall, these positive attributes of a CVT wind turbine can lead to the key commercial objective of reducing the COE associated with wind energy.

The remainder of this chapter introduces basics of wind turbine operation, continuously variable transmissions, and control. Chapter 2 explains mathematical models and simulation tools as well as deriving models used for control system design. Chapter 3 explains typical control used in variable-speed wind turbines and how it can be achieved with a CVT. Chapter 4 explains the design and tuning of classical controllers in Region 2 for CVT. Chap-

ter 5 explains various state space approaches to designing modern controllers for use with CVT, with focus on drivetrain damping. Chapter 6 compares various controllers designed throughout this thesis. Chapter 7 reviews conclusions of this work and provides suggestions for future research.

1.1 Wind Turbine Operation

As advanced as the wind turbines of today have become, the application of transforming wind energy into some usable form is ancient and key fundamentals of operation are still at work. We will begin by reviewing the basics of a typical wind turbine, i.e. one without a CVT, that are applicable to this research. For more detailed coverage, consult any one of the referenced wind energy textbooks [3, 11, 12].

1.1.1 Fundamentals

The driving force behind wind turbines transforming wind power to mechanical power is aerodynamics. Wind turbines operate on the principles of aerodynamic drag and lift. The common modern wind turbine transforms wind energy to rotational kinetic energy via lift. Drag will be present, but the positive net torque developed about the rotational axis that results in power output is driven by lift. The presence of drag will reduce the net torque and power output. Certain wind turbine designs develop positive net torque using drag, but this is not common and historically known to be less efficient than lift devices [3, 12]. Figure 1.1 illustrates drag and lift devices. The wind turbine modeled in this thesis develops positive net torque using lift.

Wind turbines can be designed to operate at fixed-speed or variable-speed, which refers

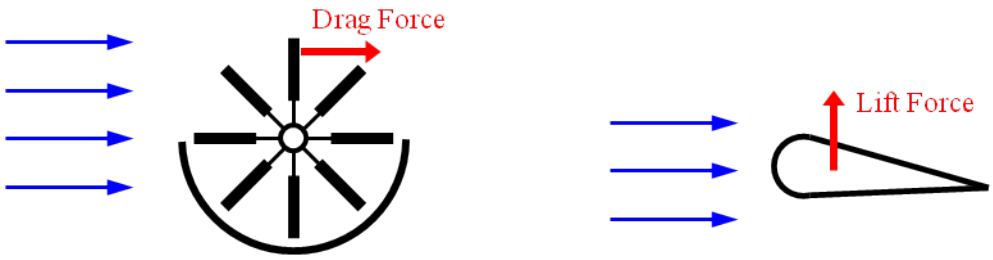

Figure 1.1: Drag and lift devices. For interpretation of the references to color in this and all other figures, the reader is referred to the electronic version of this thesis.

to the rotational speed of the rotor. The fluid mechanics of fixed-pitch blades suggest the rotor should rotate at variable speeds if peak aerodynamic efficiency is to be achieved for variable wind speeds. As the free stream air velocity increases, the angle of attack increases if rotor speed remains constant. This change in angle of attack likely results in less lift and more drag, leading to less wind power converted to mechanical power. Figure 1.2 illustrates this concept.

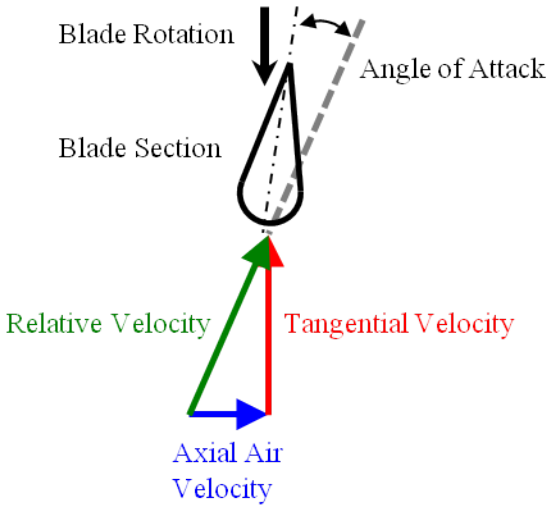

Figure 1.2: Angle of attack for a wind turbine airfoil

Another fundamental aspect of operation is orientation of the rotational axis about which wind power is transformed to mechanical power. When the axis is oriented horizontally or vertically relative to ground, it's called a horizontal axis wind turbine (HAWT) or vertical

axis wind turbine (VAWT), respectively. Typically, VAWTs are drag devices and known to be less efficient than HAWTs [3, 12]. Figure 1.3 shows an HAWT and VAWT. Most commercial wind turbines used to produce electricity are HAWTs as is the one modeled in this research.

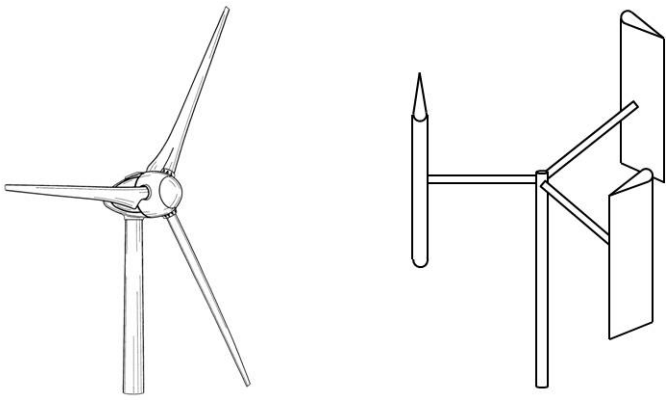

Figure 1.3: HAWT and VAWT examples

In general, the rotational speed associated with mechanical power output of a given wind turbine is either fixed- or variable-speed. In reality, there are unique designs that incorporate more than one discrete speed, but are not continuously variable between speeds during normal operation. Note that many so-called "fixed-speed" wind turbines actually have slight variations in speed, but very small relative to the operational speed. Ultimately, a variable-speed wind turbine offers the ability to store and release kinetic energy as well as track optimal aerodynamic efficiency. The former enables load alleviation during wind gusts and lulls, which is particularly important for drivetrain components. The block diagram in Figure 1.4 illustrates power flow in variable-speed wind turbines. This ability prevents captured wind power from being force-fed through the drivetrain, resulting in damaging torque spikes. This research will show a key benefit of adding a CVT to a fixed-speed wind turbine is the control it offers over system loading, effectively allowing variable-speed.

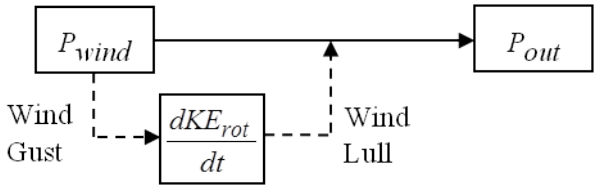

Figure 1.4: Power flow in a variable-speed wind turbine

1.1.2 Terminology

With focus strictly on HAWTs, component terminology common to large wind turbines and relevant to this research is introduced. The *rotor*, sometimes referred to as aerodynamic rotor, is comprised of the *blades* attached to a *hub*. The rotor is coupled to a *low-speed shaft* (LSS). The *gearbox* maps the LSS to a *high-speed shaft* (HSS) which is coupled to the *generator* rotor. The generator is typically connected to the *electrical grid*, sometimes with the aid of PE to enable variable-speed operation. The *nacelle* is a housing structure for the drivetrain and generator. Lastly, the nacelle is mounted atop the *tower*. Many other components are commonly used but will not be introduced here as they do not pertain to the focus of this research. On a side note, there is no gearbox for direct-drive wind turbines, hence the LSS is directly coupled to a uniquely designed generator. Figure 1.5 shows the hardware of a typical large wind turbine. This figure applies to the wind turbine modeled in this study prior to considering the hypothetical CVT configuration. In section 1.2.3, terminology specific to the CVT configuration will be reviewed.

Common actuation terms are briefly covered now. *Pitch* is the action of rotating a blade about a span oriented axis. *Yaw* is the action of rotating the nacelle, and hence rotor, about the tower axis. Yaw is not used in this research but is mentioned for completeness. Lastly, what I will call *load actuation* is the action of decreasing or increasing load torque, usually with intent to adjust the rotor angular velocity. The purpose of each actuation will be clear

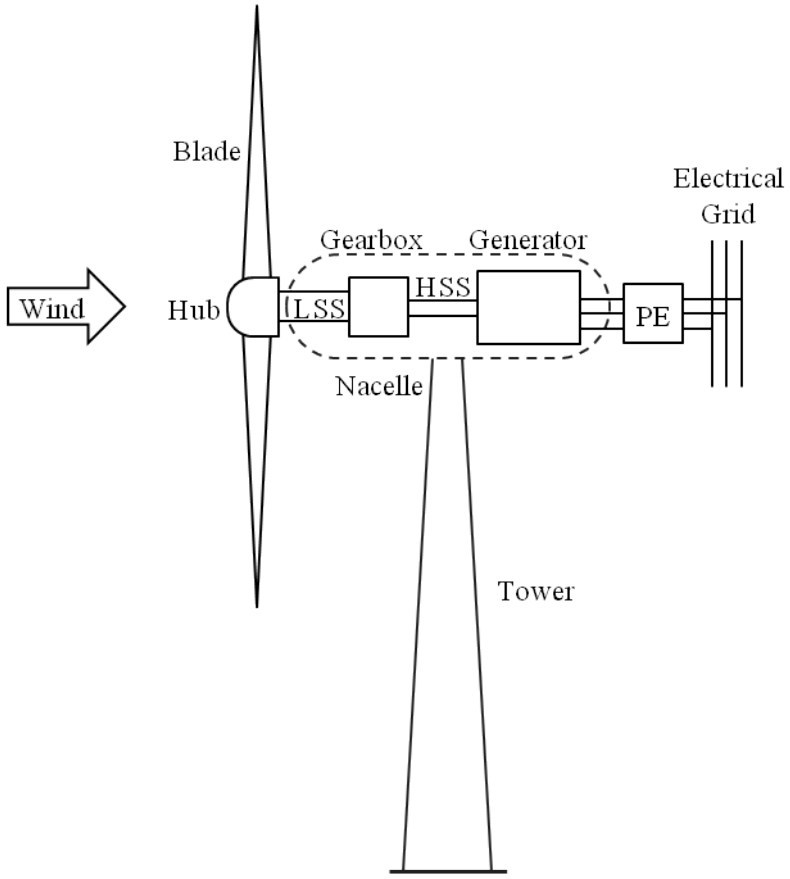

Figure 1.5: Typical wind turbine hardware

as it gets discussed in the context of control objectives. Figure 1.6 attempts to illustrate pitch and load actuation.

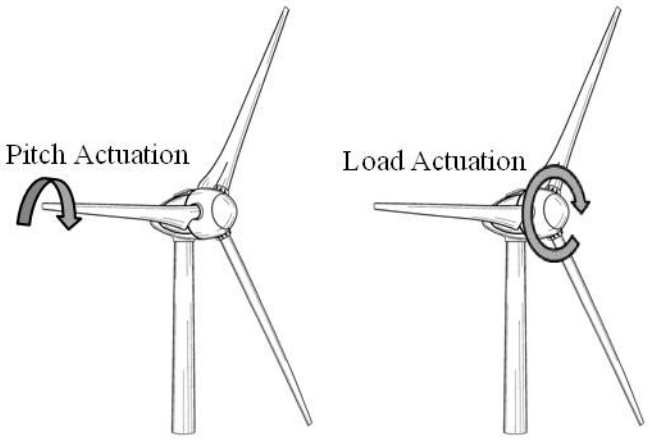

Figure 1.6: Wind turbine pitch and load actuation

1.1.3 System Load

System load refers to the components that convert rotational kinetic energy of the wind turbine to some other usable form. Typically, the system load is an electromagnetic generator connected to the electrical grid which provides consumers with alternating current (AC) power at a fixed frequency, 60 Hz in the US. However, a system load can take many other forms, such as hydraulic pump, milling grain, batteries, i.e. electrical energy storage, and even flywheels, i.e. rotational kinetic energy storage. It's also possible to have no load, other than inertial, as well as energy absorbing loads such as a viscous fluid. Figure 1.7 shows a generic illustration of a wind turbine and its system load.

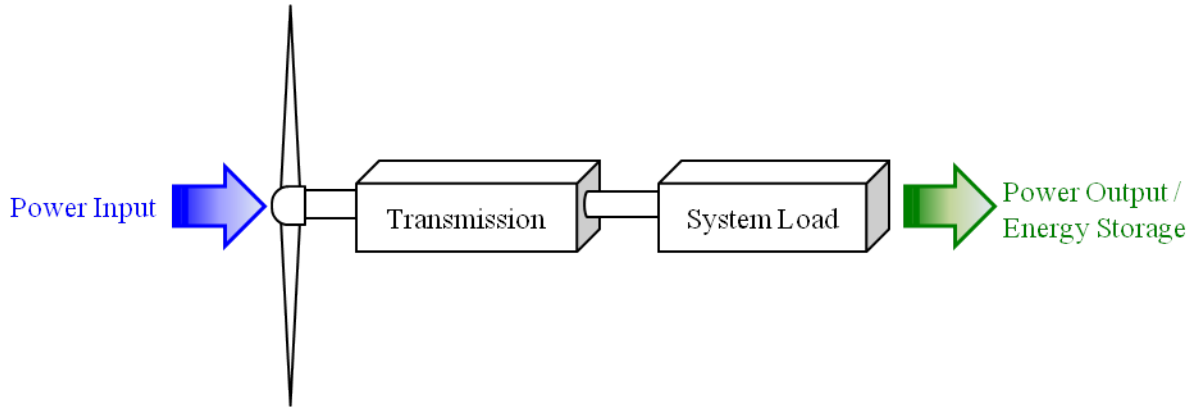

Figure 1.7: General description of system load for a wind turbine

Matching the torque-rpm characteristics of the load and aerodynamics is important to efficiency. Without matching the characteristics of each, there will be deficiencies in aerodynamic performance. A rotor capable of achieving very high peak efficiency will perform poorly if paired with a load that forces it to operate at rotor speeds well above or below its design point for a given wind speed. This study demonstrates a key advantage of using CVT is the torque control it offers when coupled to a typical fixed-speed system load. The

following statement offers insight on the ability of a CVT in a wind turbine:

CVT is to load torque what pitch actuator is to aerodynamic torque.

Figure 1.8 illustrates mismatched torque-rpm characteristics coupled by a CVT. This is precisely what's done when pairing an aerodynamic rotor to a generator that has characteristics differing from those of the optimal aerodynamics.

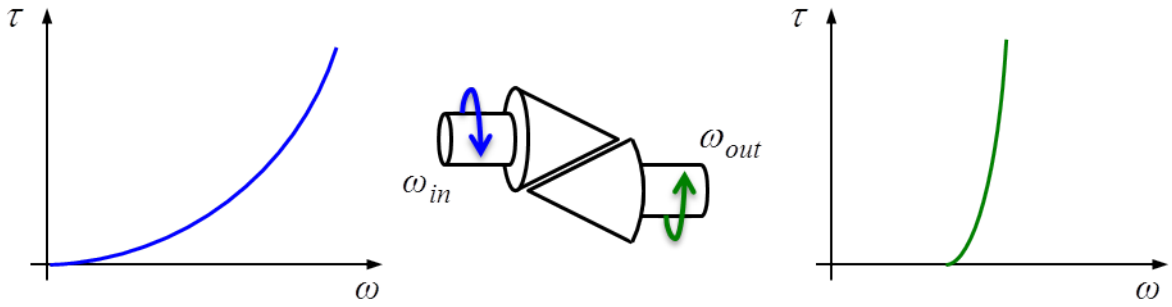

Figure 1.8: Mismatched torque-rpm characteristics coupled by a CVT

To reiterate, this study focuses on the application involving an AC electrical load with an electromagnetic generator serving as the transducer between the captured wind power and electrical power output. When a CVT is coupled to a traditional fixed-speed load, valuable control of the load torque is gained. To be discussed in full detail later, the CVT can serve as the load torque actuator thus allowing full variable-speed control.

1.1.4 Performance

Power in the wind is a function of air density, swept area, and the cube of free stream velocity. Wind power is expressed as,

$$P_w = \frac{1}{2}\rho A v^3 \tag{1.1}$$

Clearly, modern wind turbines attempt to take advantage of wind power being a function of the square of rotor radius and the cube of free stream velocity. This is illustrated by the use of long blades and tall towers reaching to heights where wind resource is more plentiful than near Earth's surface due to shear.

The power coefficient, expressed as,

$$C_p = \frac{\text{power output}}{\text{power input}} = \frac{\text{rotor mechanical power}}{\text{wind power}} = \frac{\tau_{aero}\omega_{rot}}{P_w} \tag{1.2}$$

is a measure of aerodynamic efficiency. Recalling the focus being on HAWTs operating via aerodynamic lift, Albert Betz derived a theoretical maximum power coefficient based on an actuator disc concept by applying continuity, momentum theory, and Bernoulli's equation from fluid mechanics. It's known as the Betz limit and equals 16/27, or 0.593. This occurs at an axial flow induction factor of 1/3, equivalent to an air velocity at the disc equal to 2/3 free stream velocity. This derivation can be found in wind energy textbooks [3, 11, 12].

A dimensionless parameter useful in characterizing aerodynamic performance is the tip speed ratio (TSR), denoted with λ. It's defined as the ratio of blade tip speed to free stream velocity and is written as,

$$\lambda = \frac{r\omega_{rot}}{v} \tag{1.3}$$

where r is the rotor radius. Examining the velocity vector diagram associated with the cross-section of an in-plane rotating blade reveals how TSR directly relates to angle of attack. Modeled aerodynamics of a typical wind turbine show the optimal power coefficient at a particular TSR and pitch, both relate back to angle of attack. Figure 1.9 is a plot of power coefficient versus TSR at a given pitch for a typical HAWT.

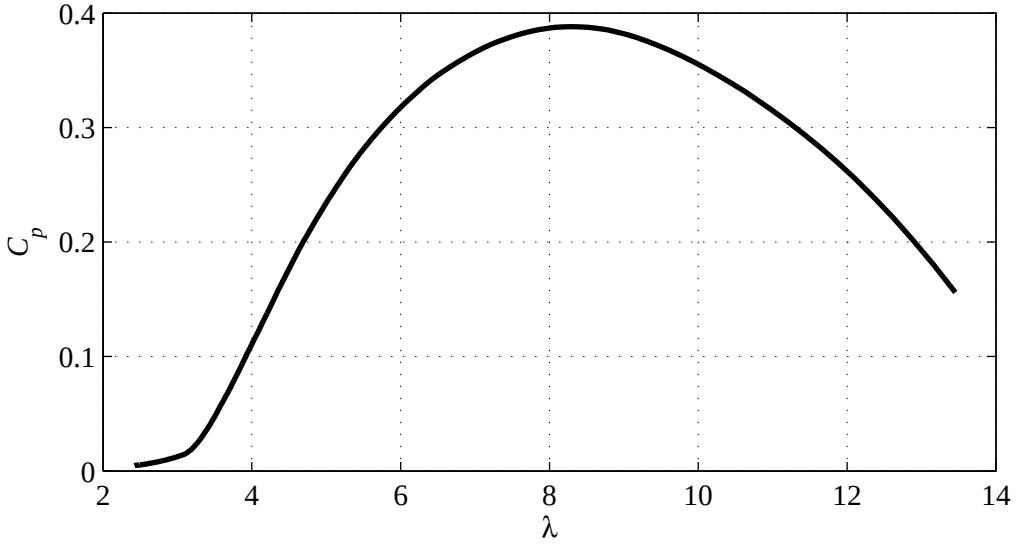

Figure 1.9: Typical power coefficient versus TSR curve at fixed pitch angle

The performance parameter of key interest to consumers is COE. The COE dictates viability of the wind energy industry. It's important for the COE from wind turbines to be competitive with that of coal and natural gas, even though wind energy has advantages for reducing CO_2 emissions and being sustainable indefinitely [13]. In 2005, the National Renewable Energy Laboratory (NREL) completed a study showing the use of CVT could reduce COE up to 7.3% compared to typical variable-speed wind turbines, but also suggested more details on CVT costs and performance are needed for in-depth analysis.

1.1.4.1 Fixed- and Variable-Speed

Differentiating performance of fixed- and variable-speed wind turbines can be done by studying the C_p versus λ curve at fixed pitch. Recall the velocity vector diagram in Figure 1.2, the blade speed vector remains unchanged in magnitude and direction regardless of wind speed for fixed-speed operation. Therefore, angle of attack changes with wind speed. Figure 1.10 explains fixed-speed operation with fixed pitch, which is usually the case in Region 2.

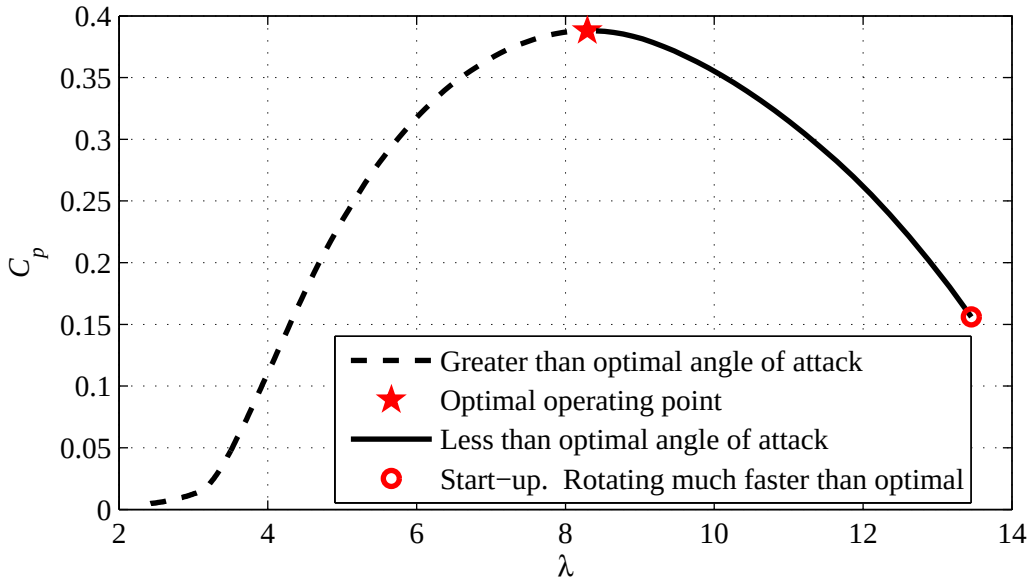

Figure 1.10: Explanation of fixed-speed and fixed-pitch operation

Alternatively, a variable-speed rotor is capable of tracking the peak C_p as wind speed varies since blade speed can vary. The power per area contour plot in Figure 1.11 shows peak power occurs along a straight line corresponding to the constant λ associated with optimal C_p.

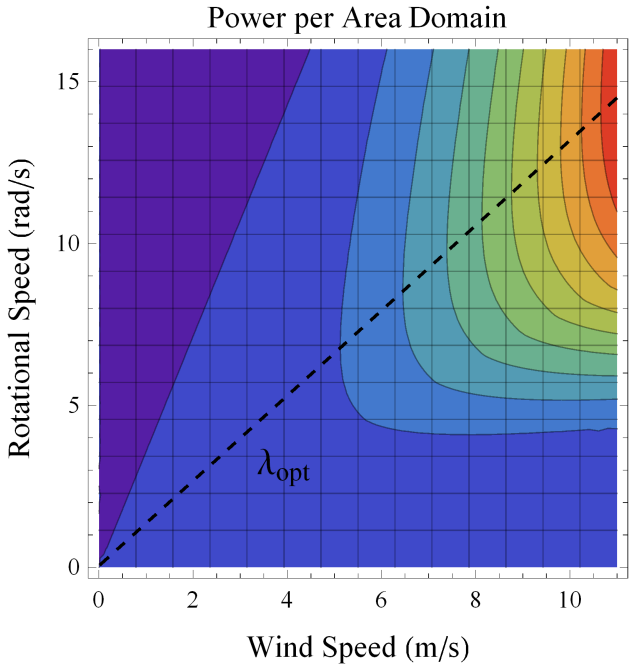

Figure 1.11: Power per area contour plot showing λ_{opt} line

1.1.5 Regions

Figure 1.12 shows a typical power curve for a wind turbine. As the figure indicates,

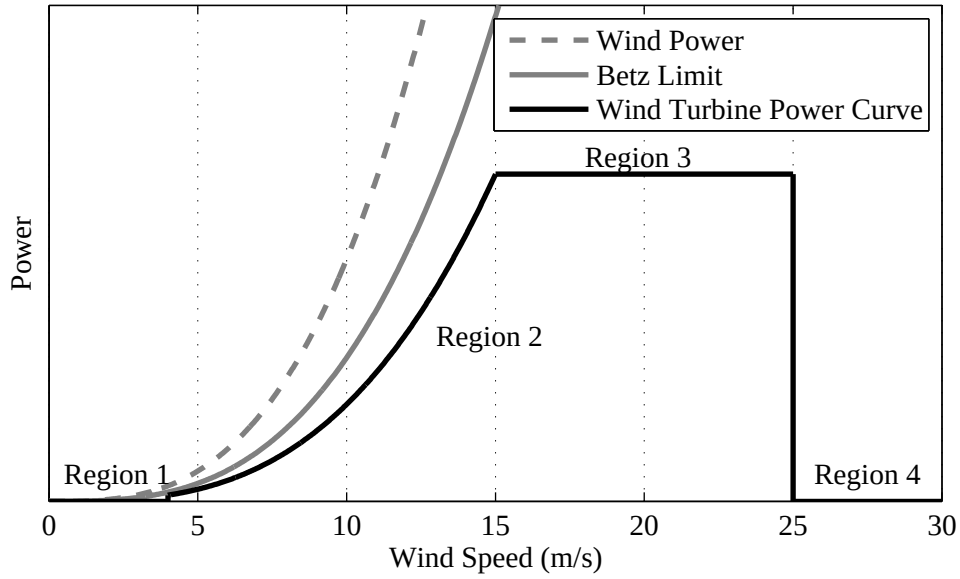

Figure 1.12: Regions of operation illustrated on a wind turbine power curve

there are four regions of operation. Region 1 is when the wind speed is below cut-in speed and the wind turbine is at a standstill. Region 2 occurs when there is sufficient wind power to operate but not more than the generator rating. Region 3 is when the wind power captured must be limited to avoid overloading the generator. Lastly, Region 4 is when the wind power reaches levels that may damage the wind turbine, therefore operation is halted. This study considers Region 2 and 3, plus a transition region known as Region 2.5. More detail regarding the three regions considered here will be covered in section 1.3.

1.2 Continuously Variable Transmission

The concept of a CVT was first documented by Leonardo da Vinci in 1490. The first patent for a CVT design, toroidal type, was filed in 1877 and 1886 for a belt and pulley type

[14]. The history of CVT research and development has been led by the automotive industry. Historically, CVT designs have struggled to handle high torque due to the transmission of torque often being friction-based. However, continued research in the automotive industry as well as emerging technologies are advancing this limitation.

1.2.1 Current Technologies

The concept of a CVT, regardless of application, is far more desirable than traditional discrete ratio transmissions, however the execution of each concept has decided their prevalence. Geared transmissions are simpler to build and have been studied extensively, resulting in reliable designs capable of transmitting very high torque and power. CVTs have not experienced the same success due to their more complicated designs combined with less research and development. A key difficulty is the unfavorable physics associated with the transfer of torque in many CVT designs, i.e. the friction-based transfer of torque and power. Let's now consider a few designs presently available.

1.2.1.1 Pulley V-Belt

This may be considered a classical design for CVTs. Recall, it was one of the first to have a patent issued. Figure 1.13 is a simple illustration how a pulley V-belt CVT is configured. Each pulley, i.e. input and output, is heavily tapered from its ends towards its center, like cones. The belt is shaped to fit the taper of the pulley, hence its name V-belt, such that contact between the belt and pulley is maximized. To maintain a constant length between each rotational axis, as one pulley is widened, the other is narrowed. This changes the radius of the belt path on each pulley, effectively changing the ratio.

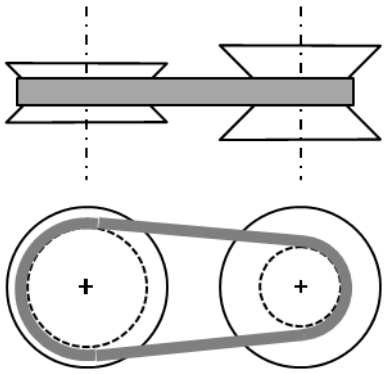

Figure 1.13: Pulley V-belt type CVT

1.2.1.2 Toroidal

Figure 1.14 is a basic layout of a toroidal CVT. A roller is located on each side of the toroid shaped drive shaft. Friction between the rollers and the toroid axles is used to transfer power from one side of the toroid to the other. As the angle of the rollers is adjusted, the contact points between the rollers and toroid axles are shifted along the toroid shape, resulting in a ratio change along the drive shaft.

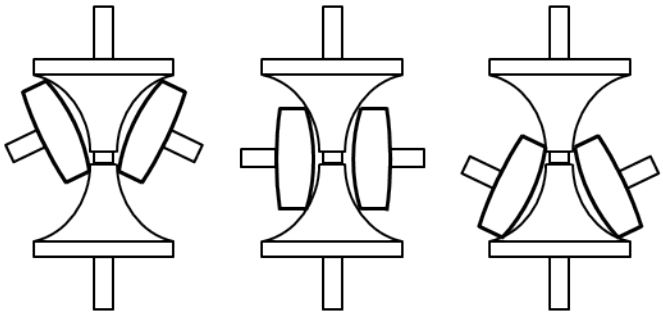

Figure 1.14: Toroidal type CVT

1.2.1.3 Hydraulic

As opposed to the previous two friction-based designs discussed above, hydraulic CVTs transfer power via hydraulic fluid and are therefore capable of handling higher torques. Two types of hydraulic CVTs are discussed here. The first type is often referred to as the hy-

drostatic CVT and operates with the use of a variable-displacement pump and hydrostatic motor [15]. As the pump varies fluid flow, the hydraulic motor output varies accordingly. This type of hydraulic CVT is common in large machinery such as farming and earth-moving

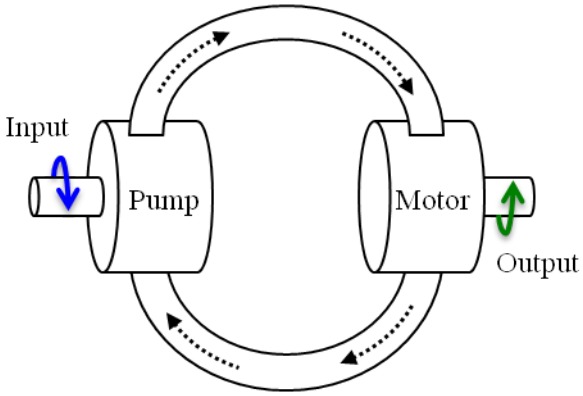

Figure 1.15: Hydrostatic type CVT

equipment, but a form of this CVT is also found in the gearbox of the 2.0 MW Wikov Wind W2000 wind turbine [16]. Its drivetrain configuration is known as the Superposition Gearbox (SPG) and is designed by ORBITAL2 Ltd. The SPG is coupled to a grid connected synchronous generator operating at constant speed, avoiding the need for frequency conversion PE [17].

Another type of hydraulic CVT is the Voith Turbo WinDrive® hydrodynamic gearbox coupled to a constant speed synchronous generator without PE [18]. The WinDrive® consists of planetary step-up gears coupled to a hydrodynamic torque converter with adjustable vane angles to vary the torque transmitted to the output drive shaft, thus providing control of the ratio. This setup is used by DeWind on their D8.2 and D9.2 models, 2.0 MW wind turbines [19].

1.2.1.4 Planetary

In particular, this refers to the NuVinci® design owned by Fallbrook Technologies Inc. They refer to their design as a Continuously Variable Planetary (CVP) transmission. This is not to be confused with traditional planetary gears, discussed in the next paragraph. However, the name is understandable when examining the design as shown in Figure 1.16. A set of planets, i.e. in both gear terminology and shape, are responsible for the transfer of power between an input and output traction ring. This is a friction-based design but uses elastohydrodynamic lubrication, and its planetary configuration provides an evenly distributed set of contact points, presumably allowing higher torque as more planets are used. A small wind turbine manufacturer, Viryd Technologies, has developed an 8.0 kW wind turbine using the NuVinci® CVP transmission and is working on a 50.0 kW design. [20, 21]

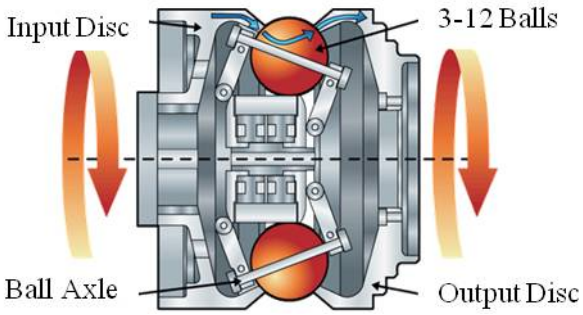

Figure 1.16: Elastohydrodynamic planetary type CVT. The image is used under license from Fallbrook Technologies Inc.

1.2.1.5 Geared

A key disadvantage of many CVT designs is their usage of friction to transmit power. Applying the concepts used in differentials, e.g. as found in automotive drivetrains, meshed gears can be configured to emulate a CVT, but there are fundamental differences between

differentials and CVTs. For CVTs, there is a single input and single output shaft, so power input must equal power output less the internal losses. For differentials emulating CVTs, there is an input, output, and at least a third shaft in which power may flow in or out, thus entering or exiting the main drive shaft of the wind turbine system. This means the third shaft must have the ability to sink and source power. When no power flows through this shaft, the differential will act as a fixed ratio geartrain. Requiring control of power flow in this shaft to adjust the input-output ratio may be viewed as the disadvantage here, but the clear advantage is the use of gears for high torque designs. A simple planetary gear set may be utilized as a differential CVT [8], see Figure 1.17. The configuration could be used with the sun gear as the input, planet carrier as output, and ring gear as the control.

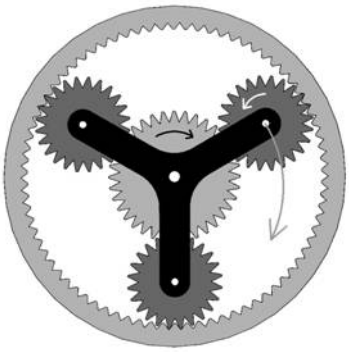

Figure 1.17: Planetary gears

1.2.1.6 Magnetic

Magnomatics Limited, based in the United Kingdom, has developed magnetic CVT technology that transmits torque without contact. It works by coupling the input and output shafts via a magnetic field created with permanent magnets. Located within this field is a rotating membrane with poles. The input-output magnetic coupling is dependent on the speed of the membrane. Therefore, the membrane's rotational speed dictates the

input-output ratio. Magnomatics claims this technology to be highly efficient, compact, and lubrication free. They do not yet provide power capacity in the megawatts range, but assert the technology is scalable. [22]

1.2.2 Wind Turbine Application

In nature, wind is highly variable and unpredictable. As dictated by the aerodynamics of fixed-pitch blades, a wind turbine rotor should rotate faster or slower for higher or lower wind speeds, respectively, if peak efficiency is to be achieved. This was previously illustrated when discussing performance of fixed- and variable-speed rotors.

Unfortunately, the common application of using an electromagnetic generator connected to a constant-frequency grid, 60 Hz in the US, results in a mismatch of torque-rpm characteristics between the system load and optimal aerodynamics. Modern wind turbines typically utilize frequency conversion PE to allow the generator to rotate at variable speeds while remaining connected to a constant-frequency grid. Without the PE, the wind turbine rotor would rotate at a constant speed, as mapped through the fixed-ratio gearbox, corresponding to the grid frequency and generator design.

Recall, a key attribute of CVT is its ability to control the load torque seen by the rotor when connected to a generator without torque control, i.e. no PE. In other words, a CVT is capable of mapping the "rigid" torque-rpm characteristics of a grid-connected generator to the desirable characteristics for a given operating condition. This means CVT provides a mechanical alternative to PE for variable-speed operation and torque regulation, given the proper controls. The expressions below, from [3], is one way to distinguish the characteristics

of fixed-speed and variable-speed systems.

$$\text{Constant-speed generator torque} = f(\text{aerodynamic torque, system dynamics}) \tag{1.4a}$$

$$\text{Variable-speed generator torque} = f(\text{generator torque control system}) \tag{1.4b}$$

Note, the "system dynamics" are part of what dictate the constant-speed generator torque. By including a CVT in the drivetrain, the system dynamics become a controllable variable of the constant-speed generator torque. This research exploits the ability of a CVT to offer control over the system dynamics, thereby achieving control objectives that would normally be applicable to only conventional variable-speed wind turbines.

1.2.3 Wind Turbine Configuration

This thesis utilizes the design of an existing wind turbine, the two-bladed Controls Advanced Research Turbine (CART) at NREL, to construct a simulation model. If the CART were to be retrofitted with a CVT, the drivetrain configuration must be considered. In particular, the torque and power capacity of the CVT must be understood along with what type of generator will be used. With this information, along with knowing the operating characteristics of the wind turbine, a CVT can be designed and implemented into the drivetrain.

Given the torque and power capacity of present CVT technology along with traditional generator designs having high rotational speeds, like the one in the CART, this dictates the drivetrain configuration to include a large step-up gearbox and for the CVT to be placed on the HSS where torque loads are much less than the LSS. This architecture is used in this research and illustrated in Figure 1.18. Details specific to the CART will be provided in the next chapter. Note the altered terminology due to the presence of a CVT. What

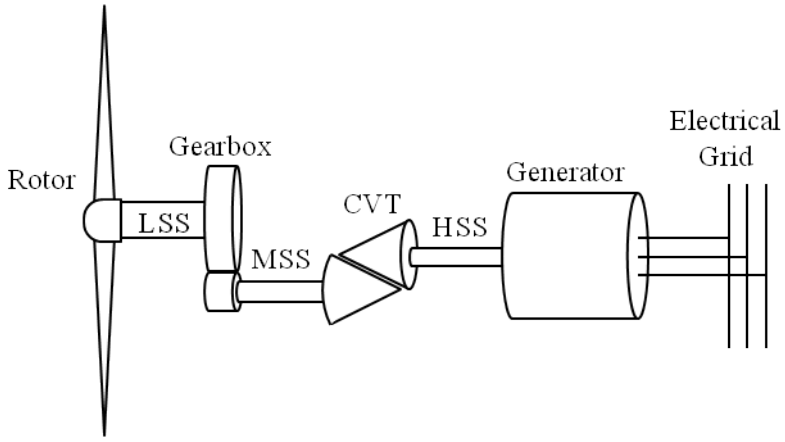

Figure 1.18: Wind turbine configuration with a CVT

was formerly the HSS now includes a CVT. To maintain consistency in notation, the shaft connected to the generator will still be called the HSS, and the shaft associated with the CVT input is the *medium-speed shaft* (MSS). In this research, this notation makes sense due to the gearbox ratio and range of CVT ratio used, but if the CVT ratio is ever less than one, the MSS would rotate faster than the HSS.

It can be helpful to view the system load as the CVT coupled to the induction generator connected to a strong electrical grid. This is illustrated in Figure 1.19. It's possible to

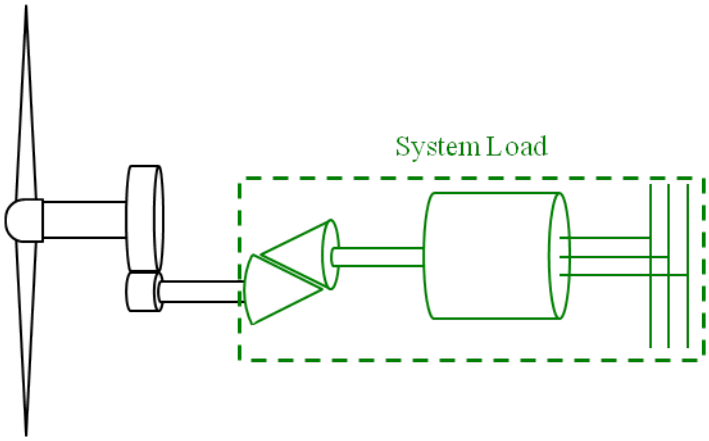

Figure 1.19: Viewing the CVT and grid-connected generator as a system load

consider only the generator as the system load, but as we will see, it's often advantageous

in our control models to consider the CVT and generator together. The CVT can be used as an actuator of the load torque and this enables CVT to transform a normally fixed-speed wind turbine into a variable-speed one. In a typical variable-speed wind turbine using PE, the generator electromagnetic torque is used as the actuating torque allowing a range of rotational speeds. The electromagnetic torque cannot be manipulated for an induction generator without PE. Therefore, the CVT will be used to map generator torque to match the desired loading condition based on the controller objective.

1.3 Control

Wind turbines experience many unpredictable operating conditions over a short period of time on any given day. To ensure stable operation and prevent extreme conditions from destroying the wind turbine components, it is necessary to implement control systems. In addition, optimal energy capture and reduced fatigue loading are desired to lower the COE. This section aims at explaining the various operational regions, objectives, and challenges associated with the control system.

1.3.1 Regions

Not only is a wind turbine required to operate in unsteady conditions continuously, but there are various regions of operation with different objectives. This research considers the controls design for a CVT wind turbine operating in Region 2 and 3, plus the transitional Region 2.5. Recall Figure 1.12 for an illustration of the regions, except Region 2.5.

Region 2 corresponds to maximizing energy capture in less than rated wind speeds. Region 3 corresponds to limiting power in above rated wind speeds due to generator capacity.

The transitional Region 2.5 exists to limit tip speed due to noise requirements. Limiting tip speed requires operating at less than optimal rotor speed, resulting in aerodynamic deficiencies and is therefore an undesirable region to have.

1.3.2 Objectives

The determination of control objectives is based on desirable performance characteristics. The objectives are not always easily measurable or designed for, especially when considering the variety of unsteady operating conditions encountered. For example, maximizing energy capture may result in different optimal controller designs for different inputs. Furthermore, different operating regions have different objectives as previously discussed, hence different control actions must be utilized. An example of an objective not easily measurable is reliability, but certain characteristics known to enhance it, such as damping, can be designed into the control scheme. We will now consider the objectives in this research for each region, but how these objectives are fulfilled is not covered until chapters on control design.

A properly designed wind turbine spends much of its time in Region 2, below rated power. To reduce the COE, it's important to capture as much energy as possible in this region. However, this should not be achieved at the expense of reliability, otherwise a benefit in COE may not be realized. It's equally important for fatigue loads to be sustained or improved in Region 2, and active damping of the drivetrain will be used to achieve this.

A wind turbine rotor with optimal aerodynamic operation requiring relatively high speeds before it reaches rated power will likely require Region 2.5. This can result from an aerodynamic rotor designed with a high λ_{opt} paired with a relatively large generator capac-

ity. Either one of these design features on its own may lead to needing a Region 2.5. Wind turbine designers should be discouraged to develop such designs since aerodynamic deficiencies result from including a Region 2.5. However, if it must be included to limit noise, then stretch it out over a range of rotor speeds to allow a smooth transition between Region 2 and 3. Without stretching out Region 2.5, the wind turbine will abruptly switch from variable- to fixed-speed operation, resulting in damaging torque spikes in the drivetrain.

Most wind turbine designs spend an appreciable amount of time in Region 3, where the primary objective is to limit power in accordance with generator capacity. Various methods exist to achieve this objective. The method used in this research involves feathering the blades, known as active pitch control, to regulate rotor speed while using the CVT to regulate the load torque seen by the rotor. Regulation of torque and angular velocity equates to regulated power. Other methods for regulating power in Region 3 include variable-speed stall, active stall, passive stall, and passive pitch. For details regarding these other methods, consult wind energy textbooks [3, 11, 12]. In addition to regulating power, another key objective in Region 3 is to limit fatigue loading by adding drivetrain damping. This is most important in Region 3 since the loads are higher than any other actively operating region.

1.3.3 Challenges

Certain challenges present themselves when attempting to meet the control objectives. The key control objectives here are maximizing energy capture, regulating power, and adding drivetrain damping with the intent of improved reliability. Due to the stochastic nature of wind and the dynamics of wind turbines, it is an ideology to truly maximize energy capture. Power regulation and drivetrain damping will not be perfect since the system is responding

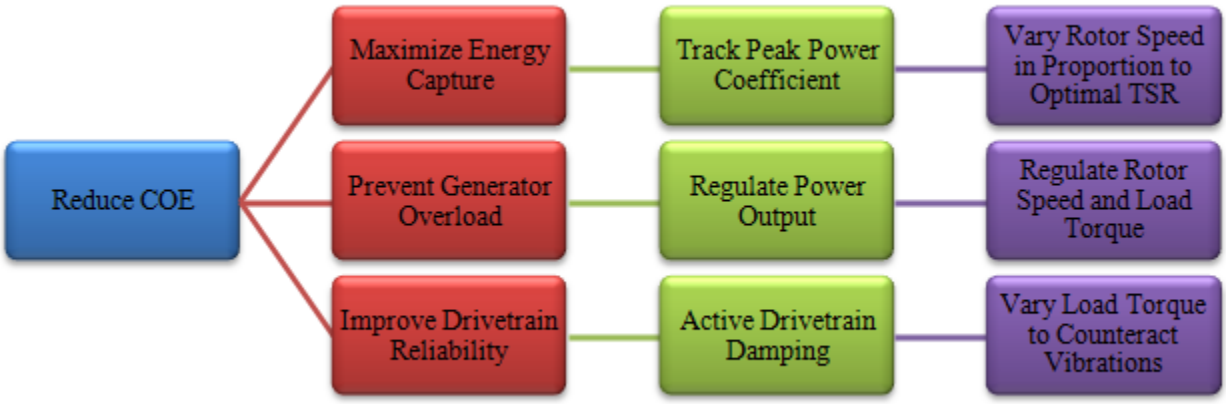

Figure 1.20: Hierarchy view of key objectives

to disturbances and speed of regulation is limited by the actuators used.

The use of mathematical models presents another challenge in designing controls intended for a physical system. Using mathematical models, we can construct simulation models meant to represent the actual physical system to the best of our ability or resources. However, mathematical models are approximations of the physical phenomena occurring in the actual system. More importantly, these models are usually constructed to be as simple as possible without ignoring any physics expected to have a strong influence on the system response. This means assumptions about the physical system will be made for the purpose of simplifying the model.

The control models, i.e. the mathematical models used for control design, are often a further simplification of the simulation model. This results in the controller design being based on an approximation of an approximation of the physical system. This is illustrated in Figure 1.21. This concludes that a control system performing as expected on a simulation model provides no guarantee of success when implemented in the physical system. A better degree of success can be expected with higher fidelity simulation and control models,

assuming the physical phenomena are accurately modeled. This research uses control and simulation models of various fidelities.

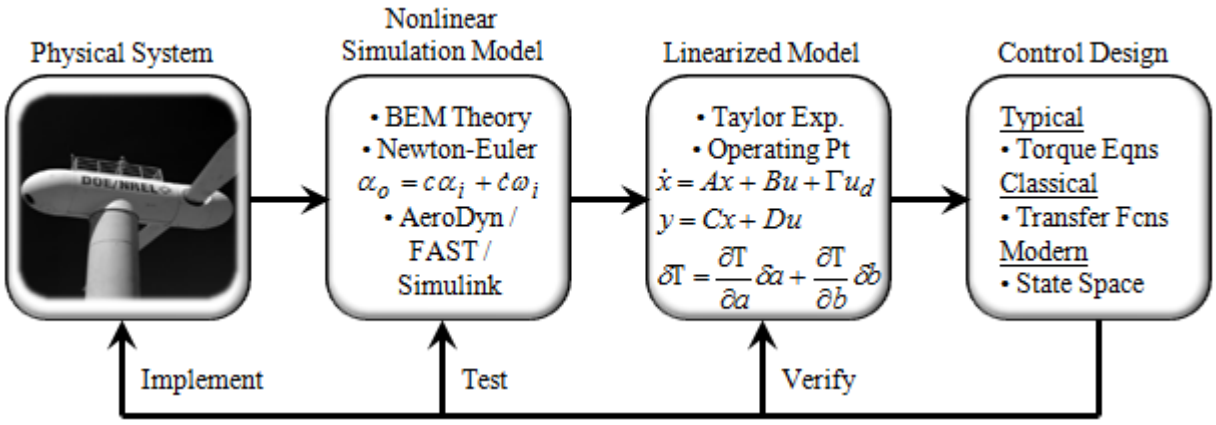

Figure 1.21: Illustration of the modeling process

Some challenges are beyond the scope of controller design. For example, regardless of how well a controller is capable of limiting fatigue or extreme loads, other physical aspects of the system will dictate its reliability. However, controller design can offer improvements for a given physical system. System dynamics and operating conditions can inherently present challenges to achieving control objectives. For example, wind input is stochastic in nature and an aerodynamic rotor has a large rotational inertia since it needs to sweep a large area yet also be durable, so this makes tracking λ_{opt} far from perfect. The presence of modeling errors also adds to the challenge of control design, however, adaptive and robust control techniques could be used to accommodate this.

1.4 Scope and Outline

The main purpose of this research is to exploit various methods of control, with focus on the use of modern control methods, for a wind turbine with a CVT and to conduct simu-

lations of the nonlinear wind turbine system for analysis of controller performance. Classical control methods, similar to what can be found in [7, 8, 9, 10], will be considered first along with additional details on developing a control model and tuning methods. Typical control for wind turbines will then be considered, but in the context of CVT rather than PE. Lastly, modern control designs will be developed with varying complexity. Results from each control methodology will be compared for various degrees of control and simulation model fidelity. Analysis of simulation results will focus on the achievement of control objectives, namely, maximizing energy capture, limiting tip speed, limiting power, and alleviating fatigue loads. From the data analysis, pros and cons of each control methodology will be deduced along with recommendations of future work.

The wind turbine modeled in this thesis is an HAWT and the control systems implemented have not been considered for VAWTs. Use of CVTs and the general approaches used here may extend to VAWTs. Furthermore, the HAWT modeled here is smaller than the average utility-scale wind turbine of present-day. However, the concept of CVT and the controller design methods used here can be extended to megawatt (MW) systems, as well as small residential systems. To be shown, modern control methods become more valuable for larger, more flexible wind turbines. The value to be obtained from this thesis is the methodology used to design an advanced control system for a CVT equipped wind turbine as well as analysis and comparison of the various control schemes.

Chapter 2

Modeling and Simulation Tools

Modeling, in this context, is the construction of a mathematical representation of physical phenomena. The purpose of modeling is to provide the designer with a mathematical representation which may be used for controller design, simulation models, and analysis. Good practice is to develop a mathematical model that is as simple as possible, but no simpler. Model complexity may then be added incrementally to include additional physics relevant to what is being studied. In this chapter, modeling a wind turbine with a CVT is explained and discussed in the context of control design and simulation.

2.1 Degrees of Freedom

Modeling specified degrees of freedom (DOF) is often of interest in the field of dynamics and controls. Control system design usually starts with a model containing minimal DOF for simplicity and then proceeds to add DOF in order of relevance. Figure 2.1 illustrates the key DOF of interest for the CVT wind turbine. The motions associated with the flexible DOF will be more pronounced for larger wind turbines. The more DOF that can be imple-

mented in the simulation model, the better the representation will be of the physical system, assuming the modeling techniques accurately depict the physical phenomena. Other DOF,

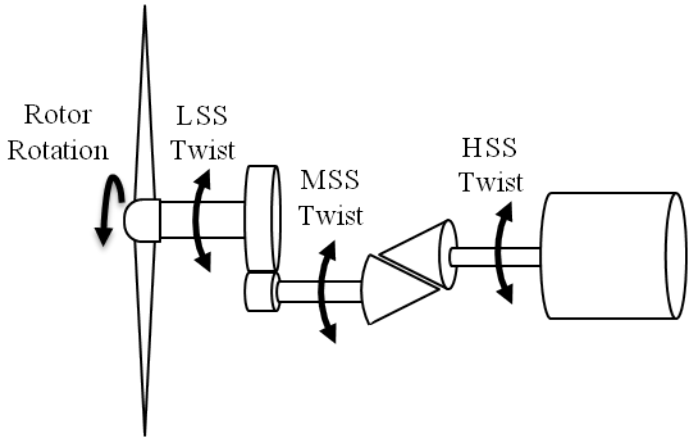

Figure 2.1: Key degrees of freedom for CVT wind turbine

such as those associated with blade and tower motions, are not considered in this thesis but may still play a role in drivetrain behavior.

Only the DOF most relevant to drivetrain behavior will be used for control model development. This includes rotor rotation, LSS twist, and MSS twist. The rotational flexibility of the HSS is not considered for control model development. The most simple of control models will consider only the rotor rotation DOF. Accounting for both DOF requires modeling the shaft torsion between the rotor and CVT input angular displacements.

2.2 Controls Advanced Research Turbine

The two-bladed upwind CART is a wind turbine located at the National Wind Technology Center (NWTC), a division of NREL located near a major mountain range. The CART generator is connected to a 60 Hz grid via frequency conversion PE. The PE allow the CART to vary its electromagnetic torque, thus enabling variable-speed operation. The

model developed here does not include PE and instead uses a CVT as a means to control load torque. The CART properties, aerodynamic performance, and CVT are now explained.

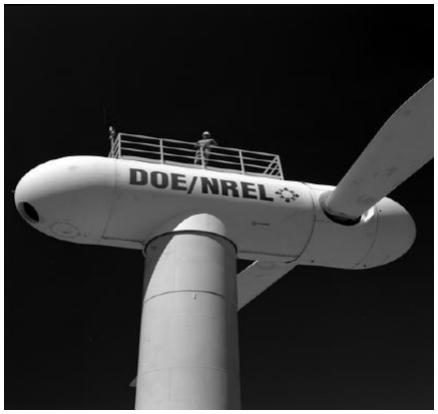

Figure 2.2: Two-bladed Controls Advanced Research Turbine

2.2.1 Properties

Basic information about the CART is listed in Table 2.1. These parameters, along

Property	**Value**	**Units**
Rotor Radius	21.34	m
Rated Rotor Speed	41.7	rpm
Rotor Inertia	3.21722 $\times 10^5$	kg-m^2
Gearbox Ratio	43.165	-
Gearbox + MSS Inertia	22.39	kg-m^2
Drivetrain Torsional Spring	2.691 $\times 10^7$	N-m/rad
Generator Rating	600	kW
Generator Poles	4	-
Grid Frequency	60	Hz
Generator Inertia	12.01	kg-m^2

Table 2.1: CART properties

with additional details, will be used to model the CVT wind turbine as covered in section 2.4. More details, including blade and tower distributed properties, can be found in [23]. Information from this table applies to both the normal CART and CVT CART, noting that what is the HSS for the normal CART will be used as the MSS for the CVT CART. The sections on modeling and control design will make use of these properties.

2.2.2 Aerodynamic Performance

Before the parameters of a CVT can be determined for the CART, the aerodynamic performance must be understood. NREL code, WT_Perf, is used to predict steady state aerodynamic performance of the CART rotor. The modeling methods used in this research are mentioned in the upcoming sections. However, the predicted aerodynamic performance is presented here so the CVT drivetrain design can be explained next. Figure 2.3 shows the power coefficient versus pitch and TSR for the CART. The plot clearly illustrates the aerodynamic behavior of the CART to be highly nonlinear, typical for a wind turbine. Table 2.2 lists the values corresponding to the peak power coefficient. This performance data will also be used for control design.

$(C_p)_{max}$	λ_{opt}	β
0.388	8.3	-1.0°

Table 2.2: Values for peak power coefficient

Figure 1.9, previously used, is a slice of the CART's power coefficient surface taken at a -1.0 degree pitch, known as the run position used for Region 2 operation.

Modeling tools can also be used for predicting noise performance, but it's not done so here. In this case, it's taken to be known that a rotor speed in the vicinity of 41.7 rpm is the

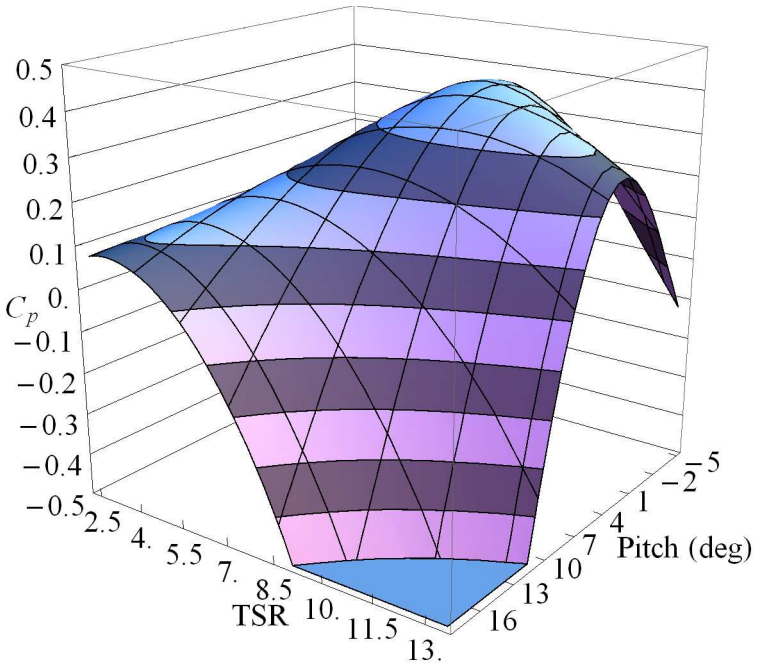

Figure 2.3: Predicted power coefficient as a function of pitch and TSR for the CART

limit for meeting noise requirements. Given the aerodynamic performance now determined with WT_Perf, it will be shown how this noise constraint hinders the Region 2 objective of tracking optimal TSR, thus needing a Region 2.5.

2.2.3 CVT Design

For a fixed-speed wind turbine, the design wind speed is when the maximum power coefficient is achieved. The normal CART has a high design wind speed if operated as a fixed-speed wind turbine. Given the optimal TSR of 8.3 as predicted by the aerodynamic performance code, and a nearly constant rotor speed around 42 rpm due to generator and gearbox designs, this leads to a design wind speed of approximately 11.3 m/s. Considering the rated rotor speed of 41.7 rpm, the CART is poorly designed in terms of fixed-speed operation. A larger gearbox ratio is one simple solution to lowering the design wind speed.

By implementing a CVT, one may view the design wind speed as variable and dependent

on the ratio of the CVT. Knowing the aerodynamic characteristics of the rotor along with the generator characteristics, the parameters of a step-up gearbox and CVT can be determined. Theoretically, there are infinite solutions to pairing a step-up ratio and CVT ratio range that will provide the ability to track optimal aerodynamic efficiency from cut-in to rated wind speed. For practical implementation, analysis of cost and reliability, among other things, should be considered.

Due to the wide variety of CVT technology and designs, this research utilizes a massless black box CVT. The internal workings of the CVT are taken to be unknown. The mechanics

Figure 2.4: Black box CVT has knowledge of input and output only

that dictate how the CVT is actuated are not modeled. No actuator effects are considered, therefore it's assumed that the commanded and actual ratio rate are equivalent.

The design of a CVT ratio range for the CART is now explained, noting that some characteristics of the generator will be used but are explained in later sections. The following equations will be used to determine the ratio range.

$$\text{CVT Upper Ratio} = \frac{\text{start-up generator speed}}{\text{start-up rotor speed} \times \text{gearbox ratio}} = \frac{(\omega_{gen})_{start}}{\lambda_{opt} v_{cut\text{-}in}/R \times N} \tag{2.1a}$$

$$\text{CVT Lower Ratio} = \frac{\text{rated generator speed}}{\text{rated rotor speed} \times \text{gearbox ratio}} = \frac{(\omega_{gen})_{rated}}{(\omega_{rot})_{rated} \times N} \tag{2.1b}$$

Using a cut-in wind speed of 4 m/s and start-up generator speed of 1800 rpm, a CVT ratio of approximately 2.8 would be required to operate at λ_{opt}. Since the CART requires a Region 2.5, it cannot track λ_{opt} up to rated speed, therefore a smaller ratio range can be used. At

rated, the rotor speed is 41.7 rpm and the generator speed is near 1816 rpm. This equates to a CVT ratio of approximately 1.0. In Region 3, perturbations about the rated point will be encountered, and using a lower ratio limit of 0.96 can accommodate this. These ratio limits will be used in the CVT model for this research. In summary, the CART requires an approximate CVT ratio range of 290% to fulfill the full range of variable speed operation.

Since a blackbox CVT is being used, ratio rate limits of present CVT technology are introduced and a practical rate limit is imposed in the CVT model for this research. The makers of NuVinci® claim it can change its ratio 5% per one-tenth of a shaft rev [6]. This implies the ratio rate in units of 1/s depends on the ratio. If a ratio change from 1.0 to 1.05 is used and a generator speed of 1800 rpm (30 rev/s), this equates to a ratio rate of 15 1/s. The magnetic CVT technology developed by Magnomatics is said to have negligible actuator effects [22]. These two examples suggest CVT ratio rates should be sufficient for wind turbines with large rotating inertia which are subject to slow changes in rotational speed. A ratio rate saturation limit of 15 1/s will be used for the CVT model in this research.

2.3 Modeling Codes

The modeling codes are a means of implementing mathematical models into a computer environment that may be used to perform simulation and analysis of the models. The computational codes used in this research are briefly introduced, but the reader is encouraged to consult the references for complete details on the operation of each code.

2.3.1 FAST

FAST (Fatigue, Aerodynamics, Structures, and Turbulence) is an NREL code, originally developed by Oregon State University and later added to and improved by NREL engineers. The code is capable of modeling the physics commonly associated with two- and three-bladed HAWTs. FAST is integrated with AeroDyn, resulting in an aeroelastic modeling package. This enables rotor aerodynamics to be modeled while also considering deflections of the wind turbine's elastic structures. FAST uses Kane's method to formulate the equations of motion which avoids needing to solve constraint forces. A fourth-order Adams-Bashforth-Moulton numerical integration method is used to solve the generalized coordinates at each time step, fixed in length as specified by the user. FAST models of the CART have been validated against experimental data and agree well with simulations using higher fidelity codes such as ADAMS [24, 25, 26].

A key feature that makes FAST an attractive modeling choice is its ability to easily include or exclude DOF as specified by the user. Table 2.3 lists the 2 out of 22 DOF used in this research that may be modeled in FAST for a two-bladed wind turbine. Refer to the FAST User's Guide [27] for more information. Although it may not be obvious here, what

Notation	**Description**
θ_{rot}	Rotor azimuth angle
θ_{gen}	Generator azimuth angle

Table 2.3: Degrees of freedom modeled in FAST

has been notated as θ_{gen} for the generator azimuth angle DOF in FAST will actually be the CVT input azimuth angle, $\theta_{cvt,i}$, for the CVT wind turbine model. An additional DOF, for rotationally flexibility of the HSS, will be modeled in Simulink.

2.3.2 AeroDyn

AeroDyn is an NREL code, developed by Windward Engineering, that is an integral part of FAST. It's built into FAST and cannot be used as a stand-alone simulator. The AeroDyn routines are responsible for calculating the aerodynamic response of the wind turbine rotor to a specified wind input. The wind input is determined by the user and provided to AeroDyn in the form of a text or binary file. The blade parameters are also provided to AeroDyn in the form of a text file containing tables of distributed blade properties. The aerodynamic response is calculated using one of two general methods available within the routines. The method used in this research, and historically the most familiar, is blade element momentum (BEM) theory. The other method, useful for modeling complex wake dynamics, is generalized dynamic-wake theory. Refer to the AeroDyn Theory Manual [28] and the AeroDyn User's Guide [29] for more information.

2.3.3 TurbSim

TurbSim is an NREL code capable of generating stochastic, full-field, turbulent-wind files that can be used as input to AeroDyn. Statistical parameters are used to define the wind characteristics. This research makes use of TurbSim's NWTCUP spectral model, developed from wind measurement data taken at the NWTC, location of the CART. Using this spectral model, three different full-field, turbulent-wind files were generated for use with AeroDyn. Details about each wind profile will be provided in the section on modeling wind. Refer to the TurbSim User's Guide [30] for more information.

2.3.4 Simulink

Simulink®, a product of MathWorks, is the simulation environment used to model and simulate the wind turbine designs used for this research. The capabilities of FAST and AeroDyn are retained in the Simulink environment by compiling their Fortran source files into an S-Function which can then be used as a block in Simulink. Input signals for the FAST block are generator torque and power, yaw position and rate, and blade pitch angles. The generator torque and power input signal would be labeled more appropriately as "system load torque and power" since its the load torque and power, from any source, on the MSS shaft (or HSS shaft for a typical wind turbine configuration). This research uses a fixed yaw angle since yaw error is not considered. Consult the FAST User's Guide [27] for more details about the use of FAST in Simulink.

An advantage of Simulink is that the wind turbine model, represented by the FAST S-Function, can easily be added to for the inclusion of new components, actuators, and controls. For this research, the addition of a CVT and its associated control system will be done using Simulink block diagrams. These modeling needs are easily accommodated by FAST's flexibility in turning on or off degrees of freedom and allowing routines outside its Fortran routines. Refer to the Simulink User's Guide [31] for more information.

2.4 Mathematical Models

This section explains the mathematical modeling involved for simulation and control models. Recall, the simulation model is meant to be a representation of the physical system, constrained to the resources available. To model the CART, mathematical representations will be developed for aerodynamics, structural mechanics, dynamics, and electromagnetics.

2.4.1 Aerodynamics

Aerodynamics are the driving force behind the operation of any wind turbine. To model the nonlinear aerodynamics of a wind turbine, two key aspects are considered: wind and blades. The fundamental task is for kinetic energy of the wind to be converted to torque by the blades.

2.4.1.1 Wind

The term wind refers to the bulk movement of air, a low density medium. Unfortunately, its motion is rather complex and unpredictable in nature. Common parameters used to model wind as a time-series include density, x-y-z component speeds, direction, vertical shear, and horizontal shear. In the case of modeling stochastic, full-field, turbulent wind as done with TurbSim, frequency-domain parameters are also used to define the model. Depending on the purpose of simulation, a mathematical model of the wind can be simple or complex. An x-y-z coordinate system is used for defining wind speed components, with the x-axis oriented along the zero-yaw axis, the y-axis points left when facing downwind, and z-axis points upward.

Simple wind models will be used to examine system response during the control design process. A simple model typically involves specifying the x-component hub-height wind speed and vertical shear for a time-series. Any changes in wind speed occur uniformly, i.e. without spatial variation. An example of a simple AeroDyn hub-height input file can be found in Appendix A. Simple multi-step wind inputs will be used for each region considered in this research. They all use a power law vertical shear exponent of 0.147. Figure 2.5 shows plots of the simple wind inputs. Note, the total duration of these inputs varies.

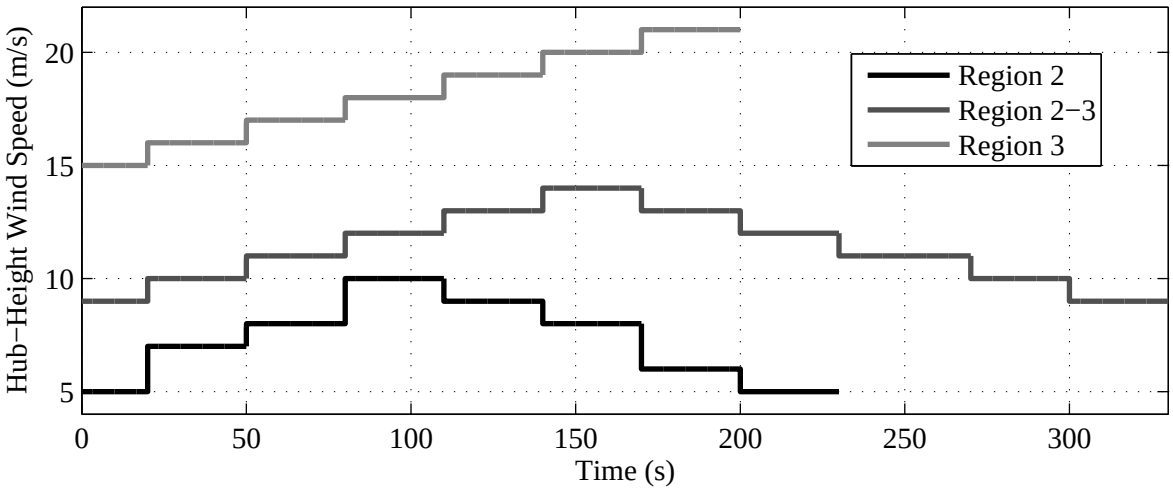

Figure 2.5: Simple hub-height wind inputs for each region

Full-field wind models will be used to analyze system behavior and controller robustness in simulations meant to represent real world conditions. These full-field models are developed by specifying a set of characteristics in TurbSim, which then generates a full-field wind file and coherent structure file compatible with AeroDyn. Figure 2.6 is a graphical representation showing the difference between these complex 3-D full-field turbulence models and the simple hub-height models. The important characteristics for the three full-field wind profiles used

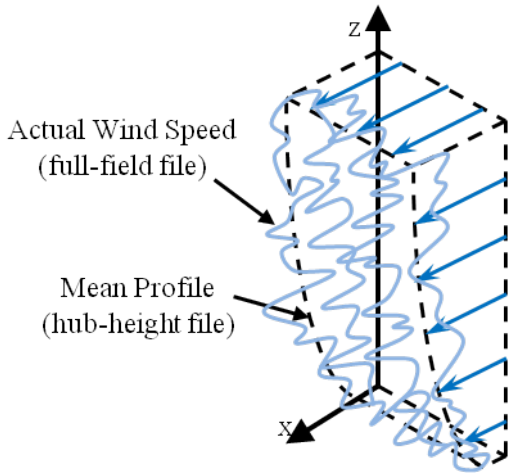

Figure 2.6: Illustration of profiles for mean and actual wind speeds

are specified in Table 2.4. Fortunately, TurbSim has an NWTCUP spectral model that is

meant to represent the conditions found at the NWTC, where the actual CART is located. This turbulence profile will be used for all three full-field wind inputs. Figure 2.7 shows plots of the full-field wind inputs, only for the x-component hub-height wind speed.

Characteristic	**Region 2**	**Region 2-3**	**Region 3**
Spectral Model	NWTCUP	NWTCUP	NWTCUP
Duration (s)	600	600	600
Frequency (Hz)	20	20	20
Gradient Richardson Number	0.05	0.05	0.05
Hub Height Mean Wind Speed (m/s)	8	13	18
Hub Height Standard Deviation (m/s)	1.41	1.83	2.75
Hub Height Min Wind Speed (m/s)	3.91	7.38	9.50
Hub Height Max Wind Speed (m/s)	13.54	17.70	27.77

Table 2.4: Characteristics of TurbSim wind files

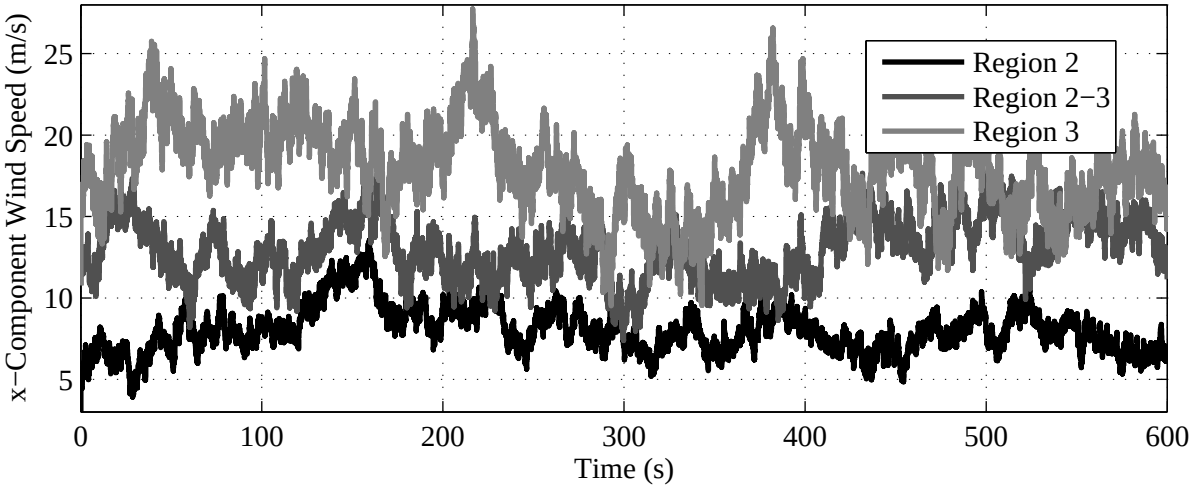

Figure 2.7: Hub-height wind speed for full-field wind inputs in each region

2.4.1.2 Blades

To model the highly nonlinear aerodynamics of the two CART blades, data is needed for the lift and drag coefficients as a function of angle of attack as well as blade geometry.

Due to the extreme angles of attack often encountered by wind turbines, data is provided for $\pm 180^{\circ}$. This data was gathered by NREL engineers and is publicly available on their web server [32]. When viewed from upwind, the blades rotate clockwise.

To solve for the aerodynamic force along each blade, BEM theory is used. The BEM routines in AeroDyn are used to model the aerodynamics of the CART blades for simulation. Similar code routines were used in WT_Perf to generate the predicted performance surface shown previously in Figure 2.3. For coverage of BEM theory, consult wind energy textbooks [3, 11] and the AeroDyn Theory Manual [28].

2.4.2 Mechanics

Two basic wind turbine models are considered for designing the CVT control system. Controllers will be designed for the single-DOF system of rotor rotation only and for the two-DOF system which considers twist between the rotor and CVT input. Modeling the mechanics associated with these DOF is required to design controllers. Other mechanics are involved in the CART's operation but will not be included in the control models.

2.4.2.1 Drivetrain

The wind turbine drivetrain involves modeling applied torques, rotating inertias, rotationally-flexible shafts, and a CVT. Several approaches are considered in this research to model the drivetrain, and are presented here in order of increasing complexity. Recall the CVT used in this research is a blackbox design, hence none of its actuating mechanics will be modeled. This is left to future research focused on a particular CVT design.

The first drivetrain model considers all bodies to be rigid, i.e. without twist. Not shown

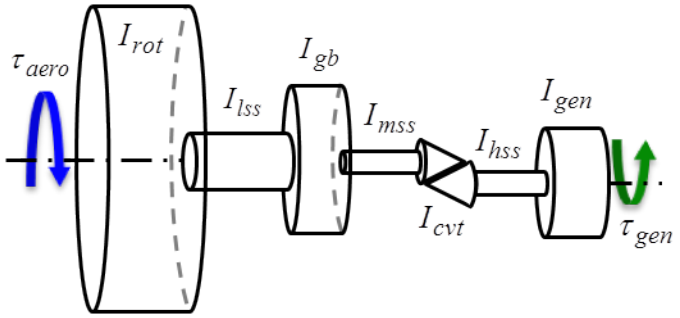

Figure 2.8: Rigid model of wind turbine drivetrain

in Figure 2.8 is the mapping of inertias across the gearbox. This will be made clear in the equations to follow. A single differential equation of motion must be derived to determine the rotor rotation. First consider the rotor and LSS,

$$(I_{rot} + I_{lss})\ddot{\theta}_{rot} = \tau_{aero} - \tau_{lss} \tag{2.2}$$

Then consider inertias in the MSS reference frame and their acceleration,

$$(I_{gb} + I_{mss} + I_{cvt,i})\ddot{\theta}_{mss} = \frac{1}{N}\tau_{lss} - \tau_{mss} \tag{2.3}$$

where I_{gb} is the gearbox inertia mapped to the MSS and N is the gearbox ratio. Lastly, consider inertias in the HSS reference frame and their acceleration,

$$(I_{cvt,o} + I_{hss} + I_{gen})\ddot{\theta}_{gen} = \frac{1}{c}\tau_{mss} - \tau_{gen} \tag{2.4}$$

where c is the CVT ratio. Now (2.4) is solved for τ_{mss} and plugged into (2.3),

$$\Sigma I_M \ddot{\theta}_{mss} = \frac{1}{N}\tau_{lss} - \left[c(\Sigma I_H \ddot{\theta}_{gen} + \tau_{gen})\right] \tag{2.5}$$

where ΣI_M and ΣI_H are the sum of inertias in the MSS (including gearbox) and HSS frames, respectively. Now, solve (2.5) for τ_{lss} and plug into (2.2),

$$\Sigma I_L \ddot{\theta}_{rot} = \tau_{aero} - N\left[\Sigma I_M \ddot{\theta}_{mss} + c(\Sigma I_H \ddot{\theta}_{gen} + \tau_{gen})\right] \tag{2.6}$$

where ΣI_L is the sum of inertias in the LSS frame.

Recall, this model assumes all bodies to be rigid, therefore the acceleration of each shaft can be written in terms of the rotor coordinate. This is where the presence of a CVT shows its effect on the system dynamics. Take derivatives of the shaft speeds written in terms of the rotor coordinate,

$$\begin{aligned} \dot{\theta}_{mss} &= N\dot{\theta}_{rot} \\ \ddot{\theta}_{mss} &= N\ddot{\theta}_{rot} \end{aligned} \tag{2.7}$$

$$\begin{aligned} \dot{\theta}_{gen} &= c\dot{\theta}_{mss} = c(N\dot{\theta}_{rot}) \\ \ddot{\theta}_{gen} &= c(N\ddot{\theta}_{rot}) + \dot{c}(N\dot{\theta}_{rot}) \end{aligned} \tag{2.8}$$

Equation (2.8) shows how a CVT can decouple the generator acceleration from the CVT input shaft acceleration. A CVT ratio change in the absence of rotor acceleration will result in generator acceleration. Alternatively, this may be viewed from the perspective of the rotor as equation (2.9) below shows. This attribute is of great value to controlling the system load

torque as will be demonstrated with controller designs in upcoming chapters.

$$\begin{aligned} \dot{\theta}_{rot} &= \frac{\dot{\theta}_{gen}}{Nc} \\ \ddot{\theta}_{rot} &= \frac{\ddot{\theta}_{gen}}{Nc} - \frac{\dot{c}\dot{\theta}_{gen}}{Nc^2} \end{aligned} \tag{2.9}$$

Now, plugging the results of equations (2.7) and (2.8) into equation (2.6) gives the rotor rotation equation of motion for this model,

$$\Sigma I_L \ddot{\theta}_{rot} = \tau_{aero} - N\big[\Sigma I_M N\ddot{\theta}_{rot} + c(\Sigma I_H(cN\ddot{\theta}_{rot} + \dot{c}N\dot{\theta}_{rot}) + \tau_{gen})\big] \tag{2.10}$$

The form of this equation is not particularly useful for developing the simulation model with FAST and Simulink. The FAST block in Simulink requires a signal containing the torque of the MSS (or HSS for a typical wind turbine). Inputting the generator torque here would be incorrect in the case of modeling a CVT wind turbine because the generator torque, and accelerations of the HSS, are transformed through the CVT onto the MSS. Therefore, equation (2.10) will be rearranged such that the torque on the MSS, called the load torque, is represented in the equation of motion.

$$(\Sigma I_L + N^2\Sigma I_M)\ddot{\theta}_{rot} = \tau_{aero} - N\big[c(\Sigma I_H(cN\ddot{\theta}_{rot} + \dot{c}N\dot{\theta}_{rot}) + \tau_{gen})\big] \tag{2.11}$$

$$\tau_{load} = c(\Sigma I_H(cN\ddot{\theta}_{rot} + \dot{c}N\dot{\theta}_{rot}) + \tau_{gen}) \tag{2.12}$$

$$(\Sigma I_L + N^2\Sigma I_M)\ddot{\theta}_{rot} = \tau_{aero} - N\tau_{load} \tag{2.13}$$

The signal fed to FAST's block diagram for torque will be computed according to equation (2.12) for the models using rigid bodies along the HSS. Notice the load torque is comprised of

an inertial load and electromagnetic torque, plus it's nonlinear. To be shown in the control chapters, a key attribute of the CVT is its ability to control the load torque. Equation (2.11) is a reflection of the system shown in Figure 2.8, whereas Figure 2.9 reflects equation (2.13).

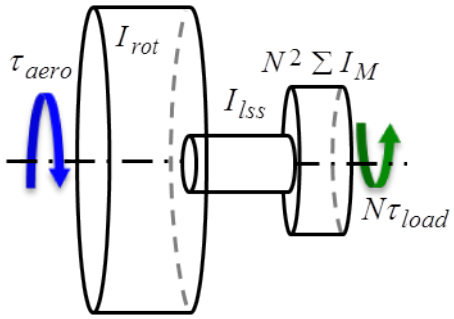

Figure 2.9: Rigid model of wind turbine drivetrain in terms of load torque

In addition to the rotor rotational DOF, consider the CVT rotational DOF. An equivalent linear torsional spring and damper between the LSS inertias and MSS inertias are used to model the first drivetrain torsion mode. This model is meant to depict the rotational flexibility of the rotor, LSS, gearbox, MSS, and CVT input. Bodies associated with the output side of the CVT will be assumed rigid. Figure 2.10 depicts the system modeled with equivalent stiffness, K_d, and damping, C_d.

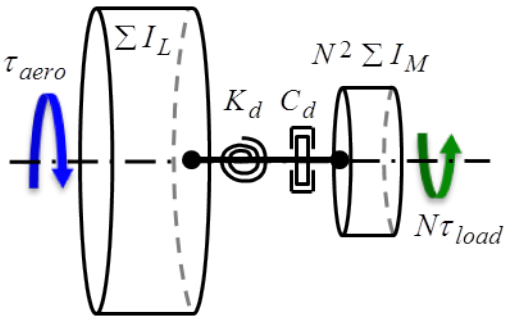

Figure 2.10: Equivalent spring and damper drivetrain model

Modal analysis conducted by NREL for the normal CART reveal the equivalent stiffness

to be 2.691×10^7 N-m/rad, but this corresponds to the first drivetrain torsion mode associated with the rotor, LSS, gearbox, typical HSS, and generator [23]. It's plausible to use this stiffness for the CVT version of the CART modeled in this research, but modal analysis would be essential for practical implementation. The drivetrain equivalent damping element is assumed zero in this research.

Equations of motion must be developed for rotor rotation and CVT rotation, which are coupled by a torsional spring and damper. The rotor equation is developed first,

$$\Sigma I_L \ddot{\theta}_{rot} = \tau_{aero} - \tau_{s,l} \tag{2.14}$$

$$\tau_{s,l} = K_d\Big(\theta_{rot} - \frac{\theta_{cvt,i}}{N}\Big) + C_d\Big(\dot{\theta}_{rot} - \frac{\dot{\theta}_{cvt,i}}{N}\Big) \tag{2.15}$$

where $\tau_{s,l}$ is the reaction torque from the torsional shaft in the LSS frame. Since K_d and C_d are defined in the LSS frame, the CVT input angle and angular velocity are mapped to the LSS by dividing each by the gearbox ratio, N. The equation of motion for rotation at CVT input can be expressed in the MSS frame as,

$$\Sigma I_M \ddot{\theta}_{cvt,i} = \frac{\tau_{s,l}}{N} - \tau_{load} \tag{2.16}$$

where τ_{load}, a function of CVT parameters, must be represented differently than it is in (2.12) due to the rotor speed and CVT input speed not being directly related by the gearbox only since the LSS and MSS shafts are flexible. The load torque for this model is expressed as,

$$\tau_{load} = c\big(\Sigma I_H(c\ddot{\theta}_{cvt,i} + \dot{c}\dot{\theta}_{cvt,i}) + \tau_{gen}\big) \tag{2.17}$$

Therefore, equation (2.16) can be expanded as,

$$\Sigma I_M \ddot{\theta}_{cvt,i} = \frac{1}{N}\left(K_d\left(\theta_{rot} - \frac{\theta_{cvt,i}}{N}\right) + C_d\left(\dot{\theta}_{rot} - \frac{\dot{\theta}_{cvt,i}}{N}\right)\right) - c\left(\Sigma I_H(c\ddot{\theta}_{cvt,i} + \dot{c}\dot{\theta}_{cvt,i}) + \tau_{gen}\right) \tag{2.18}$$

In a physical system, the input and output inertias of the CVT would be functions of the CVT ratio, but these effects are not considered here. Equations (2.14) and (2.16) are the drivetrain equations of motion for the system in Figure 2.10. The torsional shaft torque, $\tau_{s,l}$, and load torque, τ_{load}, appearing in these equations are computed from (2.15)and (2.17).

The last drivetrain model considered in this research has torsion throughout the drivetrain, including the bodies associated with the HSS, i.e. the CVT output, HSS, and generator. The drivetrain DOF are rotor rotation, CVT rotation, and generator rotation. When the HSS bodies were assumed rigid, the drivetrain torsion of the LSS and MSS bodies was modeled with an equivalent torsional spring and damper. If torsion of the HSS were to be modeled this way, the equivalent torsional spring would have a variable stiffness dependent on the CVT ratio, and similarly for the damper. Instead of doing this, the stiffness and damping of the HSS bodies will be modeled separately from the equivalent elements representing the LSS and MSS bodies. The lumped inertias are divided amongst the torsional elements as illustrated in Figure 2.11, but the gearbox mappings are not shown.

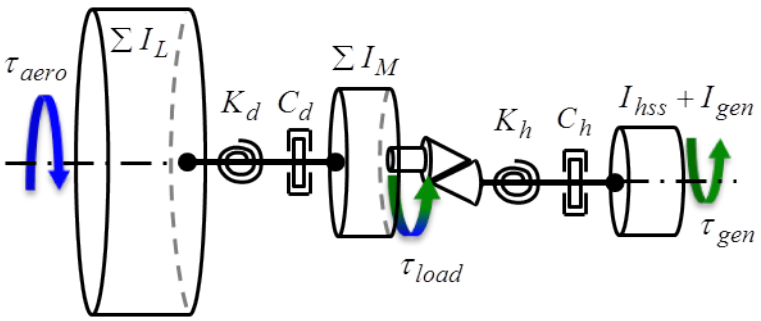

Figure 2.11: Equivalent spring and damper drivetrain model with flexible system load

The equations of motion must be developed for the rotor rotation, CVT rotation, and generator rotation. The rotor equation remains the same as (2.14) with the shaft torque still defined by equation (2.15). The CVT equation is slightly modified from equation (2.16), along with the load torque,

$$\Sigma I_M \ddot{\theta}_{cvt,i} = \frac{\tau_{s,l}}{N} - \tau_{load} \tag{2.19}$$

$$\tau_{load} = c(I_{cvt,o}(c\ddot{\theta}_{cvt,i} + \dot{c}\dot{\theta}_{cvt,i}) + \tau_{s,h}) \tag{2.20}$$

$$\tau_{s,h} = K_h(\theta_{cvt,o} - \theta_{gen}) + C_h(\dot{\theta}_{cvt,o} - \dot{\theta}_{gen}) \tag{2.21}$$

where $\tau_{s,h}$ is the reaction torque of the torsional HSS and K_h and C_h are the stiffness and damping coefficient, respectively. This research assumes zero damping for the HSS torsion. The difference between equations (2.12) and (2.20) is the inertia used and the shaft torque, $\tau_{s,h}$, is used instead of generator torque.

Lastly, the generator equation for the fully torsional drivetrain system can be written as,

$$(I_{hss} + I_{gen})\ddot{\theta}_{gen} = \tau_{s,h} - \tau_{gen} \tag{2.22}$$

which now concludes the equations of motion, (2.14), (2.19), and (2.22), required to model the fully torsional wind turbine drivetrain with a CVT. The torsional LSS torque, $\tau_{s,l}$, load torque, τ_{load}, and torsional HSS torque, $\tau_{s,h}$, appearing in these equations are computed from (2.15), (2.20), and (2.21).

As previously illustrated, the aerodynamics of the CART are nonlinear. The aerodynamic torque, as modeled in this research, is a nonlinear function of wind speed, rotor speed, and blade pitch. Explained in the next section, generator torque is modeled as a nonlinear, although nearly linear, function of generator speed. Furthermore, the generator torque

appears in the expression for load torque, equation (2.12), as do other nonlinearities. Therefore, use of linear control theory will require linearizing these nonlinear functions. Deriving linearized models is explained in section 2.5.

An important note about creating the simulation model with FAST and Simulink must be made. The dynamics of a CVT and generator are coupled, as illustrated by the expression for load torque, therefore modeling the generator outside the FAST S-Function will be required. This division of modeling tasks is illustrated in Figure 2.12. Remember, the

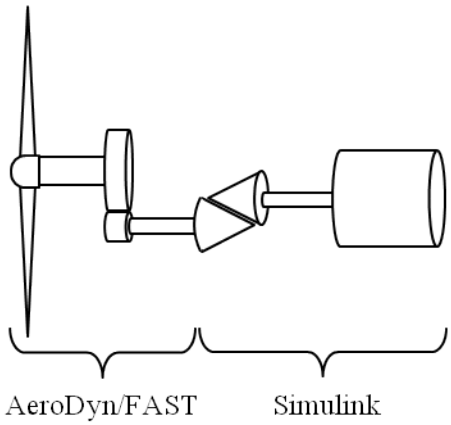

Figure 2.12: Modeling tasks assigned to FAST and Simulink

torque applied to the MSS is what must be fed to FAST, and since the generator torque appears in equation (2.12), it must computed outside of FAST. The same goes for modeling the torsional HSS.

2.4.3 Electrical

The most common application of wind turbines transforms wind power into electrical power, usually a form of AC power which is sometimes converted to direct current (DC) for special applications such as battery storage. All real AC circuits have resistance, capacitance, and inductance with the latter two causing current and voltage sinusoids to be out of phase.

Two types of power result in circuits with current and voltage out of phase, real and reactive power. Apparent power is the the vector sum of the two, where θ is the phase angle. Real

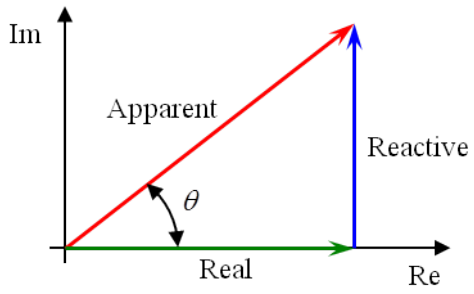

Figure 2.13: Vector diagram of real, reactive, and apparent power

power is the portion that results in positive energy flow, i.e. useful power. Reactive power is the portion that results in reversing energy flow due to the presence of energy storage circuit components. A purely reactive or capacitive circuit, with current lagging or leading voltage by 90°, respectively, has zero net energy flow. Capacitive circuits produce reactive power while inductive ones consume it. The power factor of a circuit is the ratio of real power to apparent power or the cosine of phase angle.

$$\text{power factor} = \frac{\text{real power}}{\text{apparent power}} = \cos(\theta) \tag{2.23}$$

The scope of this research does not require knowledge of line currents and voltages during wind turbine operation, hence the information just presented will not be elaborated on or considered in the simulation model but was introduced for completeness.

For the CART electrical system, only a model of electromagnetic torque is required in this research to study drivetrain behavior for various methods of CVT control. This section introduces the principles of generators, with focus on the induction generator used here, and shows how the electromagnetic torque is modeled.

2.4.3.1 Generator

The fundamental principles of electric generators lie within the physics of electromagnetism. In short overview, a magnetic field is induced around a conductor with current flow. This is the principle used in the creation of an electromagnet, with the magnetic field strength being proportional to the current and number of coil loops. In reverse effect, altering a magnetic field in the presence of a conductor induces an electromotive force resulting in current flow. Ampere's Law describes induced magnetic fields while Faraday's Law describes induced electromotive force. For information on modeling electromagnetics, consult physics textbooks, including those on rotating electric machines [33, 34].

A generator has a rotor and stator, with the design of each dependent on the type of generator. Armature windings are found on the stator, where induced voltage results in current flow in the coils which transmits electrical power from the generator to the grid or auxiliary electrical equipment. Field windings, responsible for creating the magnetic field, may be found on the rotor or stator depending on generator design.

There are three aspects dictating the rotational speed of a generator directly connected to an AC electrical grid: number of poles, grid frequency, and number of phases. The number of poles refers to magnetic poles of the generator's stator. Grid frequency refers to the sinusoidal frequency of the grid's AC current and voltage. The number of phases refers to the conductors responsible for transmitting electrical power in the generator (armature windings) and grid. Commonly used 3-phase AC, with 120° phase-shifted voltages, has the ability to create a rotating electromagnetic field in the stator. Below is a schematic of a 2-pole, 3-phase system showing how the rotating magnetic field corresponds to current flow in each phase. Notice there are two poles per phase, thus a total of six poles in the stator.

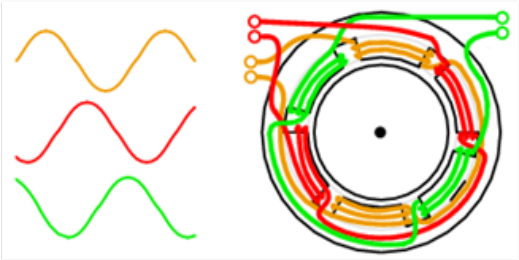

Figure 2.14: Illustration of stator windings for a 2-pole, 3-phase generator

If there were six poles per phase, the magnetic field would rotate at 1/3 the speed.

If a generator is connected directly to the grid without frequency conversion PE, then it must produce AC power at grid frequency. The mechanical speed of the generator rotor that corresponds to grid frequency is referred to as the synchronous speed. Synchronous speed is calculated as,

$$\omega_{syn} = \frac{60f}{P/2} \tag{2.24}$$

where f is frequency of AC in Hz, and P is number of poles per phase. Therefore, the system shown in Figure 2.14 has a synchronous speed of 3600 rpm if expected to output 60 Hz AC.

In general, three types of electric generator designs exist: synchronous, asynchronous, and parametric. The name of the former two refers to the rotational speed of the generator rotor. If the generator rotor rotates at synchronous speed, as defined by (2.24), then it's the synchronous type, otherwise it's asynchronous. As for parametric type, also known as doubly salient, some consider these as synchronous type. Basics of the synchronous and asynchronous type will be covered here. For full coverage of the various types of electric generators, see [34].

Synchronous generators output voltage and current frequency that is synchronized with the rotor mechanical frequency. Direct connection to a grid requires synchronization of

frequency and phase. Figure 2.15 shows the basic configuration of synchronous generators. Electromagnets are created from the field windings of the rotor with an externally controlled DC current. The stator contains multiple windings of the armature with 3-phase AC from the grid producing a fixed-speed rotating magnetic field. No relative motion exists between the fields when the rotor is at synchronous speed. If the rotor has no load, the fields

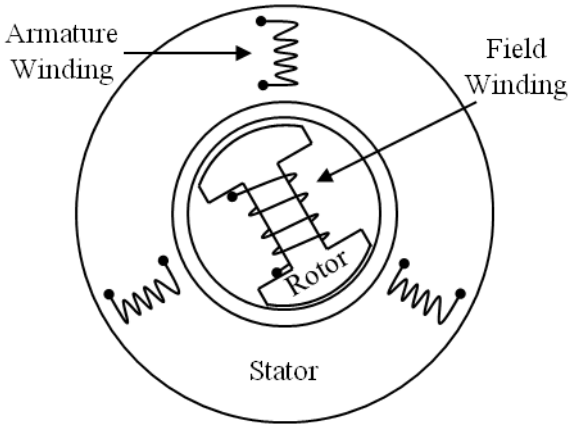

Figure 2.15: Illustration of synchronous generator

will be aligned. As load is applied to the rotor, misalignment of the rotor and stator fields results in an electromagnetic torque that tries to maintain alignment. Although misaligned under load, the fields remain in sync with the same angular velocity. The angle between the rotor and stator field is known as the load angle, δ, sometimes referred to as power angle. Electromagnetic torque is greatest for $\delta = 90°$, however $\delta = 30°$ is suggested for stable operation. In mechanical terms, load angle may be thought of as a very stiff spring. This results in a nearly rigid coupling between the generator and grid, meaning very little load absorption. [3, 10]

Asynchronous generators, often called induction, rely on the grid for excitation and operate at angular speeds slightly higher than synchronous speed. Figure 2.16 shows the basic configuration of induction generators. Stator windings are excited by a 3-phase AC

grid, providing the terminal voltage regulation and resulting in a magnetic field rotating at synchronous speed, therefore the stator contains both armature and field windings. The squirrel-cage rotor, consisting of aluminum or copper bars parallel to the rotational-axis and connected to aluminum end-rings, achieves current flow due to electromagnetism from the rotating stator field. Electromagnets in the rotor result from the squirrel-cage current

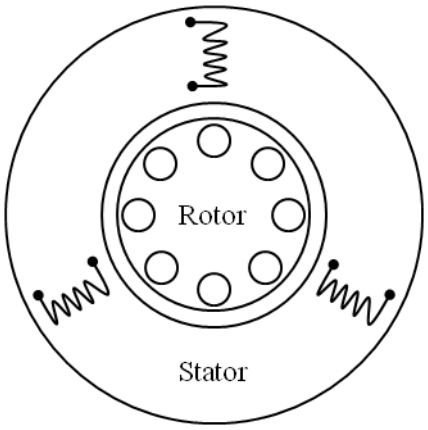

Figure 2.16: Illustration of induction generator

flow. When the rotor is at synchronous speed, no electromagnetism occurs and there is no real power flow. However, there is always reactive power consumption to energize the field windings. If rotor angular speed becomes greater than synchronous, real power is sent to the grid. This relative motion between the rotor and stator fields is called slip,

$$s = \frac{\omega_{syn} - \omega_{gen}}{\omega_{syn}} \tag{2.25}$$

where ω_{gen} is angular speed of the generator rotor. Slip is often presented as a percentage by multiplying (2.25) by 100. Typical values are around 1-2%, negative when generating and positive when motoring. For the drivetrain dynamics, this slip is valuable because it acts as a damper, absorbing loads but at the cost of efficiency. Another key advantage to induction

generators is that no voltage control or synchronization is required, as it's provided by the grid in the stator windings.

To summarize key attributes mentioned above, Tables 2.5 and 2.6 list advantages and disadvantages of synchronous and induction generators [3, 10, 11]. In the context of fixed-

Advantages	Disadvantages
power factor control	dynamic loads
efficiency	external control of field
weak grid stability	

Table 2.5: Synchronous generator

Advantages	Disadvantages
rugged construction	low power factor
relatively inexpensive	consumes reactive power
grid synchronization	
load absorption	

Table 2.6: Induction generator

speed wind turbines, a mechanical analogy is shown in Figure 2.17 to illustrate the effect synchronous and induction generators have on the drivetrain. In the case of variable speed

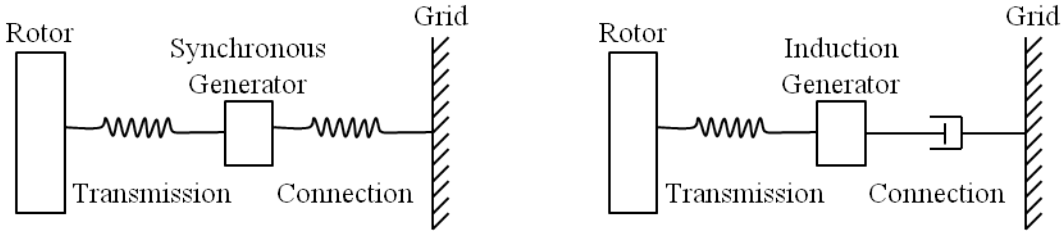

Figure 2.17: Mechanical analogy of grid-connected induction and synchronous generators

wind turbines, load can be absorbed by an increase in rotational kinetic energy. Given the very rigid coupling between a synchronous generator and the grid, the CVT control system would require a bandwidth on the order of 60 Hz in comparison to the approximate 3 Hz

suggested for use with an induction generator [6].

The normal CART has a 600 kW induction generator connected to a constant 60 Hz grid with frequency conversion PE. This research decides to use the same induction generator, but without PE. A model of the electromagnetic torque is needed to study the mechanical behavior of the drivetrain for various methods of CVT control.

A steady state induction generator model is used for this research. When the frequency of wind-induced torque in the drivetrain is less than that of the grid electrical frequency, as is typically the case, this approach is acceptable [3]. To model this, the equivalent circuit shown in Figure 2.18 is used. Using this circuit, all the generator characteristics necessary

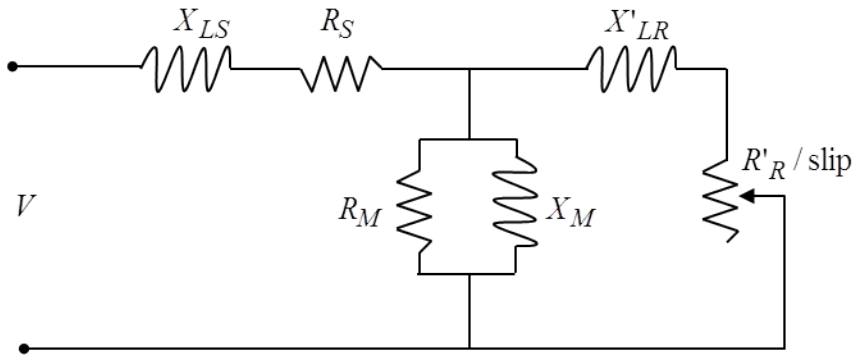

Figure 2.18: Equivalent circuit used to model the induction generator

for this research can be obtained, assuming the circuit data is known.

Engineers at NREL provided the necessary equivalent circuit data for the CART, which they received from the generator manufacturer. The CART generator equivalent circuit parameters and values are listed in Table 2.7. Consult Appendix B to see the equivalent circuit calculations used to obtain the mechanical characteristics of the CART's induction generator. The resulting mechanical torque as a function of slip is displayed in Figure 2.19 and key values are in Table 2.8.

Recall in section 1.1.3, the importance of matching system load characteristics to those of

Circuit Parameter	Symbol	Value	Units
Terminal voltage	V	460	V
Stator leakage reactance	X_{LS}	0.10104	p.u.
Stator resistance	R_S	0.00798	p.u.
Rotor leakage reactance	X'_{LR}	0.07324	p.u.
Rotor resistance	R'_R	0.00847	p.u.
Magnetizing reactance	X_M	3.73419	p.u.
Core loss resistance	R_M	108.5131	p.u.
Base ohms	Ω_{base}	0.32600	Ω

Table 2.7: Equivalent circuit data for CART generator

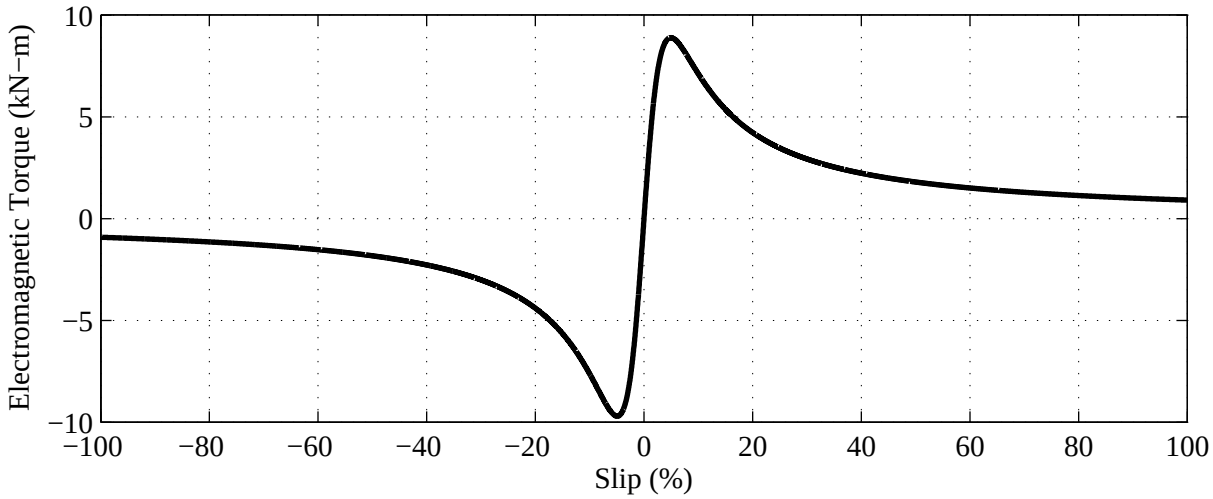

Figure 2.19: Mechanical torque as a function of slip for the modeled induction generator

Parameter	Symbol	Value	Units
Rated torque	$(\tau_{gen})_{rated}$	-3212	N-m
Rated slip	s_{rated}	-0.87	%
Pull out torque	$\tau_{pullout}$	-8887	N-m

Table 2.8: Key mechanical parameters of the CART generator

the aerodynamics. Unfortunately, this common application of high-speed electric generators connected to the fixed-frequency grid makes for a poorly matched system load in wind

turbines. Large gearboxes in combination with frequency conversion PE are often used to match the load characteristics better. However, this research focuses on the use of a CVT, allowing the generator to produce grid quality power without PE. The focus of this research is on control techniques for the CVT, which will now be introduced.

2.4.4 Controls

Linear time-invariant (LTI) control theory is used to develop both classical and modern controls for closed-loop control of the CVT wind turbine in this thesis. Therefore, any nonlinear models are first linearized about a specified operating point. The linearized physical plants can then be used for control system design. In addition, typical wind turbine torque control is used but in the context of CVT actuation instead of the usual generator torque. To ensure robustness, the controllers are then simulated with the nonlinear physical plant. Recall Figure 1.21 for this process.

The nonlinear wind turbine simulator is still a deviation from the actual CART since it too is just a mathematical model that does not account for all physical phenomena. It's important to understand that control system design is based on a simplified model of the actual system, which is represented by a simulation model in this thesis.

Control actuation of a CVT involves commanding either the CVT ratio or ratio rate. Throughout this thesis, the CVT ratio rate is chosen as the variable to command. By specifying an initial condition, the CVT ratio is easily determined as needed for the simulation model. Equation (2.26) shows this.

$$c(t) = \int \dot{c}\, dt \quad \text{with } c(0) = c_o \tag{2.26}$$

A brief explanation of each control method will be introduced next, and the chapters to follow detail each controller design for the CVT CART.

2.4.4.1 Typical Control

Typical control for variable-speed wind turbines involves commanding a load torque, typically the generator torque, based on modeled aerodynamic torque-rpm characteristics. For Region 2, these characteristics are for peak power coefficient at fixed pitch, recall Figure 1.9 , requiring a variable-speed rotor. A non-zero net torque on the drivetrain will accelerate or decelerate the inertias accordingly. By matching the torque-rpm characteristics of the load to the optimal aerodynamics, the rotor will track the modeled peak power coefficient. For Region 2.5, the torque-rpm characteristics should provide a smooth transition between Region 2 and 3 while limiting rotor speed. Like Region 2, this requires variable-speed operation but with a different objective. Lastly, for Region 3, the load torque must be held constant while a pitch controller regulates rotor speed, thus achieving the Region 3 objective of regulating power output. This research does not consider a generator with torque control, used in typical variable-speed wind turbines, therefore it must be understood how the CVT is capable of controlling torque when coupled to a generator with rigid torque-rpm characteristics.

Recall in section 1.1.3 and Figure 1.19, it was said that it can be advantageous to view the CVT and generator, together, as the system load. The torque at the CVT input will be considered the load torque, τ_{load}, in this approach. Recall this from equations (2.11) to (2.13). The mathematical approach to this perspective will be formulated in Chapter 3.

2.4.4.2 Classical Theory

Using classical linear control theory, it quickly becomes difficult to design controls that will account for multiple DOF. This is because a single control loop in classical theory represents a single-input single-output (SISO). For wind turbine control, the single-output of a classical control loop is particularly troublesome since it's often desirable to control more than a single system variable. It's possible to design multiple control loops in attempt to achieve multi-input multi-output (MIMO) control. Other variations of this include single-input multi-output (SIMO) and multi-input single-output (MISO) controllers. However, since each control loop is designed independently, undesirable controller interactions may result. As an advantage, classical theory is typically less sensitive to modeling errors than modern theory [35].

For classical control, controller input is an error signal, $e(t)$, calculated based on a setpoint. The setpoint depends on the control objective, which varies with region in the case of a wind turbine. Once an error signal is formulated, the input-output description of the closed-loop system can be represented by a transfer function in the Laplace domain, assuming a linear mathematical model of the system is available. With classical control, the plant has a single output so its fidelity is very limited. The approach used is briefly mentioned next and applied in Chapter 4.

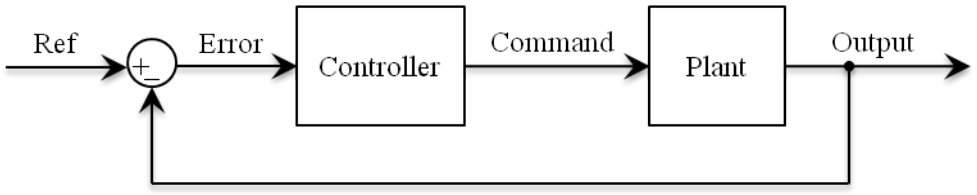

Figure 2.20: Classical control loop with single-input single-output

Tuning controller gains (or plant parameters, if able) will modify system response.

This research uses a proportional-integral-derivative (PID) controller as its classical method, therefore there are three tunable gains. A PID controller is shown mathematically, in time and Laplace domains, by equations (2.27) and (2.28).

$$f(t) = K_P\, e(t) + K_I \int e(t)\, dt + K_D \frac{d}{dt} e(t) \tag{2.27}$$

$$F(s) = \Big(K_P + \frac{K_I}{s} + K_D s\Big) E(s) \tag{2.28}$$

In this research, $f(t)$ will be the CVT ratio rate. The Laplace variable, s, isn't to be confused with the variable used for generator slip as defined in (2.25).

2.4.4.3 Modern Theory

Modern linear control theory allows controllers with higher fidelity, e.g. MIMO, to be designed in a single control loop. More control objectives can be achieved this way. However, a more accurate model may be required than with classical control to achieve robust operation [35]. With the inclusion of more parameters than would be used in the model for classical theory, it may be necessary to use gain scheduling or design the controller at multiple operating points for a nonlinear system. Without doing so, the system will deviate from its designed response and may become unstable. The methods used are briefly mentioned next and applied in Chapter 5.

Modern control of the CVT in Region 2 will be done with Disturbance Tracking Control (DTC) theory. To see the study of DTC theory in the context of wind turbines, consult [36, 37]. The purpose of DTC is to track input disturbances without measuring them. The key fundamental to DTC theory is that it uses an assumed disturbance waveform. Knowl-

edge of the input and output along with an assumed waveform allows the disturbance to be estimated, and tracked in the case of DTC. This is valuable for Region 2 control since the primary objective is to track λ_{opt}.

Modern control of the pitch actuator in Region 3 could be done with Disturbance Accommodating Control (DAC) theory [24, 38], but this thesis sticks with PI pitch control while the CVT will use typical torque control. Always using PI pitch control makes it easier to compare CVT controllers. Additionally, drivetrain damping will be added by designing a realizable modern controller for the CVT that allows torque perturbations about its setpoint torque.

2.5 Linearized Models

If linear control analytics are to be conducted, linearized mathematical models are needed. This section focuses on linearization of the models but does not consider their use in the context of controller design, which is covered in the following chapters on control. Let's now look at linearizing models to formulate transfer functions and state space representations, which will prove useful for control design.

2.5.1 Rigid Drivetrain Linearization

The rigid body equation of motion expressed by (2.13) is reprinted here for convenience,

$$(\Sigma I_L + N^2 \Sigma I_M)\dot{\omega}_{rot} = \tau_{aero} - N\tau_{load}$$

To simplify notation, it will be rewritten as,

$$I_{dr}\dot{\omega}_{rot} = \tau_{aero} - \tau_{lss} \tag{2.29}$$

This equation will be linearized for use in designing controls based on the rigid body model.

Both torque terms in (2.29) are nonlinear, therefore they need to be linearized about an operating point. To express these as linear functions, a Taylor series expansion will be performed for each, where the function and its derivatives are evaluated at a specified operating point. This is done for the aerodynamic torque as,

$$\begin{aligned}
\tau_{aero} &= f\{\omega_{rot}, \beta, v\} \\
&= \tau_{aero}\{\omega_{rot_o}, \beta_o, v_o\} + \delta\tau_{aero} \\
&= (\tau_{aero})_o + \frac{\partial \tau_{aero}}{\partial \omega_{rot}}\delta\omega_{rot} + \frac{\partial \tau_{aero}}{\partial \beta}\delta\beta + \frac{\partial \tau_{aero}}{\partial v}\delta v + \cancel{\text{hots}}
\end{aligned} \tag{2.30}$$

where the higher order terms (hots) are assumed negligible. The delta terms represent perturbations about the operating point. This linearized aerodynamic torque model includes perturbations of rotor speed, blade collective-pitch, and wind speed. If the LSS torque is linearized as is, i.e. without expanding it to include the rigid body load torque expression of (2.12), then it's written as,

$$\begin{aligned}
\tau_{lss} &= f\{\omega_{rot}, \dot{\omega}_{rot}, c, \dot{c}\} \\
&= \tau_{lss}\{\omega_{rot_o}, \dot{\omega}_{rot_o}, c_o, \dot{c}_o\} + \delta\tau_{lss}
\end{aligned} \tag{2.31}$$

Generator torque does not appear in this expression because it's a function of generator speed which is a function of the CVT ratio and rotor speed for the rigid drivetrain model.

If (2.31) is expanded like aerodynamic torque was, it can be written as,

$$\tau_{lss} = (\tau_{lss})_o + \frac{\partial \tau_{lss}}{\partial \omega_{rot}} \delta\omega_{rot} + \frac{\partial \tau_{lss}}{\partial \dot{\omega}_{rot}} \delta\dot{\omega}_{rot} + \frac{\partial \tau_{lss}}{\partial c} \delta c + \frac{\partial \tau_{lss}}{\partial \dot{c}} \delta\dot{c} + \cancel{\text{hots}} \tag{2.32}$$

Combining equations (2.30) and (2.31) back into (2.29), a linearized form of the rigid drivetrain equation of motion is,

$$I_{dr}\big((\dot{\omega}_{rot})_o + \delta\dot{\omega}_{rot}\big) = (\tau_{aero})_o + \frac{\partial \tau_{aero}}{\partial \omega_{rot}} \delta\omega_{rot} + \frac{\partial \tau_{aero}}{\partial \beta} \delta\beta + \frac{\partial \tau_{aero}}{\partial v} \delta v - \big((\tau_{lss})_o + \delta\tau_{lss}\big) \tag{2.33}$$

All operating points will be chosen at steady state, i.e. with no acceleration, therefore the aerodynamic torque and LSS torque must equal one another at equilibrium, otherwise there would be rotor acceleration. This also means the CVT ratio rate will be zero at equilibrium, because a non-zero ratio rate causes acceleration. These conditions simplify (2.33) to,

$$I_{dr}\delta\dot{\omega}_{rot} = \frac{\partial \tau_{aero}}{\partial \omega_{rot}} \delta\omega_{rot} + \frac{\partial \tau_{aero}}{\partial \beta} \delta\beta + \frac{\partial \tau_{aero}}{\partial v} \delta v - \delta\tau_{lss} \tag{2.34}$$

Using the same operating point assumptions, equations (2.30) and (2.32) can be formulated back into (2.29), which gives the expanded form as,

$$\begin{aligned} I_{dr}\delta\dot{\omega}_{rot} = {} & \frac{\partial \tau_{aero}}{\partial \omega_{rot}} \delta\omega_{rot} + \frac{\partial \tau_{aero}}{\partial \beta} \delta\beta + \frac{\partial \tau_{aero}}{\partial v} \delta v - \left(\frac{\partial \tau_{lss}}{\partial \omega_{rot}} \delta\omega_{rot} + \frac{\partial \tau_{lss}}{\partial \dot{\omega}_{rot}} \delta\dot{\omega}_{rot} \right. \\ & \left. + \frac{\partial \tau_{lss}}{\partial c} \delta c + \frac{\partial \tau_{lss}}{\partial \dot{c}} \delta\dot{c} \right) \end{aligned} \tag{2.35}$$

Grouping terms reveals another useful form of the linearized rigid drivetrain model,

$$\left(I_{dr} + \frac{\partial \tau_{lss}}{\partial \dot{\omega}_{rot}}\right)\delta\dot{\omega}_{rot} = \left(\frac{\partial \tau_{aero}}{\partial \omega_{rot}} - \frac{\partial \tau_{lss}}{\partial \omega_{rot}}\right)\delta\omega_{rot} - \frac{\partial \tau_{lss}}{\partial c}\delta c - \frac{\partial \tau_{lss}}{\partial \dot{c}}\delta\dot{c} + \frac{\partial \tau_{aero}}{\partial \beta}\delta\beta + \frac{\partial \tau_{aero}}{\partial v}\delta v \tag{2.36}$$

As a side note, the nonlinear generator torque is linearized for the rigid drivetrain model as,

$$\begin{aligned} \tau_{gen} &= f\{\omega_{gen}\} = f\{\omega_{rot}, c\} \\ &= \tau_{gen}\{\omega_{rot_o}, c_o\} + \delta\tau_{gen} \\ &= (\tau_{gen})_o + \frac{\partial \tau_{gen}}{\partial \omega_{rot}}\delta\omega_{rot} + \frac{\partial \tau_{gen}}{\partial c}\delta c + \cancel{\text{hots}} \end{aligned} \tag{2.37}$$

which allows τ_{gen} to be expressed in terms of $\delta\omega_{rot}$ and δc. This is why the generator torque does not appear explicitly in the linearization of LSS torque because it will appear in the rotor speed and CVT ratio terms.

The chapters on control will use both forms of the linearized rigid drivetrain equations, (2.34) and (2.36), for controller design. The derivatives will be evaluated symbolically and numerically for the CART as needed in those chapters.

2.5.1.1 Typical Region 2

The typical Region 2 law, not yet derived, will be linearized and the characteristic equation associated with the wind speed input to rotor speed output will be evaluated. This will prove useful for tuning classical and modern controllers. Start with the rigid drivetrain equation of motion, (2.29), which is rewritten as,

$$I_{dr}\dot{\omega}_{rot} = \tau_{aero} - \tau_c \tag{2.38}$$

where τ_c is a control torque commanded according to the typical law for Region 2, equal to $K_\tau \omega_{rot}^2$, where K_τ is a fixed gain. This expression will be derived later. This commanded torque is nonlinear but may be linearized using a Taylor series expansion with the function and its derivative evaluated at the operating point,

$$\begin{aligned} \tau_c &= f\{\omega_{rot}\} = K_\tau \omega_{rot}^2 \\ &= \tau_c\{\omega_{rot_o}\} + \frac{d\tau_c}{d\omega_{rot}}\delta\omega_{rot} \\ &= (\tau_c)_o + 2K_\tau \omega_{rot_o}\delta\omega_{rot} \end{aligned} \tag{2.39}$$

The purpose of this linearization is to obtain a transfer function between the wind speed and rotor speed. The transfer function poles will give insight into the rotor speed response. This information may then be used as a reference tuning point for classical and modern controllers. Reformulate the equation of motion, (2.29), using the linearized expressions, (2.30) and (2.39), along with the assumptions of no acceleration at the operating point,

$$I_{dr}\delta\dot{\omega}_{rot} = \frac{\partial\tau_{aero}}{\partial\omega_{rot}}\delta\omega_{rot} + \frac{\partial\tau_{aero}}{\partial\beta}\cancelto{0}{\delta\beta} + \frac{\partial\tau_{aero}}{\partial v}\delta v - 2K_\tau\omega_{rot_o}\delta\omega_{rot} \tag{2.40}$$

where pitch perturbation is zero for Region 2. Transforming to the Laplace domain gives,

$$I_{dr}s\Delta\Omega_{rot} = \frac{\partial\tau_{aero}}{\partial\omega_{rot}}\Delta\Omega_{rot} + \frac{\partial\tau_{aero}}{\partial v}\Delta V - 2K_\tau\omega_{rot_o}\Delta\Omega_{rot} \tag{2.41}$$

which can be rearranged to formulate the transfer function,

$$\frac{\Delta\Omega_{rot}}{\Delta V} = \frac{\frac{\partial\tau_{aero}}{\partial v}}{I_{dr}s - \frac{\partial\tau_{aero}}{\partial\omega_{rot}} + 2K_\tau\omega_{rot_o}} \tag{2.42}$$

The characteristic equation, denominator of (2.42), has a single root at,

$$p_1 = \frac{\frac{\partial \tau_{aero}}{\partial \omega_{rot}} - 2K_\tau \omega_{rot_o}}{I_{dr}} \tag{2.43}$$

whose value depends on the point of linearization. In summary, attributes of this linearized typical control model will be used as a reference for tuning the classical and modern controllers designed in this research.

2.5.1.2 Transfer Functions

The linearized rigid drivetrain model expressed by (2.36) will prove to be useful for designing the classical controllers for the CVT and pitch actuator. By developing a Region 2 control law that commands the CVT ratio rate as a function of measured rotor speed and wind speed, the closed-loop transfer function can be derived between the wind speed input and rotor speed output. Controller gains will then be tuned to provide a satisfactory system response. Similar statements can be made about designing a classical pitch controller. The classical controller designs and tuning will be done in Chapter 4.

Transforming the linearized equation of motion, (2.36), to the Laplace domain, with the collective pitch perturbation set to zero for Region 2, gives,

$$(\dot{\omega}_{rot} \text{ terms}) s\Delta\Omega_{rot} = (\omega_{rot} \text{ terms})\Delta\Omega_{rot} - (c \text{ terms})\Delta C - (\dot{c} \text{ terms}) s\Delta C + (v \text{ terms})\Delta V \tag{2.44}$$

where the linearized terms haven't been written explicitly, since the point is to understand how a useful transfer function can be formulated. If the controller uses a TSR setpoint that computes the ratio rate, $\dot{c}(t)$, based on measurements of rotor and wind speed, then the

Laplace ratio perturbation can be expressed as a function of perturbed rotor and wind speed as well as any tunable gains, i.e. $\Delta C = f\{\Delta\Omega_{rot}, \Delta V, \text{gains}\}$. By expressing (2.44) in this way, a transfer function can be found between the wind speed input and rotor speed output.

2.5.1.3 State Space: 1-State

A state space representation with 1-state, perturbed rotor speed, can be formulated based on (2.34). The control input is perturbed load torque and the disturbance input is perturbed wind speed. Perturbed collective-pitch is also a control input variable, however it will cancel for Region 2 operation since pitch is fixed. The state equation for (2.34), a 1-state system, is written as,

$$\delta\dot{\omega}_{rot} = A\delta\omega_{rot} + B\begin{bmatrix}\delta\tau_{load}\\ \delta\beta\end{bmatrix} + \Gamma\delta v \tag{2.45}$$

$$A = \frac{\frac{\partial\tau_{aero}}{\partial\omega_{rot}}}{I_{dr}}, \quad B = \begin{bmatrix}\frac{-N}{I_{dr}} & \frac{\frac{\partial\tau_{aero}}{\partial\beta}}{I_{dr}}\end{bmatrix}, \quad \Gamma = \frac{\frac{\partial\tau_{aero}}{\partial v}}{I_{dr}}$$

Note the perturbed load torque, $\delta\tau_{load}$, is where all the CVT dynamics are contained, making this an attractive model due to its simplicity.

2.5.1.4 State Space: 2-State

A state space representation with two states, perturbed rotor speed and CVT ratio, can be formulated based on (2.36). The control input is perturbed CVT ratio rate and the disturbance input is perturbed wind speed. Perturbed collective-pitch is also a control input variable, however it's zero for Region 2 operation since pitch is fixed. The state equation for

(2.36), a 2-state system, is written as,

$$\begin{bmatrix} \delta\dot{\omega}_{rot} \\ \\ \delta\dot{c} \end{bmatrix} = A \begin{bmatrix} \delta\omega_{rot} \\ \\ \delta c \end{bmatrix} + B \begin{bmatrix} \delta\dot{c} \\ \\ \delta\beta \end{bmatrix} + \Gamma\delta v \tag{2.47}$$

$$A = \begin{bmatrix} \frac{\frac{\partial\tau_{aero}}{\partial\omega_{rot}} - \frac{\partial\tau_{lss}}{\partial\omega_{rot}}}{I_{dr} + \frac{\partial\tau_{lss}}{\partial\dot{\omega}_{rot}}} & \frac{-\frac{\partial\tau_{lss}}{\partial c}}{I_{dr} + \frac{\partial\tau_{lss}}{\partial\dot{\omega}_{rot}}} \\ \\ 0 & 0 \end{bmatrix}, \; B = \begin{bmatrix} -\frac{\frac{\partial\tau_{lss}}{\partial\dot{c}}}{I_{dr} + \frac{\partial\tau_{lss}}{\partial\dot{\omega}_{rot}}} & \frac{\frac{\partial\tau_{aero}}{\partial\beta}}{I_{dr} + \frac{\partial\tau_{lss}}{\partial\dot{\omega}_{rot}}} \\ \\ 1 & 0 \end{bmatrix}, \; \Gamma = \begin{bmatrix} \frac{\frac{\partial\tau_{aero}}{\partial v}}{I_{dr} + \frac{\partial\tau_{lss}}{\partial\dot{\omega}_{rot}}} \\ \\ 0 \end{bmatrix}$$

This representation is sensitive to the operating point due to the equilibrium CVT ratio being in some terms. This could lead to unstable operation away from the operating point, or require the controller to be designed at multiple operating points.

2.5.2 Torsional Drivetrain Linearization

The equations of motion for the flexible drivetrain model, which are expressed by (2.14) and (2.16), are reprinted here for convenience,

$$\Sigma I_L \dot{\omega}_{rot} = \tau_{aero} - \tau_{s,l}$$

$$\Sigma I_M \dot{\omega}_{cvt,i} = \frac{\tau_{s,l}}{N} - \tau_{load}$$

which are the rotor rotation and CVT input rotation equations. Also, recall (2.15) for the shaft reaction torque, $\tau_{s,l}$, expression. These equations, (2.14) and (2.16), are expressed with three torque terms. The shaft reaction torque, $\tau_{s,l}$, was modeled with a linear spring and linear damping element, therefore only the aerodynamic torque and load torque require linearization. The aerodynamic torque is linearized exactly the same as before, see (2.30).

The shaft torque is written as,

$$\begin{aligned}\tau_{s,l} &= f\{\theta_{rot}, \theta_{cvt,i}, \omega_{rot}, \omega_{cvt,i}\} \\ &= \tau_{s,l}\{\theta_{rot_O}, \theta_{cvt,i_O}, \omega_{rot_O}, \omega_{cvt,i_O}\} + \delta\tau_{s,l} \\ &= (\tau_{s,l})_o + K_d(\delta\theta_{rot} - \frac{1}{N}\delta\theta_{cvt,i}) - C_d(\delta\omega_{rot} - \frac{1}{N}\delta\omega_{cvt,i})\end{aligned} \tag{2.49}$$

For the operating point to have no accelerations, the aerodynamic torque must equal the shaft reaction torque at equilibrium, $(\tau_{aero})_o = (\tau_{s,l})_o \implies (\dot{\omega}_{rot})_o = 0$. Under these conditions, the linearized rotor equation for the torsional drivetrain is,

$$\Sigma I_L \delta\dot{\omega}_{rot} = \frac{\partial\tau_{aero}}{\partial\omega_{rot}}\delta\omega_{rot} + \frac{\partial\tau_{aero}}{\partial\beta}\delta\beta + \frac{\partial\tau_{aero}}{\partial v}\delta v - K_d(\delta\theta_{rot} - \frac{1}{N}\delta\theta_{cvt,i}) - C_d(\delta\omega_{rot} - \frac{1}{N}\delta\omega_{cvt,i}) \tag{2.50}$$

To derive the CVT input rotation equation, an expression for the linearized load torque is needed. If it's linearized as is, i.e. without expanding it to include the load torque expression, (2.17), then it's written as,

$$\begin{aligned}\tau_{load} &= f\{\omega_{cvt,i}, \dot{\omega}_{cvt,i}, c, \dot{c}\} \\ &= \tau_{load}\{\omega_{cvt,i_O}, \dot{\omega}_{cvt,i_O}, c_o, \dot{c}_o\} + \delta\tau_{load}\end{aligned} \tag{2.51}$$

Combine (2.49) and (2.51) into (2.16) while using the same operating point conditions, $\frac{1}{N}(\tau_{s,l})_o = (\tau_{load})_o \implies (\dot{\omega}_{cvt,i})_o = 0$, and a linearized form of the CVT input rotation equation is written as,

$$\Sigma I_M \delta\dot{\omega}_{cvt,i} = \frac{1}{N}\big(K_d(\delta\theta_{rot} - \frac{1}{N}\delta\theta_{cvt,i}) + C_d(\delta\omega_{rot} - \frac{1}{N}\delta\omega_{cvt,i})\big) - \delta\tau_{load} \tag{2.52}$$

The chapters on control will use the linearized CVT rotation equation, (2.52), and the linearized rotor equation, (2.50), for controller design. The derivatives of aerodynamic torque will be evaluated numerically for the CART as needed in those chapters.

2.5.2.1 State Space: 3-State

For an equivalent spring and damper used to represent the drivetrain torsion properties of the LSS and MSS, a state space representation can be formulated with three states. For this torsional model, the rotor and CVT input rotations are degrees of freedom. The state variables are perturbed rotor speed, perturbed equivalent shaft deflection torque, and perturbed CVT input speed. The control and disturbance inputs are perturbed load torque, collective-pitch, and wind speed, analogous to the 1-state model.

The state equation is based on (2.50) and (2.52),

$$\dot{x} = A \begin{bmatrix} \delta\omega_{rot} \\ K_d\left(\delta\theta_{rot} - \dfrac{\delta\theta_{cvt,i}}{N}\right) \\ \delta\omega_{cvt,i} \end{bmatrix} + B \begin{bmatrix} \delta\tau_{load} \\ \delta\beta \end{bmatrix} + \Gamma\delta v \tag{2.53}$$

$$A = \begin{bmatrix} \dfrac{\frac{\partial\tau_{aero}}{\partial\omega_{rot}} - C_d}{\Sigma I_L} & \dfrac{-1}{\Sigma I_L} & \dfrac{C_d/N}{\Sigma I_L} \\ K_d & 0 & -K_d/N \\ \dfrac{C_d/N}{\Sigma I_M} & \dfrac{1/N}{\Sigma I_M} & \dfrac{-C_d/N^2}{\Sigma I_M} \end{bmatrix}, \quad B = \begin{bmatrix} 0 & \dfrac{\frac{\partial\tau_{aero}}{\partial\beta}}{\Sigma I_L} \\ 0 & 0 \\ \dfrac{-1}{\Sigma I_M} & 0 \end{bmatrix}, \quad \Gamma = \begin{bmatrix} \dfrac{\frac{\partial\tau_{aero}}{\partial v}}{\Sigma I_L} \\ 0 \\ 0 \end{bmatrix}$$

where $\dot{x}$, the state derivatives, notation is used for convenience. Again, note that all the CVT dynamics are contained within the perturbed load torque, $\delta\tau_{load}$.

Chapter 3

Typical Control

To use typical variable-speed control for the CART with a CVT, a mathematical model must be developed for the CVT that illustrates its ability to control load torque. Imagine a scenario in which the load torque, in the MSS reference frame, must match a torque setpoint, τ_{set}, in the LSS reference frame. The load torque is easily mapped to the LSS by multiplying it with the gearbox ratio, N. This is written as,

$$N\tau_{load} = \tau_{set} \tag{3.1}$$

Inserting the CVT expression for load torque defined by (2.12) for a rigid drivetrain gives,

$$Nc(\Sigma I_H(cN\dot{\omega}_{rot} + \dot{c}_c N\omega_{rot}) + \tau_{gen}) = \tau_{set} \tag{3.2}$$

Solving this for the commanded variable, $\dot{c}_c$, results in,

$$\dot{c}_c = \frac{\tau_{set}/N - c^2\Sigma I_H N\dot{\omega}_{rot} - c\tau_{gen}}{c\Sigma I_H N\omega_{rot}} \tag{3.3}$$

Commanding the CVT ratio rate with expression (3.3) results in a load torque equal to the setpoint torque mapped to the MSS frame. This CVT control law will be referred to as the ratio rate law, but in the context of typical control it will be called the typical torque (TT) method. The ratio rate law will prove to be very useful for both typical and modern control. Specifying a setpoint torque (fixed or as a function of rotor speed), plus measuring rotor speed and generator torque is needed to implement this CVT ratio rate command for the rigid drivetrain model.

A simplified version of the TT method will also be tested, which ignores the inertial effects of the HSS and estimates generator torque. In other words, it's an approximate steady state approach to deriving the control law. The CVT input shaft acceleration and CVT ratio rate are terms that involve the summed inertia associated with the HSS, and since both will be ignored by the control law, they are set to zero in equation (3.2). The generator torque is estimated as a linear function of generator speed, with a slope of Q_r. This estimation will be done for each region. Thus, (3.2) can be written for this simplified method as,

$$Nc_cQ_r(Nc_c\omega_{rot} - \omega_{syn}) = \tau_{set} \tag{3.4}$$

Generator speed is written in terms of rotor speed and the CVT ratio since setpoint torque will be derived as a function of rotor speed. Solving for the commanded CVT ratio, c_c, gives,

$$c_c = \frac{\sqrt{Q_r}\omega_{syn} + \sqrt{Q_r\omega_{syn}^2 + 4\tau_{set}\omega_{rot}}}{2\sqrt{Q_r}N\omega_{rot}} \tag{3.5}$$

This version of typical control will be called the steady state typical torque (SSTT) method. The appeal of this control law is it only requires a rotor speed measurement. To understand

how (3.3) and (3.5) can be used to achieve the control objectives, the setpoint torque must be determined for each region of operation, namely, Region 2, 2.5, and 3.

3.1 Region 2

The key objective of Region 2 is to track λ_{opt} while pitch is fixed at -1.0°. To derive the rotor τ-ω characteristics associated with λ_{opt}, begin with the equation for wind power captured by a rotor at peak power coefficient,

$$P_{aero} = \frac{1}{2}\rho A v^3 (C_p)_{max} \tag{3.6a}$$

$$\tau_c\, \omega_{rot} = \frac{1}{2}\rho \pi r^2 v^3 (C_p)_{max} \tag{3.6b}$$

where control torque, τ_c, is the rotor torque needed to achieve $(C_p)_{max}$. Solving the TSR equation, (1.3), for wind speed, v, with $\lambda = \lambda_{opt}$ and plugging it into (3.6b) gives,

$$\tau_c\, \omega_{rot} = \frac{1}{2}\rho \pi r^2 \left(\frac{r\omega_{rot}}{\lambda_{opt}}\right)^3 (C_p)_{max} \tag{3.7}$$

Simplifying this equation and solving for τ_c results in,

$$\tau_c\{\omega_{rot}\} = \frac{\rho \pi r^5 (C_p)_{max}}{2\lambda_{opt}^3}\ \omega_{rot}^2 = K_\tau \omega_{rot}^2 \tag{3.8}$$

where all parameters of the torque gain, K_τ, are known from the modeling process, therefore the desired control torque is a function of squared rotor speed. For the CART, as modeled in this research using WT_Perf, the torque gain is computed as 4854.2 N-m/rad/s^2. With this, (3.8) will be the Region 2 setpoint torque, τ_{set}, to use in TT law (3.3), and SSTT law

(3.5). The generator torque slope, Q_r, used for Region 2 estimation is 2001.4 N-m/rad/s.

3.2 Region 2.5

The key objective of Region 2.5 is to smoothly transition from Region 2 to Region 3 while limiting rotor speed to 41.7 rpm, the rated speed. Pitch will be fixed at $-1.0°$. The high end of Region 2.5 is dictated by the start of Region 3, but the low end is left to the discretion of the control engineer. A rotor speed of 39.2 rpm will be used for the starting point of Region 2.5. The τ-ω characteristics for Region 2.5 are determined by deriving an equation for the torque, similar to what was done for Region 2 above. Region 2.5 will be designed as a linear interpolation of the torque between Region 2 and 3, as a function of rotor speed. This approach for torque control has been used by [38, 37].

$$\tau_c\{\omega_{rot}\} = \frac{\tau_{rated} - \tau_{2f}}{\omega_{3i} - \omega_{2f}}(\omega_{rot} - \omega_{2f}) + \tau_{2f} \tag{3.9}$$

τ_{rated} and ω_{3i} are the rated rotor torque and Region 3 transition rotor speed, while τ_{2f} and ω_{2f} are the rotor torque and speed at the end of Region 2. An ω_{3i} of 0.3 rpm less than rated rotor speed is used to avoid continual operation at the transition point in Region 3. Previously, it was decided that $\omega_{2f} = 39.2$ rpm. This equates to an MSS range of 95 rpm for Region 2.5. The torque, τ_{2f}, is easily computed using the Region 2 torque equation, (3.8). This gives $\tau_{2f} = 81.791$ kN-m. Rated rotor torque is known to be 139.857 kN-m. With these values, (3.9) will be the Region 2.5 setpoint torque, τ_{set}, to use in TT law (3.3), and SSTT law (3.5). The generator torque slope used in Region 2 is left unchanged here.

3.3 Region 3

The key objective of Region 3 is to regulate power output. This will be done by using pitch control for rotor speed regulation in conjunction with CVT control for torque regulation. A classical PI pitch controller is used, see Appendix C for details. For Region 3 CVT control, no derivation is required for the rotor torque as a function of speed, as was done for Region 2 and 2.5 with equations (3.8) and (3.9), respectively. The torque to be used for the Region 3 setpoint torque, τ_{set}, in (3.3) and (3.5) is simply the rated torque, τ_{rated}, a fixed value. The generator torque slope used for Region 3 is 1966.3 N-m/rad/s.

3.4 Summary of Torque Method

The torque control, to be accomplished with CVT actuation by using the TT method, (3.3), or SSTT method, (3.5), may now be summarized for all three operating regions considered in this research. Figure 3.1 offers a pictorial representation of typical control. Notice if the Region 2 torque law was used up to rated torque, which would be ideal for energy

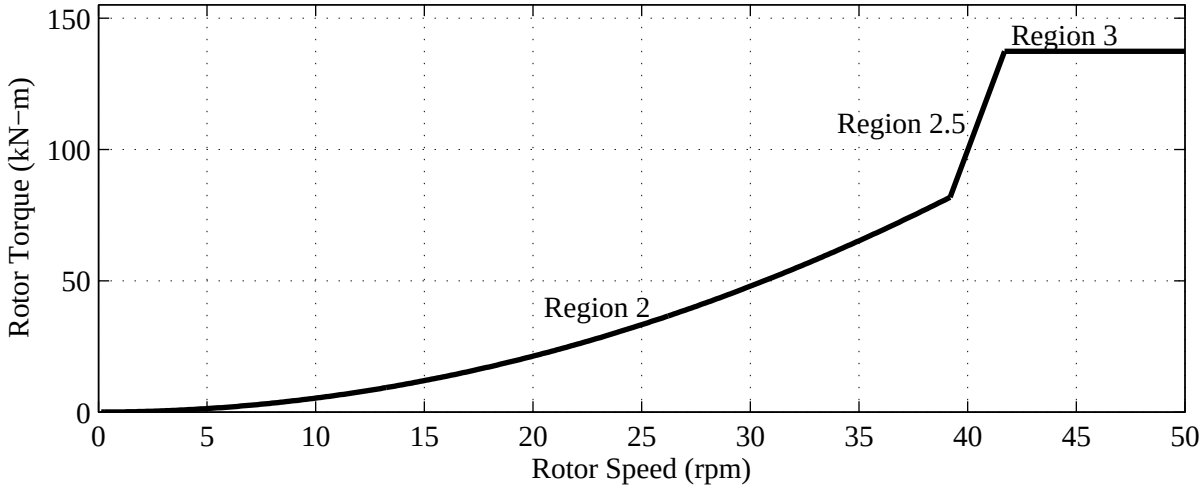

Figure 3.1: Graphical summary of typical torque control

capture, then rotor speed would exceed the speed allowed to meet noise requirements. This is why Region 2.5 must exist for the CART.

The SSTT method will only be used in this chapter. It's not considered in the development of any other controller. However, since it's easier to practically implement than TT control, it's suggested for future research.

3.5 Modified Torque Method

To adjust rotor speed response to be faster or slower than what's achieved with typical torque control, what has been labeled as the Optimally Tracking Rotor (OTR) law can be used [39]. With the typical torque law, the setpoint torque, τ_{set}, in (3.3) and (3.5) is simply equal to the derived expressions for control torque: (3.8), (3.9), and τ_{rated}. For OTR law, setpoint torque for each region now involves additional terms and is expressed as,

$$\tau_{set} = \tau_c - G_\tau(\tau_{aero} - \tau_c) \tag{3.10}$$

where τ_c is defined the same as before for each region. Analyzing scenarios for the OTR law will help to understand it. See Table 3.1 for this.

Wind Condition	**Compare Torques**	**Compare Laws**	**OTR Response**
Gust	$\tau_{aero} > \tau_c$	$(\tau_{set})_{OTR} < (\tau_{set})_{typ}$	more acceleration
Lull	$\tau_{aero} < \tau_c$	$(\tau_{set})_{OTR} > (\tau_{set})_{typ}$	more deceleration
Steady	$\tau_{aero} = \tau_c$	$(\tau_{set})_{OTR} = (\tau_{set})_{typ}$	same operating pt

Table 3.1: Analyzing the Optimally Tracking Rotor law for $G_\tau > 0$

To avoid measuring τ_{aero}, it can be calculated as,

$$\tau_{aero} = I_{rot}\dot{\omega}_{rot} + \tau_{set} \tag{3.11}$$

Inserting (3.11) into (3.10) and solving for the setpoint torque gives,

$$\tau_{set} = \frac{\tau_c - G_\tau(I_{rot}\dot{\omega}_{rot} - \tau_c)}{1 + G_\tau} \tag{3.12}$$

which is the expression to be used in (3.3) and (3.5), in conjunction with the torque equations associated with each region, (3.8), (3.9), and τ_{rated}. Together, all these expressions define the OTR law for the CVT. Note, $G_\tau < 0$ should be used in Region 3 for better regulation.

3.6 Simulations

The TT and SSTT methods for typical torque control are easily implemented into the Simulink environment as a controller for the CVT. The output of TT and OTR controllers is commanded CVT ratio rate, which is used as the actual ratio rate and sent through an integrator to get the CVT ratio. Both are then used by the CVT and HSS dynamics equations to simulate the system coupled to the MSS, where the FAST model ends. Note, an air density of 1.03 kg/m^3 will be used for all simulations and linearizations.

3.6.1 Region 2

The simple Region 2 wind input is used to test the fundamental ability of the Region 2 controllers to track λ_{opt}. The results of this simulated with the nonlinear model using

the typical torque controllers is shown in Figure 3.2. The ideal λ_{opt} signal is also shown for reference. The rotor speed resulting from SSTT control is indistinguishable from TT

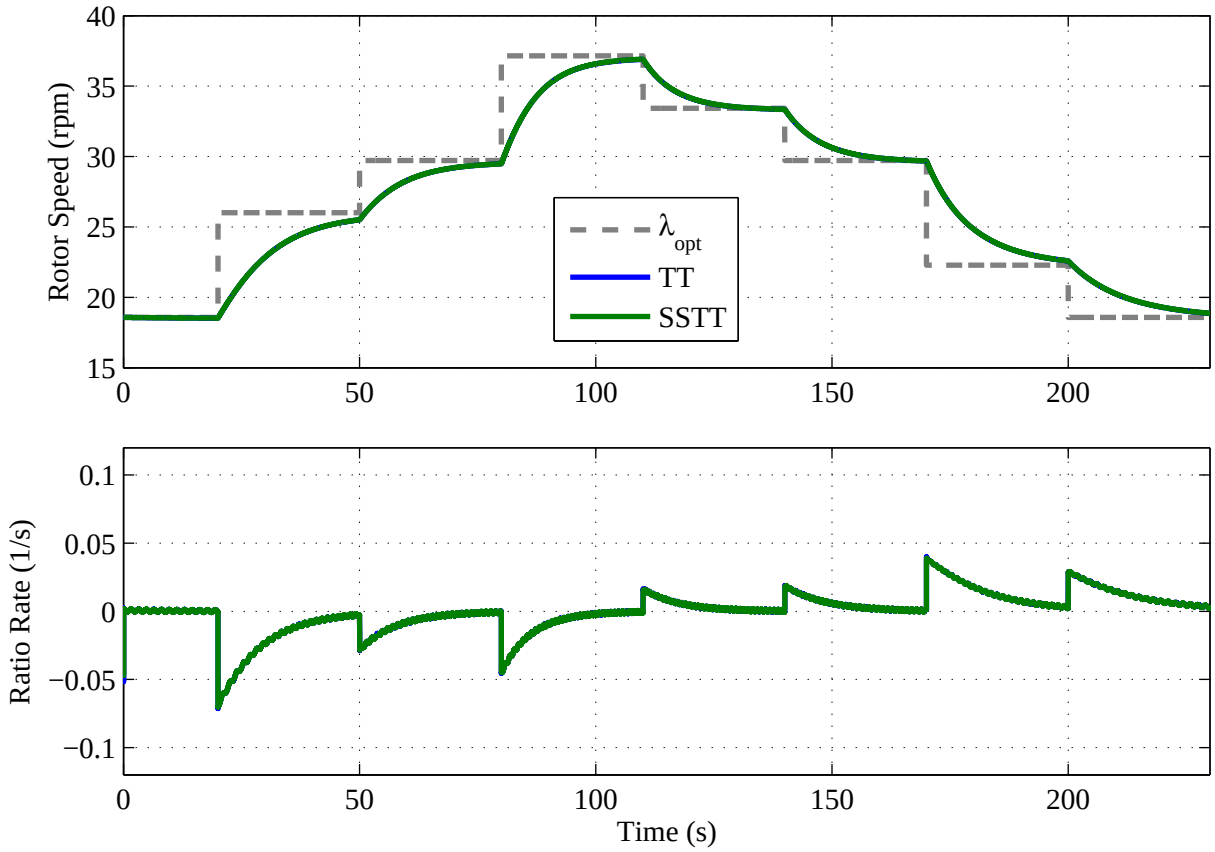

Figure 3.2: Rotor speed and ratio rate for typical control with simple Region 2 wind input

control. Clearly, both typical torque controllers are capable of closely tracking λ_{opt} and the CVT ratio rates are well within the limits.

It's important that generator torque does not decrease a lot when the CVT actuates, because this could result in motoring. This will happen if the CVT control is too aggressive as it will attempt to create a very large torque differential capable of quickly accelerating the rotor. Figure 3.3 shows the generator speed from the multi-step simulation. Observation of the generator torque for these sudden disturbances suggests the CVT control action is not too aggressive. In fact, more aggressive control can used without motoring.

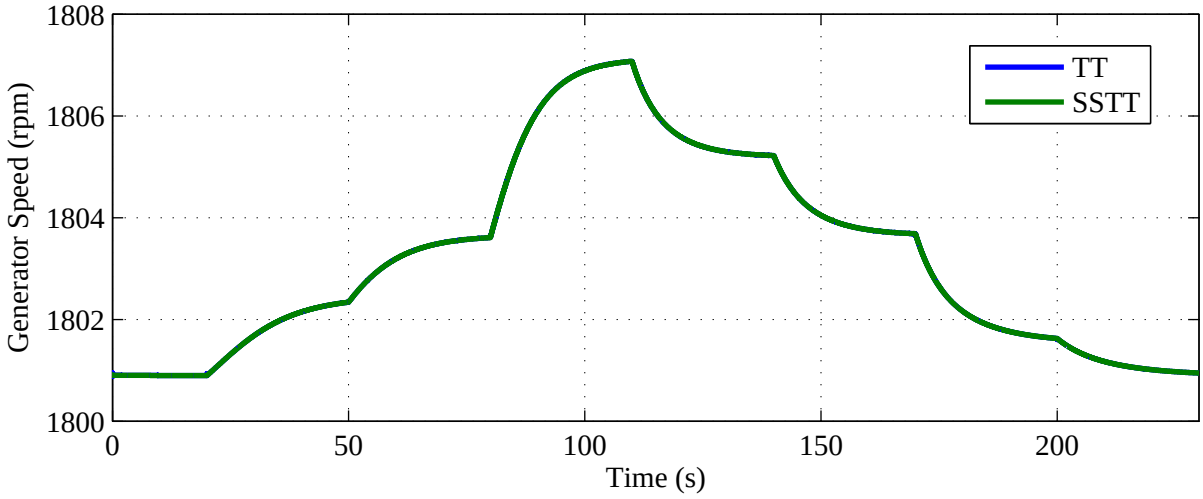

Figure 3.3: Generator speed for typical control with simple Region 2 wind input

The OTR law will now be used with the TT method by setting $G_\tau = 0.5$ to create higher rotor accelerations, allowing for quicker tracking of λ_{opt}. The OTR gain was subjectively tuned by observing step responses for different gains. For easy comparison, the results of this simulation are plotted with the previous TT results, see Figure 3.4. The results show better tracking of λ_{opt} for the OTR law but at the cost of higher CVT ratio rates. The ratio rates aren't so aggressive that motoring is occuring (plot not shown). It's therefore feasible to use OTR for better energy capture but CVT reliability may be sacrificed as a consequence. A more detailed study is required to make knowledgeable decisions about these tradeoffs.

Nonlinear simulations are now run with full-field wind input and accompanied by data analysis useful in establishing the success of control objectives. A common data analysis, dependent on model fidelity and region of operation, will be used for all nonlinear simulations with a turbulent wind input. This applies to the upcoming chapters for classical and modern control as well. This will allow different controller designs to be compared quantitatively. Table 3.2 lists data analysis parameters to be used. Note that some data is useful for specific model fidelity and region of operation.

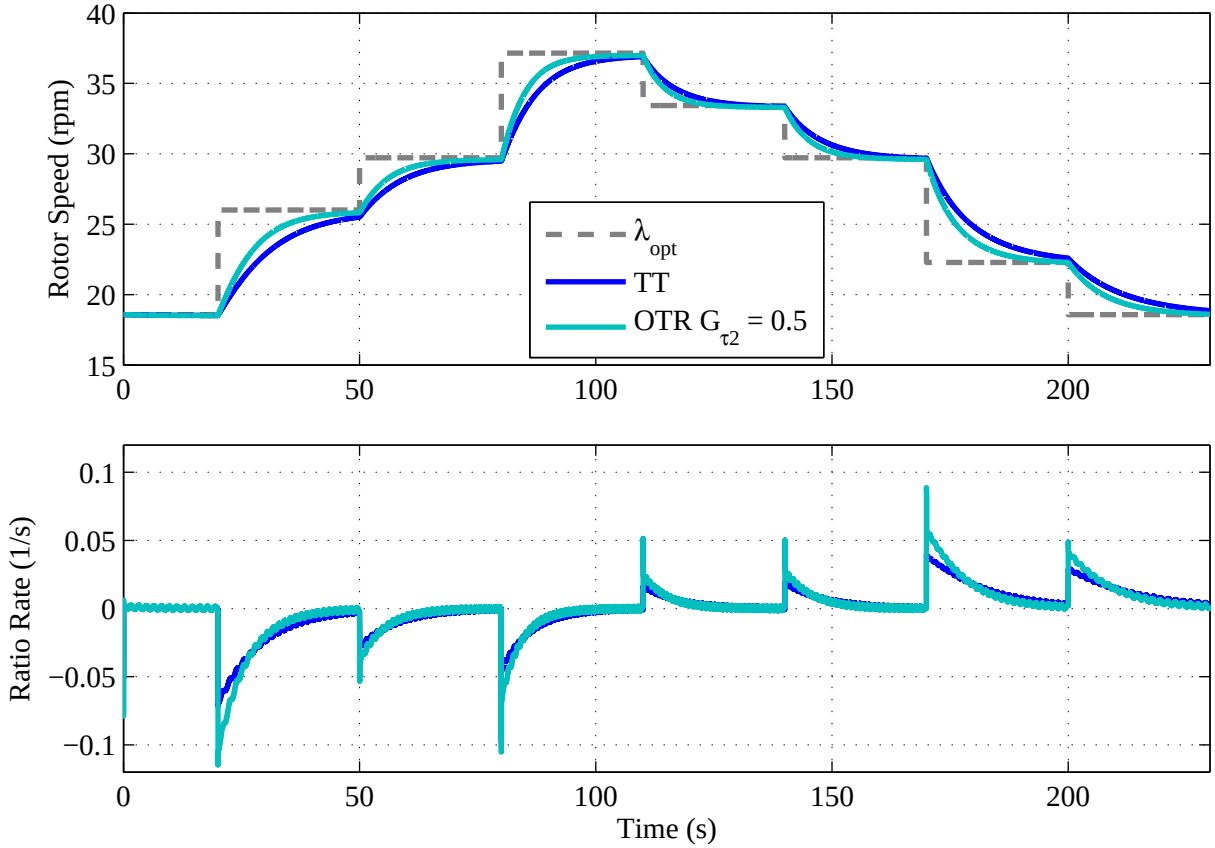

Figure 3.4: Rotor speed and ratio rate for OTR control with simple Region 2 wind input

Each typical torque controller and the OTR controller, with $G_\tau = 0.5$, is simulated with the nonlinear model using the Region 2 turbulent input. Key results of this are presented in Table 3.3. The TT and SSTT controllers produce very similar results, with the biggest difference being a slightly higher max ratio acceleration for SSTT, but even this is minuscule. The OTR controller has a few significant differences, namely, max rotor acceleration, max ratio rate and acceleration, min generator speed, max generator acceleration, and energy capture. All these differences were expected since OTR uses more aggressive CVT control action to achieve better λ_{opt} tracking, hence higher accelerations and better energy capture. The generator is close to motoring, thus a potential problem at low wind speeds. Maximum ratio acceleration was 140% higher for OTR compared to TT control. The energy capture

Parameter	Region	Description & Significance
Max $\lvert\dot{\beta}\rvert$	3	Max pitch rate indicates actuation within saturated limits.
RMS $\dot{\beta}$	3	RMS pitch rate indicates overall actuator workload.
Max $\lvert\ddot{\beta}\rvert$	3	Max pitch acceleration indicates peak actuator load.
Max ω_{rot}	All	Max rotor speed indicates if blade noise meets requirements.
RMS $\Delta\omega_{rot}$	3	RMS rotor speed error indicates rotor speed regulation success.
Max $\lvert\dot{\omega}_{rot}\rvert$	All	Max rotor acceleration indicates peak transient load.
RMS $\Delta\omega_{dr}$	All	RMS drivetrain twist rate indicates the degree of cyclic loads.
Max $\lvert\dot{c}\rvert$	All	Max CVT ratio rate indicates actuation within saturated limits.
RMS $\dot{c}$	All	RMS CVT ratio rate indicates overall actuator workload.
Max $\lvert\ddot{c}\rvert$	All	Max CVT ratio acceleration indicates peak actuator load.
Min ω_{gen}	All	Min generator speed indicates if motoring occurred.
Max ω_{gen}	All	Max generator speed indicates peak electrical load.
RMS $\Delta\omega_{gen}$	3	RMS generator speed error indicates power regulation success.
Max $\lvert\dot{\omega}_{gen}\rvert$	All	Max generator acceleration indicates peak transient load.
RMS $\Delta\lambda$	2	RMS of TSR error indicates λ_{opt} tracking success.
E_{cap}	2	Total energy captured indicates overall performance.

Table 3.2: Simulation data analysis for turbulent wind inputs

Parameter	Units	TT	SSTT	OTR
Max ω_{rot}	rpm	40.19	40.21	40.31
Max $\lvert\dot{\omega}_{rot}\rvert$	deg/s^2	5.536	5.545	7.187
Max $\lvert\dot{c}\rvert$	1/s	5.713E-02	5.710E-02	7.737E-02
RMS $\dot{c}$	1/s	1.293E-02	1.295E-02	1.720E-02
Max $\lvert\ddot{c}\rvert$	1/s^2	0.3315	0.4171	0.7943
Min ω_{gen}	rpm	1801.3	1801.3	1800.8
Max $\lvert\dot{\omega}_{gen}\rvert$	deg/s^2	281.6	281.2	383.4
RMS $\Delta\lambda$	-	0.9082	0.9080	0.8457
E_{cap}	kW-hr	25.89	25.89	25.98

Table 3.3: Data from typical torque and OTR control with Region 2 turbulent wind input

is only 0.35% better for OTR, which may not be worth the added CVT workload.

To illustrate some key behavioral differences, plots are used to see what's happening during the simulations. The statistical values from Table 3.3 suggest better λ_{opt} tracking and more control action, so Figure 3.5 was created to show this. It's evident from the rotor

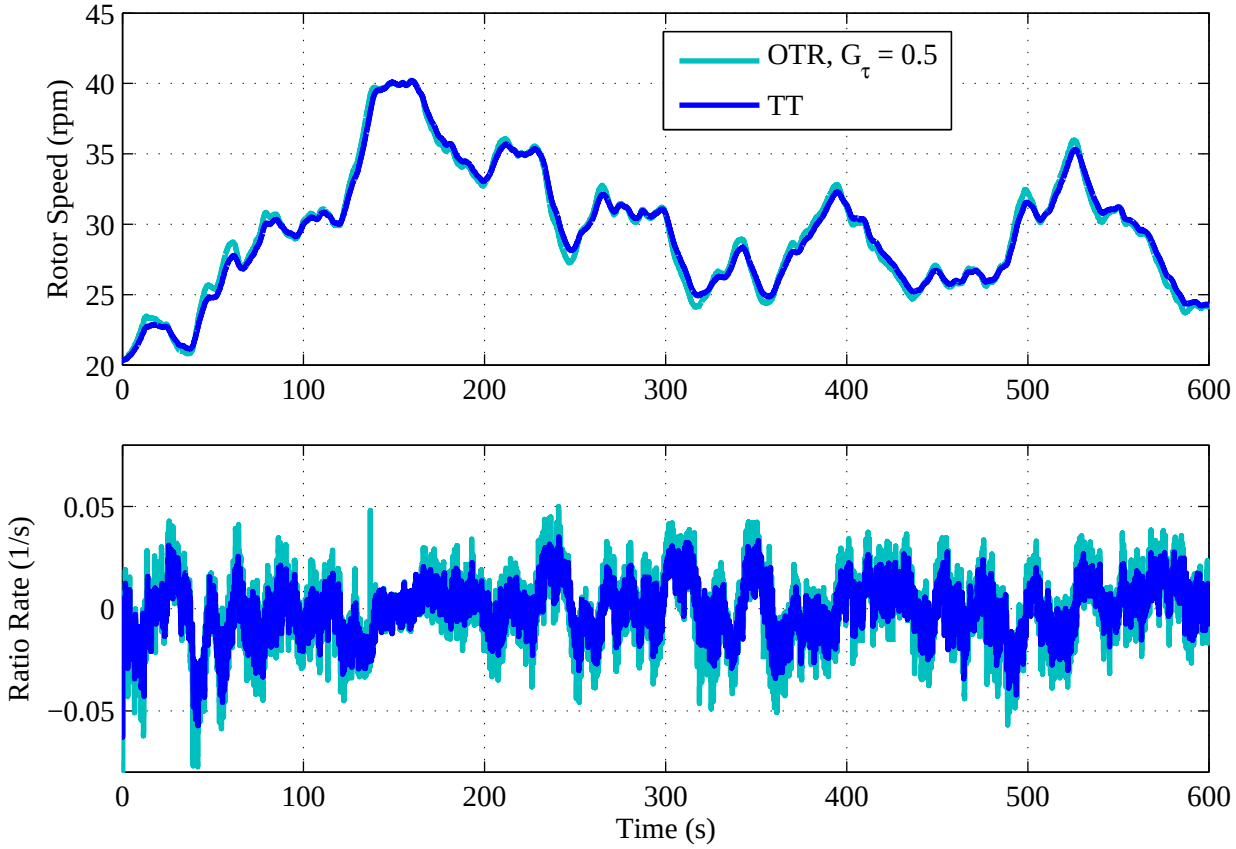

Figure 3.5: Rotor speed and ratio rate for typical and OTR control with full-field Region 2 wind input

speed plot that OTR tracks λ_{opt} quicker, but at a cost of more aggressive control action, as the ratio rate plot shows. More in-depth study is required to understand the tradeoffs between energy capture and CVT reliability. In summary, all three controllers proved to be stable and achieve some degree of success in tracking λ_{opt}.

3.6.2 Region 3

The simple Region 3 wind input is used to test key control objectives in Region 3, namely to regulate rotor speed and load torque via pitch and CVT control, respectively. The interest to this reserach is the ability of CVT to regulate load torque. Figure 3.6 shows the load torque and generator power output for the nonlinear model simulation.

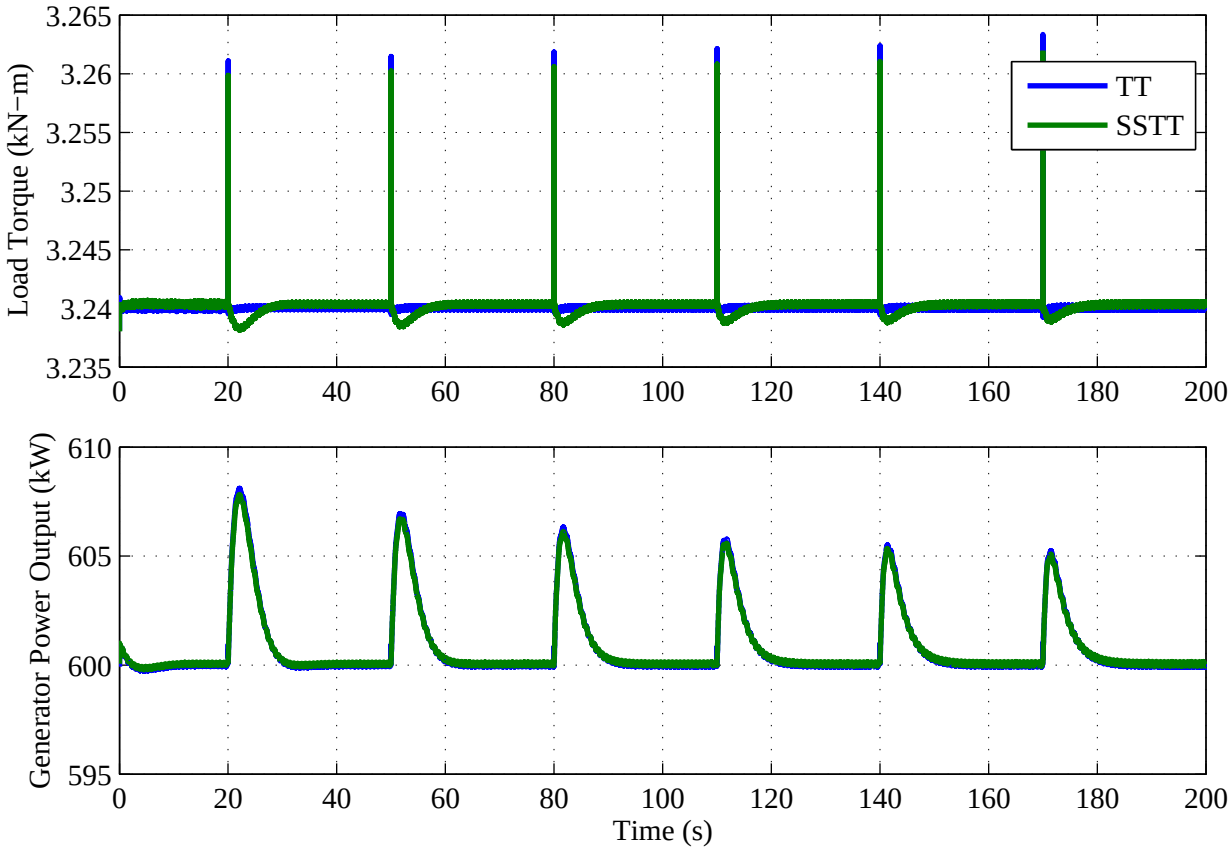

Figure 3.6: Load torque and power output for typical control with simple Region 3 wind input

The results suggest the CVT is capable of regulating load torque in conjunction with the PI pitch controller regulating rotor speed. The maximum generator power output was only 1.3% above ideal. Since the load torque is regulated sufficiently fast, the OTR law is not considered for Region 3 even though it could be easily implemented.

The typical torque controllers for Region 3 are now simulated with the nonlinear model using the Region 3 turbulent input. Key data results are presented in Table 3.4. The TT

Parameter	**Units**	**TT**	**SSTT**
Max $\lvert\dot{\beta}\rvert$	deg/s	4.234	4.196
RMS $\dot{\beta}$	deg/s	1.015	1.007
Max $\lvert\ddot{\beta}\rvert$	deg/s^2	74.29	79.43
Max ω_{rot}	rpm	43.37	43.19
RMS $\Delta\omega_{rot}$	rpm	0.4282	0.4162
Max $\lvert\dot{c}\rvert$	1/s	4.295E-02	4.424E-02
RMS $\dot{c}$	1/s	1.019E-02	1.015E-02
Max $\lvert\ddot{c}\rvert$	1/s^2	0.8078	6.606
Min ω_{gen}	rpm	1812.9	1813.0
Max ω_{gen}	rpm	1816.2	1816.2
RMS $\Delta\omega_{gen}$	rpm	0.5258	0.5892
Max $\lvert\dot{\omega}_{gen}\rvert$	deg/s^2	390.8	403.1

Table 3.4: Data from typical torque control with Region 3 turbulent wind input

and SSTT controllers produce very similar results again, with the biggest difference being the max ratio acceleration. For SSTT, it's over eight times larger than for TT control. This is due to the Region 2.5 transition point. Even though the simulation is focused on Region 3, it does occasionally transition to the Region 2.5 CVT controller. Improving this transition is suggested for practical implementation, but is not explored here. In summary, both controllers proved stable and successful at regulating load torque.

3.6.3 Region 2 to 3

The transition from Region 2 to 3 and vice versa is important to test because the control laws are changing from one region to the next. A conditional statement is used to switch

between controllers. If the controllers don't transition smoothly, there could be undesirable excitations or extreme loads encountered. First, the simple Region 2-3 wind input is simulated with the nonlinear model for both types of typical torque controllers. The rotor speed plot for both typical torque controllers is in Figure 3.7. The transition between regions

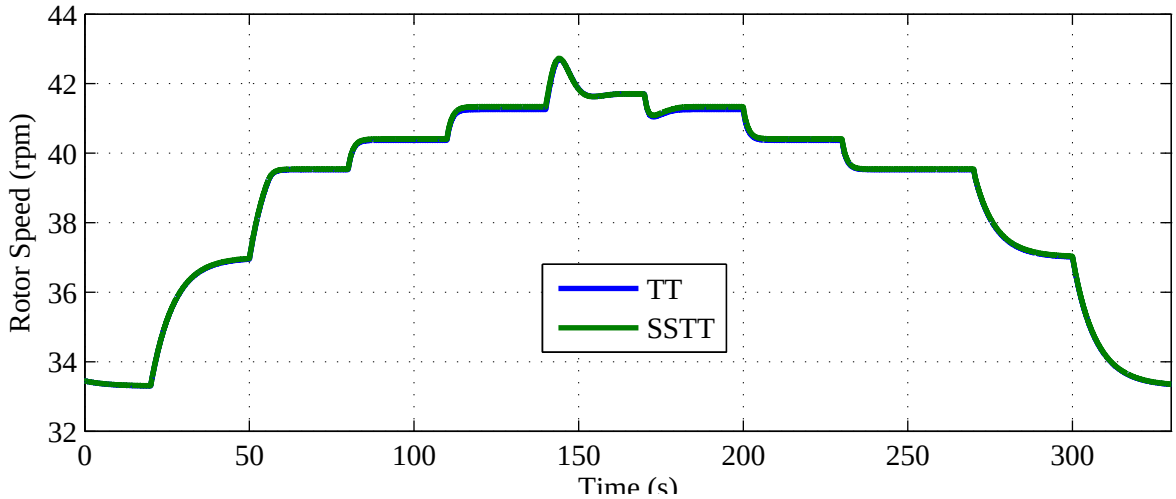

Figure 3.7: Rotor speed and ratio rate for typical control with simple Region 2-3 wind input

appears smooth for the rotor speed response of the multi-step input.

The Region 2-3 turbulent input will now be used to perform simulations with the nonlinear model for each controller. In addition to tabular results, graphical results will also be used to analyze each controllers performance. The wind inputs of graphical interest, occuring over particular time domains of the 600 seconds of Region 2-3 turbulent input, are shown in red in Figure 3.8. These wind inputs correspond to transitions between Region 2 and 3 over a short period of time. The rotor speed, not plotted, transitions smoothly between regions with a max speed of 42.4 rpm. Figure 3.9 shows plots of ratio rate for the short wind inputs. The CVT ratio rate transitions smoother for TT control, with SSTT control having a few spikes which equates to larger ratio accelerations. Key data is presented in Table 3.5.

The results here are analogous to the Region 3 turbulent simulations, in that TT and

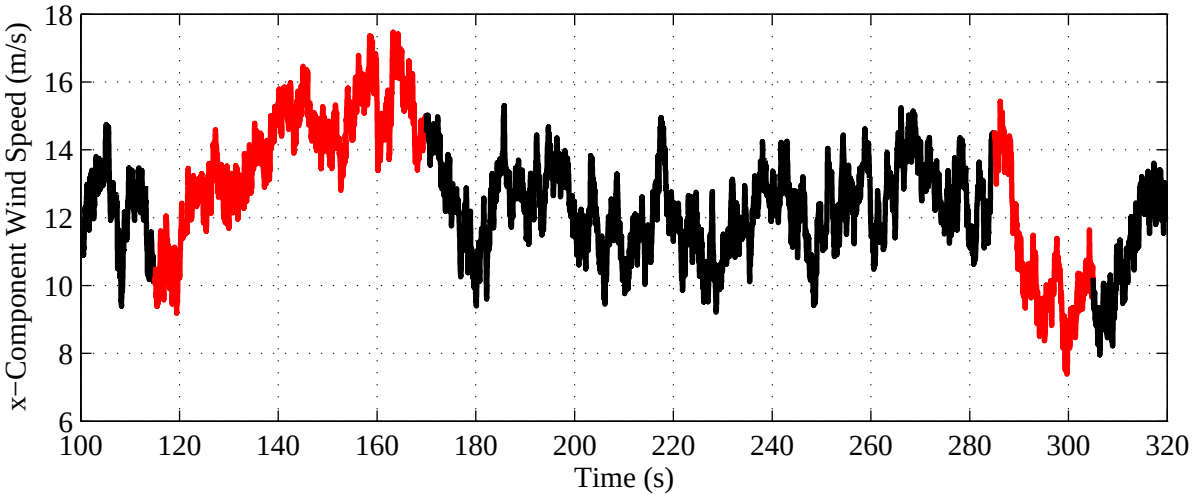

Figure 3.8: Transition time periods for full-field Region 2-3 wind input

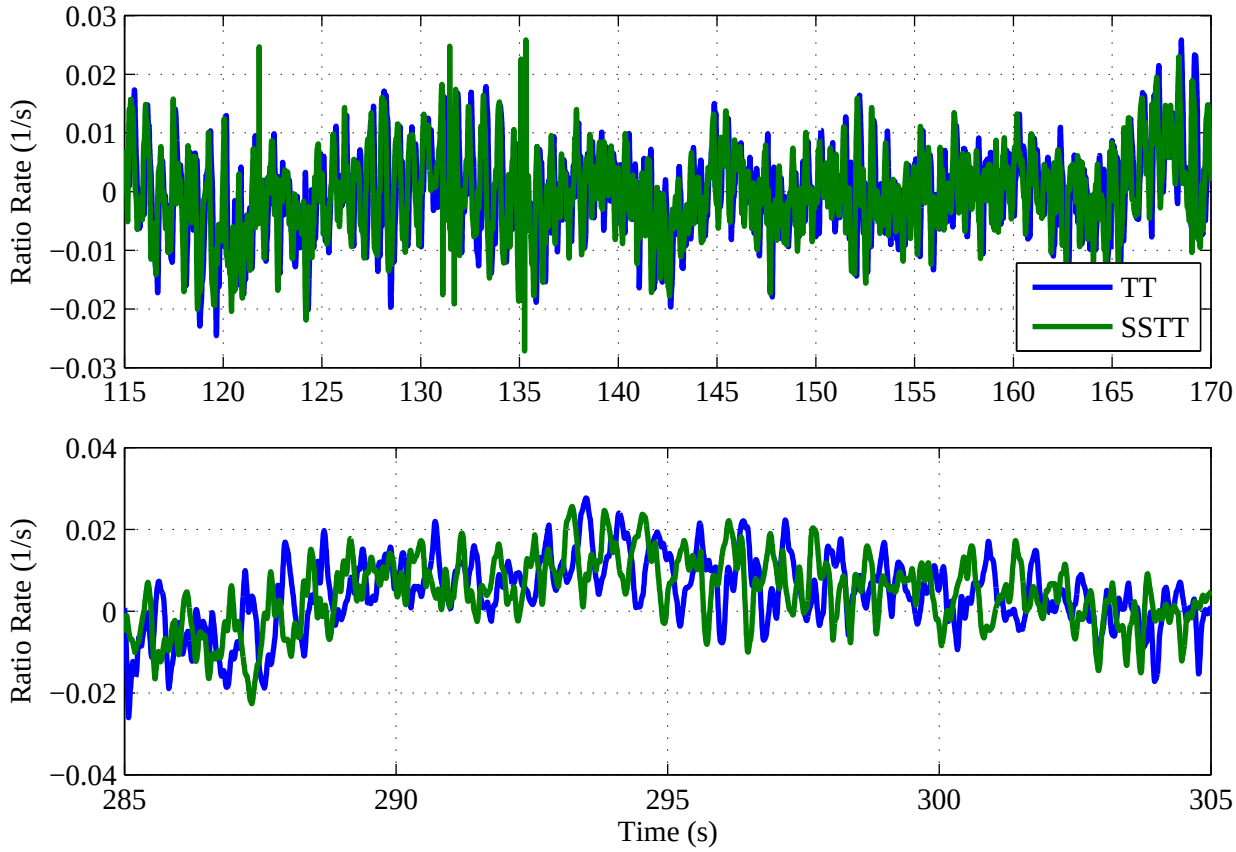

Figure 3.9: Ratio rate for full-field Region 2-3 wind input transitions

SSTT control are very similar except for max ratio acceleration. Again, this is due to poor transitioning between regions for the SSTT controller. Future research should focus on im-

Parameter	**Units**	**TT**	**SSTT**
Max ω_{rot}	rpm	43.61	43.65
Max $\lvert\dot{\omega}_{rot}\rvert$	deg/s^2	9.280	9.955
Max $\lvert\dot{c}\rvert$	1/s	3.694E-02	3.876E-02
RMS $\dot{c}$	1/s	8.180E-03	8.168E-02
Max $\lvert\ddot{c}\rvert$	1/s^2	0.5684	6.438
Min ω_{gen}	rpm	1807.2	1807.2
Max ω_{gen}	rpm	1816.3	1816.3
Max $\lvert\dot{\omega}_{gen}\rvert$	deg/s^2	351.0	371.3
E_{cap}	kW-hr	86.77	86.70

Table 3.5: Data from typical torque control with Region 2-3 turbulent wind input

proving these transitions. In summary, both controllers proved to be stable and achieve some degree of success in transitioning between regions, with TT control being smoother.

Chapter 4

Classical Control

Classical control was already demonstrated above for the pitch controller. To use classical control for the CVT, a setpoint is needed to formulate the error signal sent to the CVT controller. In this research, PID control and variations of it will be considered. Recall (2.28) for a general mathematical description of a PID controller. Classical controllers will only be designed for Region 2, while Region 2.5 and 3 will use TT control.

4.1 Region 2

For Region 2, the key objective is optimal energy capture, which may be achieved by tracking λ_{opt}, with blade pitch fixed at -1.0° for the CART. To track λ_{opt} using a setpoint, the wind speed must be measured since it's a disturbance with no ability to control it. Therefore, the only way to exercise control of TSR is to adjust rotor speed in accordance with the wind speed and λ_{opt}, hence variable-speed operation. This setpoint methodology is illustrated in Figure 4.1.

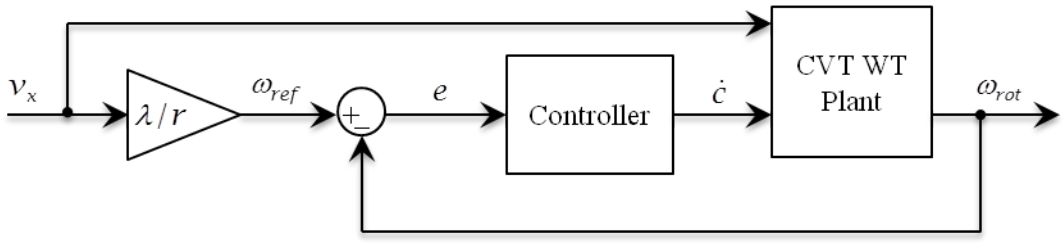

Figure 4.1: Block diagram illustration of classical approach to CVT control

The PID controller for CVT in Region 2 can be expressed in the time domain as,

$$\dot{c}(t) = K_p\left(\omega_{ref} - \omega_{rot}\right) + K_i \int \left(\omega_{ref} - \omega_{rot}\right) dt + K_d \frac{d}{dt}(\omega_{ref} - \omega_{rot}) \tag{4.1}$$

where ω_{ref} is a setpoint that varies with wind speed and is computed as $\lambda_{opt} v/r$, and ω_{rot} is measured rotor speed. For the linearized model, this PID controller is expressed in the Laplace domain as,

$$s\Delta C = \left(K_p + \frac{K_i}{s} + K_d s\right)\left(\frac{\lambda_{opt}}{r}\Delta V - \Delta\Omega_{rot}\right) \tag{4.2}$$

Now that the perturbed CVT ratio is expressed in terms of perturbed rotor speed, perturbed wind speed, and controller gains, (4.2) can be substituted into (2.44) with pitch perturbation set to zero for Region 2. Grouping terms and solving for the closed-loop transfer function between wind speed and rotor speed results in,

$$\frac{\Delta\Omega_{rot}}{\Delta V} = \frac{(B_{11}K_d\lambda)s^3 + (A_{12}K_d\lambda + B_{11}K_p\lambda + \Gamma_1 r)s^2 + (A_{12}K_p\lambda + B_{11}K_i\lambda)s + A_{12}K_i\lambda}{r(B_{11}K_d + 1)s^3 + r(-A_{11} + A_{12}K_d + B_{11}K_p)s^2 + r(A_{12}K_p + B_{11}K_i)s + rA_{12}K_i} \tag{4.3}$$

where $\lambda = \lambda_{opt}$ and A_{11}, A_{12}, B_{11}, and Γ_1, using index notation, are defined by (2.47). The linearized aerodynamic torque terms are determined by running a FAST linearization.

Symbolic computations of the linearized LSS torque terms evaluated at the operating point, thus $(\dot{\omega}_{rot})_o = 0$ and $\dot{c}_o = 0$, are given by,

$$\begin{aligned}
\frac{\partial \tau_{lss}}{\partial \dot{\omega}_{rot}} &= N^2 c_o^2 \Sigma I_H \\
\frac{\partial \tau_{lss}}{\partial \omega_{rot}} &= N c_o \frac{\partial \tau_{gen}}{\partial \omega_{rot}} = N^2 c_o^2 \frac{d\tau_{gen}}{d\omega_{gen}} \\
\frac{\partial \tau_{lss}}{\partial c} &= N(\tau_{gen})_o + c_o \frac{\partial \tau_{gen}}{\partial c} = N(\tau_{gen})_o + N c_o (\omega_{rot})_o \frac{d\tau_{gen}}{d\omega_{gen}} \\
\frac{\partial \tau_{lss}}{\partial \dot{c}} &= N^2 c_o \Sigma I_H (\omega_{rot})_o
\end{aligned} \tag{4.4}$$

where the derivative of generator torque with respect to generator speed will be calculated at the operating point using finite differences on the equivalent circuit torque data.

To numerically compute the linearized LSS torque terms of (4.4) as well as obtain values for the linearized aerodynamic torque using FAST, a Region 2 operating point must be chosen. To perform a Region 2 linearization with FAST, the hub-height wind speed, vertical shear exponent, blade pitch, and rotor speed at equilibrium are specified as,

$$\begin{aligned}
v_o &= 8 \text{ m/s} \\
\alpha_o &= 0.147 \\
\beta_o &= -1.0^\circ \\
(\omega_{rot})_o &= 29.7 \text{ rpm}
\end{aligned} \tag{4.5}$$

where the wind speed was chosen around the middle of Region 2 and rotor speed was chosen to coincide with $\lambda_{opt} = 8.3$. The FAST linearization trims what has been labeled as load torque in this research to satisfy the operating point conditions. Recall that FAST is only capable of modeling up through the MSS in this research, therefore the CVT and induction generator are not included in the linearization. However, the CVT ratio and generator torque

at equilibrium are needed to compute the linearized LSS torque terms of (4.4). To determine the CVT ratio at equilibrium, it's a matter of satisfying the equilibrium condition. FAST trims the load torque and the gearbox ratio is known, giving both torque and rotational speed of the MSS. Therefore, the CVT ratio that satisfies the power condition between the MSS and generator will be the ratio at equilibrium. Since the generator torque is not expressed as a function but rather as a lookup table, the solution to this problem is obtained iteratively,

(1) Guess an initial c

(2) Compute $\tau_{gen} = \dfrac{\tau_{load}}{c}$

(3) Look up ω_{gen}

(4) Compute new $c = \dfrac{\omega_{gen}}{N\omega_{rot}}$

(5) Repeat from (2) until converged

A Region 2 linearization is run with FAST for the operating point of (4.5) and the load torque is trimmed to 1075.7 N-m. The equilibrium CVT ratio is found to be 1.4060. The derivative of generator torque with respect to generator speed is computed with finite differences as 2001.4 N-m/rad/s. With this information, all the linearized LSS torque terms can be computed for this operating point. Using the FAST linearization results, the linearized aerodynamic torque terms for this Region 2 operating point are,

$$\begin{aligned} \frac{\partial \tau_{aero}}{\partial \omega_{rot}} &= -1.4563 \times 10^4 \\ \frac{\partial \tau_{aero}}{\partial v} &= 1.7268 \times 10^4 \end{aligned} \tag{4.7}$$

where the linearized pitch term is not reported because pitch is not a control input for Region 2. Now the PID gains for the Region 2 classical controller can be tuned such that

CVT actuation provides satisfactory rotor speed response to wind input. Analytical tuning will be done for a proportional controller only, while a complete analytical tuning of the PID controller is suggested for future research.

Classical control is not considered for Region 2.5 and 3 in this thesis. Refer to the previous chapter, on typical control, for the TT control laws in Region 2.5 and 3. These will be used in conjunction with the classical Region 2 controllers.

4.1.1 Tuning

Multiple tuning methods are considered for the Region 2 PID controller. First, a sequential tuning of the PID gains will be done to find the gains that have the most energy capture for a given turbulent wind input. This approach was used by [7, 9]. Next, multivariable tuning of the PD gains will be done. This is nearly the same procedure used for the sequential tuning except the controller gains, only proportional and derivative, are varied simultaneously to capture interactions between the gains. The sequential method ignores this. Visually, this could be viewed as constructing a surface of energy capture versus proportional gain versus derivative gain. The third tuning method uses the proportional control transfer function, a simplified version of (4.3), to analytically design the closed-loop system for a rotor speed response similar to a typical torque controller.

The sequential PID tuning method is partly subjective because it requires the choice of a wind input. There are infinite choices when it comes to this, but this research focuses on three key attributes for the wind input to be used: turbulence intensity, average wind speed, and duration of wind input. It was decided to use the first 70 seconds of the full-field Region 2 wind file. This has a hub-height x-component average wind speed of 6.9 m/s with

a standard deviation of 1.14 m/s. The 70 second duration is chosen since this will limit computational resources and is long enough to capture a wide range of Region 2 wind speeds, i.e. from 3.9 to 9.9 m/s. Figure 4.2 shows the x-component hub-height wind speed used for this tuning process.

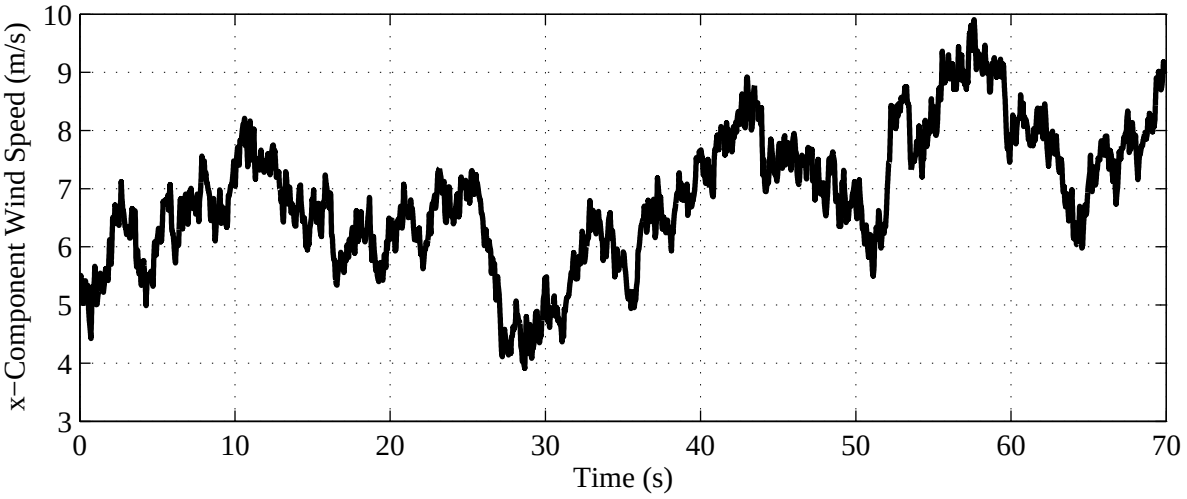

Figure 4.2: Turbulent wind input used for classical controller tuning

Simulations were first run with integral and derivative gains set to zero and varying the proportional gain incrementally over a wide range of gains. Any simulations detected as unstable or with excessive motoring are discarded from the data. The energy captured from each stable simulation run is measured with the following correction for rotational kinetic energy (KE) which has been added to the system,

$$E_{cap} = E_{out} + (\mathrm{KE}_f - \mathrm{KE}_i) \tag{4.8}$$

where E_{out} is the time integral of measured electrical power output and KE_f and KE_i are the final and initial rotational KE of the system. All simulations are started with the same initial conditions which correspond to λ_{opt}. After finding the K_p gain that results in the

most energy capture, the gain is fixed and then the integral gain is varied. Lastly, the derivative gain is varied. The results of this sequential PID tuning process are presented in Table 4.1. Notice integral control was found to only negatively effect energy capture, no matter

K_p	K_i	K_d	**Energy Captured**
-0.04468	0.00	-0.01816	1.6358 kW-hr

Table 4.1: Sequential PID tuning for Region 2 full-field wind input

what gain value is used. Its effect on CVT control action or drivetrain loading may be more impactful but isn't considered in this research.

The next tuning method, multi-variable PD, uses the same approach as the sequential tuning except that it samples an array of points in the PD plane, measuring energy capture for each. The wind input in Figure 4.2 is used here too, therefore this tuning process is also somewhat subjective. The integral gain is not included in this tuning because it would increase the total simulation time drastically since the PD plane would need to be sampled for each integral gain tested. The results of multi-variable PD tuning are in Table 4.2. Interestingly, the result is nearly identical to the sequential tuning process. This suggests

K_p	K_i	K_d	**Energy Captured**
-0.04468	n/a	-0.02195	1.6359 kW-hr

Table 4.2: Multi-variable PD tuning for Region 2 full-field wind input

that tuning the proportional gain has the biggest impact on energy capture. Even with the derivative gain set to zero, the energy capture is still 1.6341 kW-hr. Therefore, the addition of derivative control action is nearly negligible in terms of energy capture. Its effect on other aspects, such as CVT actuation or drivetrain loads, is not considered in this research.

Lastly, and perhaps the most useful, the proportional control closed-loop transfer function is tuned to behave similar to typical control for Region 2. This transfer function is written as,

$$\frac{\Delta\Omega_{rot}}{\Delta V} = \frac{(B_{11}K_p\lambda + \Gamma_1 r)s + A_{12}K_p\lambda}{rs^2 + r(-A_{11} + B_{11}K_p)s + rA_{12}K_p} \tag{4.9}$$

where $\lambda = \lambda_{opt}$ and A_{11}, A_{12}, B_{11}, and Γ_1, using index notation, are defined by (2.47). These terms are evaluated at the Region 2 operating point, (4.5), see Table 4.3. Tuning is done

$\boldsymbol{A_{11}}$	$\boldsymbol{A_{12}}$	$\boldsymbol{B_{11}}$	$\boldsymbol{\Gamma_1}$
-18.12	-40.11	-0.2402	0.04236

Table 4.3: Region 2 linearization of 1-state with CVT inputs

by placing one of the closed-loop poles in the same location of the complex plane as the pole of (2.42), the linearized typical control law for Region 2. To be shown, the other pole will be located near the zero of (4.9), thus canceling its effect on the system response.

The linearized typical law for Region 2 is evaluated at the operating point, (4.5), resulting in its pole located at -0.1232. Now, the proportional gain is calculated to create a similar rotor speed response. The poles of the proportional controller are,

$$p_{1,2} = \frac{1}{2}\Big(A_{11} - B_{11}K_p \pm \sqrt{-4A_{12}K_p + (-A_{11} + B_{11}K_p)^2}\Big) \tag{4.10}$$

The only zero is given by,

$$z_1 = \frac{-A_{12}K_p\lambda_{opt}}{B_{11}K_p\lambda_{opt} + \Gamma_1 r} \tag{4.11}$$

Setting the first pole equal to -0.1232 and solving for K_p yields a value of -0.05532. This makes the other pole equal to -18.01 and the zero equal to -18.17. This zero effectively

removes any small effects the fast pole may have exhibited, thus the pole at -0.1232 is the dominant pole. The proportional controller tuned this way should behave similar to the TT controller, at least in the vicinity of the operating point. To verify this, an 8 to 9 m/s wind input step response was simulated for each controller with the nonlinear model.

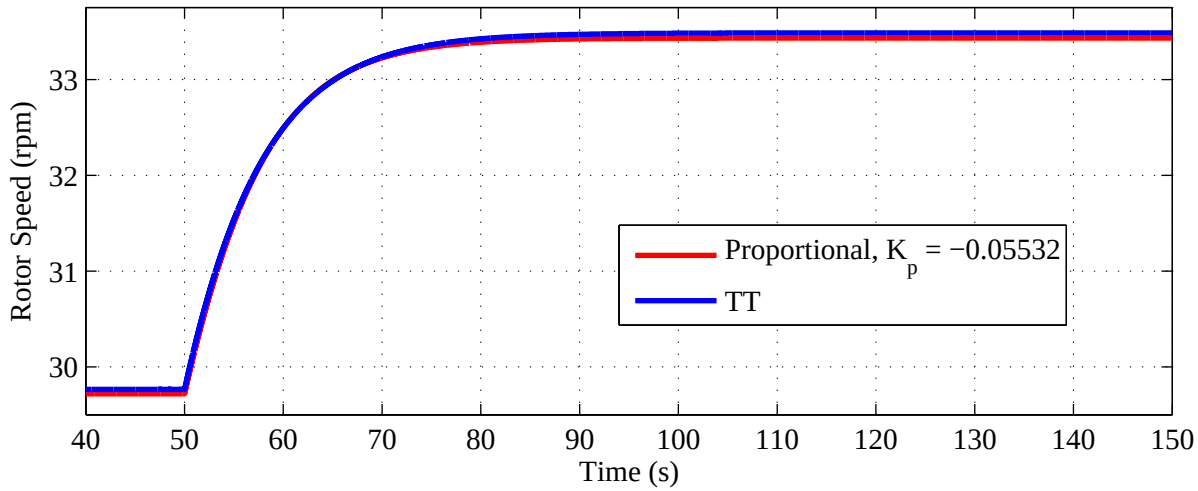

Figure 4.3: Step response, 8-9 m/s, of nonlinear model with proportional and typical control

Figure 4.3 illustrates the response of both closed-loop systems being similar, thus verifying the proportional controller tuning method. For a more aggressive response, the K_p gain should be made more negative. Lastly, when simulated with the 70 seconds of turbulent wind input used above, an energy capture of 1.6277 kW-hr was measured.

Consider operation away from the linearization operating point. Figure 4.4 shows the step response, a 5 to 6 m/s wind input, of the nonlinear model using typical and proportional controllers. As expected, both controllers have slower responses since less wind energy is available to create a torque differential that would help the rotor accelerate. Being further from the operating point, the controllers no longer actuate the CVT as similarly. Therefore, two more operating points are considered, one near the low end and one near the high end of Region 2. The additional operating points are chosen at 5 m/s and 11 m/s hub-height

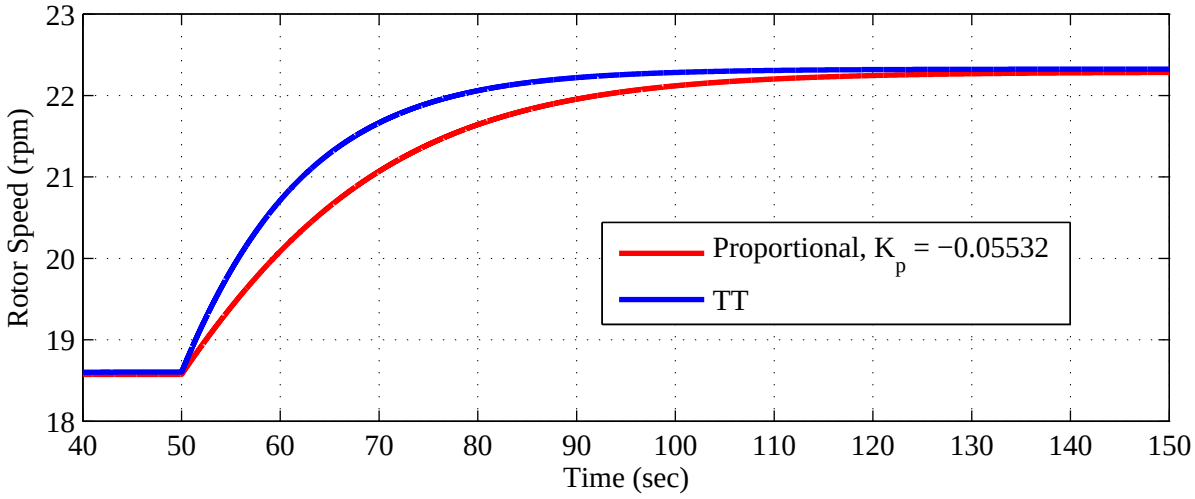

Figure 4.4: Step response, 5-6 m/s, of nonlinear model with proportional and typical control

wind speeds, still with 0.147 vertical shear and rotor speeds corresponding to λ_{opt}. The pole of the linearized typical law, (2.42), for each operating point is summarized in Table 4.4.

Wind Speed (m/s)	5	8	11
Rotor Speed (rpm)	18.57	29.72	40.86
Pole Location	-0.07695	-0.1232	-0.1694

Table 4.4: Linearized typical Region 2 law pole location

Gain scheduling of K_p will be done as a function of rotor speed. Figure 4.5 illustrates the gain scheduling to be used, with the three points corresponding to Table 4.4. Using this gain scheduling, the simulations of Figure 4.4 are repeated and displayed in Figure 4.6. When simulated with the 70 seconds of turbulent wind input of Figure 4.2, an energy capture of 1.6333 kW-hr was measured. For a more aggressive response across the entire range of Region 2 control, the constant term of the gain scheduling function should be made more negative. There is a tradeoff between better tracking of λ_{opt} and CVT actuation. Simulations and results will focus on this proportional gain scheduling (P-GS) controller more than the other Region 2 classical controllers.

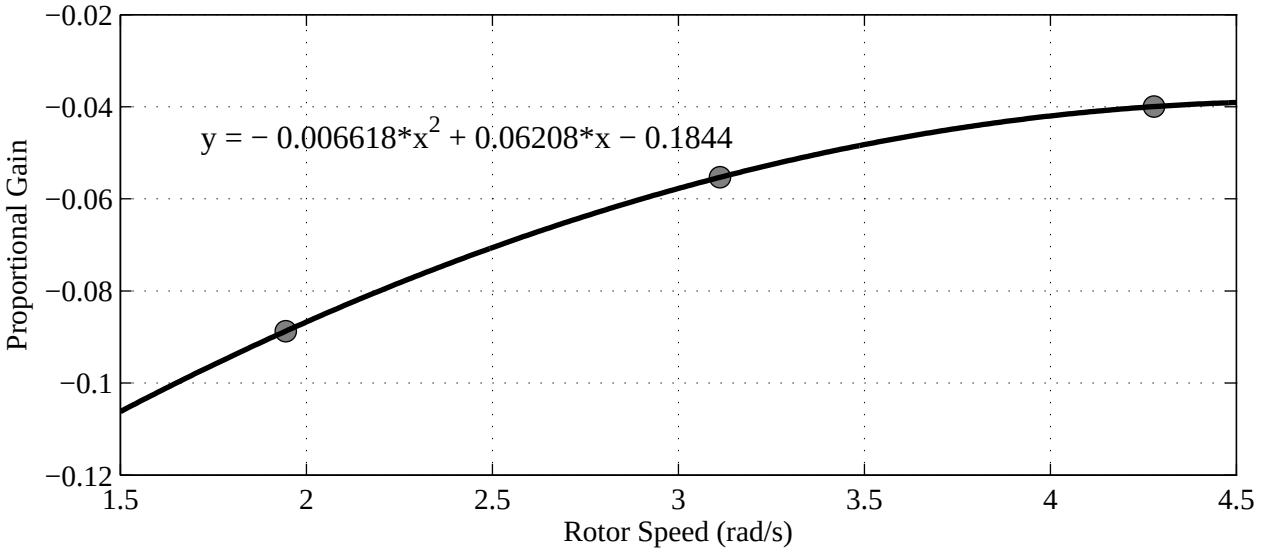

Figure 4.5: Plot of gain scheduling used for proportional controller

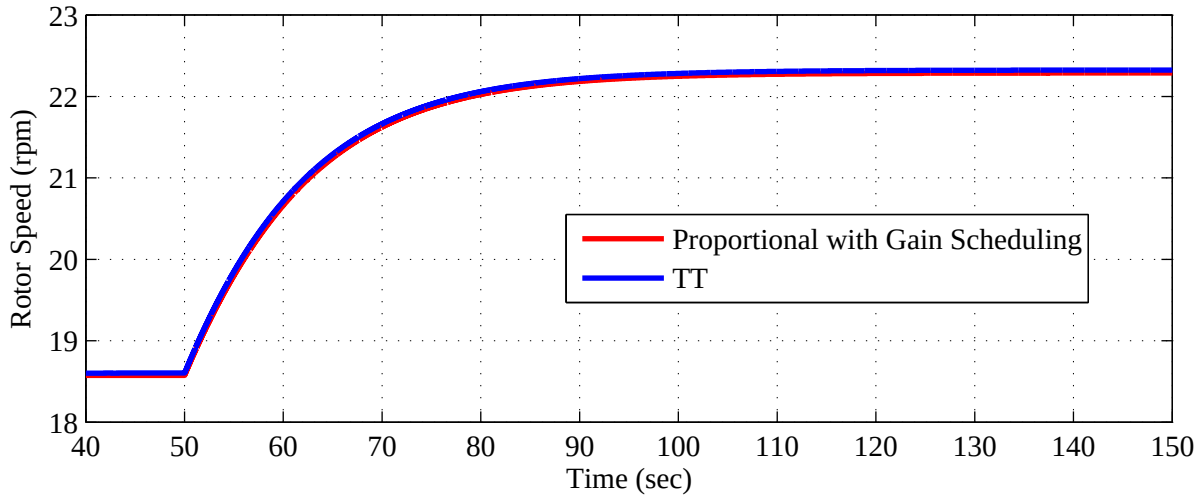

Figure 4.6: Step response, 5-6 m/s, of nonlinear model using proportional gain scheduling

4.2 Simulations

Before continuing, a note about the Region 2 classical controllers is made. None are easily realizable, i.e. implementable in nature, since the setpoint requires measurement of wind speed. Measuring wind speed is difficult because use of an anemometer at hub-height, away from the turbine wake, is costly and still only provides measurement at a single point.

However, it's not impractical, so this research still includes these controllers for analyzing different control schemes in a CVT wind turbine. Three different methods of tuning were considered for Region 2, but the sequentially tuned PID control will no longer be considered since it was tuned so similar to the PD control. Region 2.5 and 3 will not be tested since they use the TT control designed and tested in the previous chapter.

4.2.1 Region 2

The simple Region 2 wind input is used to test the ability of the classical Region 2 controllers to track λ_{opt}. The resulting rotor speed and CVT ratio rate are plotted in Figure 4.7 with the ideal λ_{opt} rotor speed as reference. The P-GS controller tracks λ_{opt} better

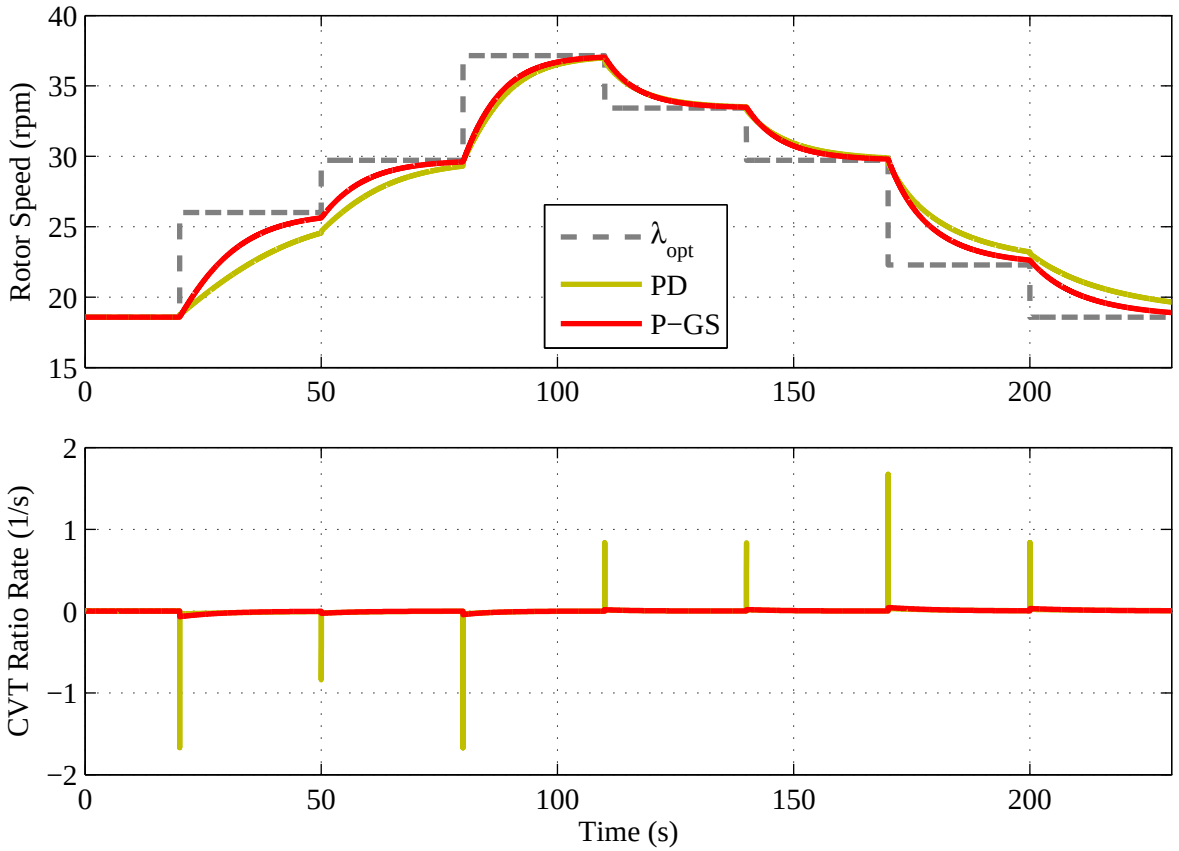

Figure 4.7: Rotor speed and ratio rate for classical control with simple Region 2 wind input

throughout most of Region 2, particularly the lower part. The PD controller unjustifiably has CVT ratio rates and accelerations (not shown) that far exceed those of P-GS control. This is likely unacceptable in practice but it will continue to be tested.

Similar to OTR, the constant term of the gain scheduling function, see Figure 4.5 , can be adjusted accordingly. Making it more negative will result in a quicker response, but at the cost of more aggressive CVT control action. Reduced control action is achieved by making the constant less negative. These tuning abilities are not explored here but may be applicable to future research.

The PD and P-GS controllers will now be simulated with the nonlinear model using the Region 2 turbulent input. Key results are presented in Table 4.5. The PD controller

Parameter	**Units**	**PD**	**P-GS**
Max ω_{rot}	rpm	42.22	40.71
Max $\lvert\dot{\omega}_{rot}\rvert$	deg/s^2	19.57	7.100
Max $\lvert\dot{c}\rvert$	1/s	1.459E-01	6.478E-02
RMS $\dot{c}$	1/s	3.332E-02	1.723E-02
Max $\lvert\ddot{c}\rvert$	1/s^2	23.09	1.481
Min ω_{gen}	rpm	1797.9	1800.1
Max ω_{gen}	rpm	1814.5	1811.6
Max $\lvert\dot{\omega}_{gen}\rvert$	deg/s^2	901.7	335.3
RMS $\Delta\lambda$	-	1.055	0.8648
E_{cap}	kW-hr	25.39	25.85

Table 4.5: Data from PD and P-GS control with Region 2 turbulent wind input

does not perform well in comparison to P-GS control. Its statistics are less favorable in every category, yet the energy capture is less. Furthermore, PD control results in motoring with generator speeds less than synchronous. To further illustrate the excessive PD control action, the CVT ratio rate is plotted in Figure 4.8 from a portion of the simulation. Around

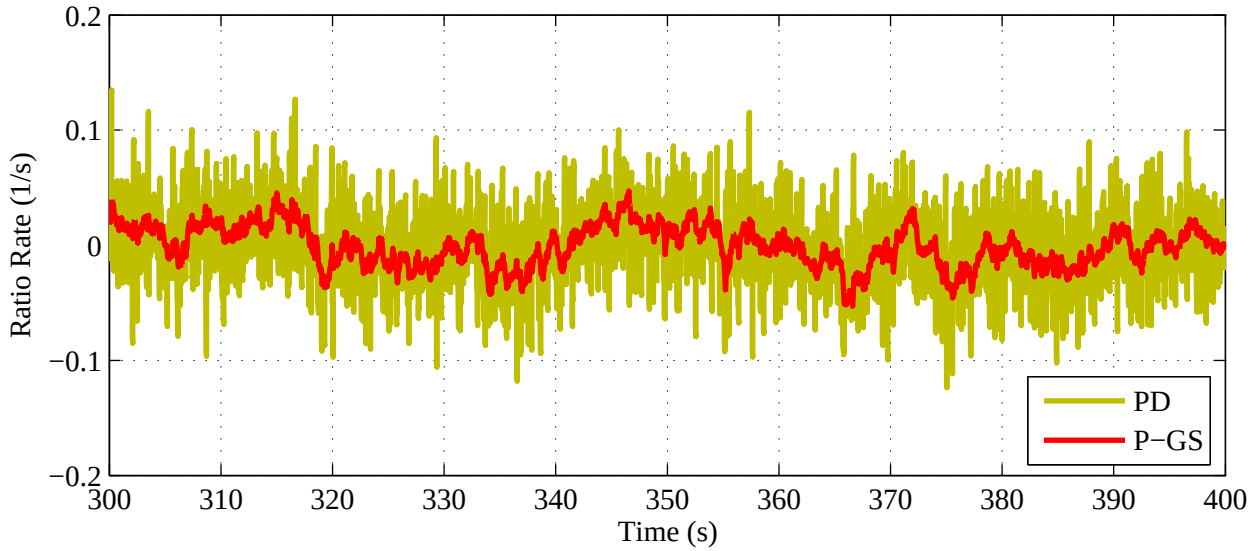

Figure 4.8: Ratio rate for classical control with full-field Region 2 wind input

200 seconds, the CVT temporarily uses Region 2.5 and 3 TT controllers, hence the reduced rates. PD control, as tuned here, is not recommended due to its excessive control action, motoring, and less energy capture.

In summary, the PD controller proved to be impractical since its excessive CVT control action results in extreme loads and frequent motoring, while the P-GS controller is stable and successful in tracking λ_{opt}. PD control will no longer be considered. Note, it has been verified that P-GS control is capable of operating in conjunction with the Region 2.5 TT controller.

Chapter 5

Modern Control

Modern control relies on the use of state space representations to develop control laws. A key advantage of state space models is the ability to express more complex systems that modern control techniques can use in a single control loop. As shown in the sections on linearized models, a state space model was developed for the wind turbine that includes drivetrain torsion. Using modern control techniques, this drivetrain torsion mode can be damped with CVT actuation. This will be demonstrated for Region 2, 2.5, and 3. The pitch system is also capable of damping the drivetrain torsion mode in Region 3 if DAC theory were used [24, 38, 40].

Recall the control objectives of section 1.3 and the brief intro to modern control methods in section 2.4.4.3. The use of DTC theory, realizable drivetrain dampers, and PI pitch will be used to achieve control objectives in each region. Table 5.1 summarizes the various modern control designs developed in this research for controlling the CVT. Three different modern controllers are designed for Region 2, while Region 2.5 and 3 will each have a single design. Notice the shorthand notation in the left column.

Method	Region 2
T2	$\delta\tau_{load}$ model with ratio rate law (DTC)
C2	$\delta\dot{c}$ model (DTC)
R2	TT method with realizable damper
	Region 2.5
R25	Interpolated torque method
	Region 3
R3	TT method with realizable damper

Table 5.1: Summary of modern controllers designed for CVT

Only Region 2 makes use of DTC theory since that's the only time the wind disturbance should be tracked. The PI pitch controller reviewed in Appendix C is used for regulating rotor speed in above rated conditions. This research is interested in using a CVT in conjunction with the pitch system to regulate power.

It should be noted that modern control methods applied here for CVT rely on equations (2.12) and (2.20) being accurate mathematical models for load torque, i.e. torque at the CVT input shaft. Modern control will first be used by considering the simple rotor rotation model and then advancing to the more complex model with drivetrain torsion.

5.1 1-State Model

The 1-state model refers to the linear mathematical description of the wind turbine with perturbed rotor speed as the state. This is a rigid drivetrain model with perturbed

load torque as an input. The state space representation for the 1-state system is given by,

$$\delta\dot{\omega}_{rot} = A\delta\omega_{rot} + B\begin{bmatrix}\delta\tau_{load}\\ \delta\beta\end{bmatrix} + \Gamma\delta v \tag{5.1}$$

$$y = C\delta\omega_{rot}$$

where the state equation was previously given by (2.45), refer to it for A, B, and Γ. As the output equation shows, the only output will be rotor speed in units of rad/s for $C = 1$.

5.1.1 Region 2

A DTC controller will be designed for the state space representation given in (5.1). The ratio rate law, the basis for TT control in Chapter 3, will be used to command the CVT ratio rate to achieve the commanded torque. Recall, the idea behind the ratio rate law is that a specified load torque can be achieved by commanding the CVT ratio rate according to (3.3). The disadvantage of commanding the CVT ratio rate this way is that knowledge of the rotor speed, rotor acceleration, and HSS torque is required. The rotor speed will be measured anyway, and its time derivative will give acceleration, but HSS torque needs to be measured or estimated.

This control method refers to T2 in Table 5.1. To obtain a numerical state equation, an operating point must be chosen for A, B, and Γ to be known. This was done for classical control of Region 2, except the model was different. The same Region 2 operating point defined in (4.5) is used here. The FAST linearization evaluated in the context of this control

model is summarized as,

$$\begin{aligned} A &= \frac{\frac{\partial \tau_{aero}}{\partial \dot{\omega}_{rot}}}{I_{dr}} = -0.04007 \\ b_\tau &= \frac{-N}{I_{dr}} = -1.1877 \times 10^{-4} \\ \Gamma &= \frac{\frac{\partial \tau_{aero}}{\partial v}}{I_{dr}} = 0.04752 \end{aligned} \tag{5.2}$$

where b_β is not reported because pitch angle is fixed for Region 2, thus $\delta\beta = 0$.

State feedback will be used to command the input, $\delta\tau_{load}$, as a function of the state. The general form of the state feedback control law is written as,

$$u = F_x x + q \tag{5.3}$$

where $F_x \in \mathbb{R}^{m \times n}$ is the feedback gain matrix and $q \in \mathbb{R}^m$ is a reference input vector. In the context of this 1-state model, the state feedback law is written as,

$$\delta\tau_{load} = F_x \delta\omega_{rot} + q \tag{5.4}$$

The commanded load torque is then sent to the CVT controller for actuation, where the CVT ratio rate is commanded based on (3.3). The feedback matrix, F_x, is computed to provide a satisfactory transient response by placing the eigenvalues/poles of the closed-loop system in a desired location of the complex plane. Before F_x is computed for eigenvalue assignment, the pair $\{A, B\}$ must be checked for controllability. For nonzero B, as is the case here, the pair is controllable for this 1-state model. Plugging (5.4) into the state equation of (5.1)

allows the closed-loop system with state feedback to be written as,

$$\delta\dot{\omega}_{rot} = (A + BF_x)\delta\omega_{rot} + Bq + \Gamma\delta v \tag{5.5}$$

Therefore, the eigenvalue of $A + BF_x$ dictates the transient response of the perturbed rotor speed state. Note that the disturbance input, perturbed wind speed, has not been accounted for in the control law. Instead, there is an arbitrary reference input, $q(t)$, that does not incorporate the disturbance. So, even though the transient response can be manipulated via F_x, the control law of (5.3) is not designed to track disturbances which is an objective for Region 2. This is illustrated in Figure 5.1 with plots of a multiple step input to the linear and nonlinear plants using state feedback, with $F_x = 3872.5$ such that the closed loop eigenvalue is at -0.5 to provide an arbitrarily fast rotor response. The disturbance input steps from a perturbed wind speed of -2 m/s up to 2 m/s in increments of 1 m/s, where 0 m/s signifies 8 m/s for the nonlinear plant, or physical system. The linear and nonlinear simulations are very comparable, however, it's clear that rotor speed does not track the reference speed

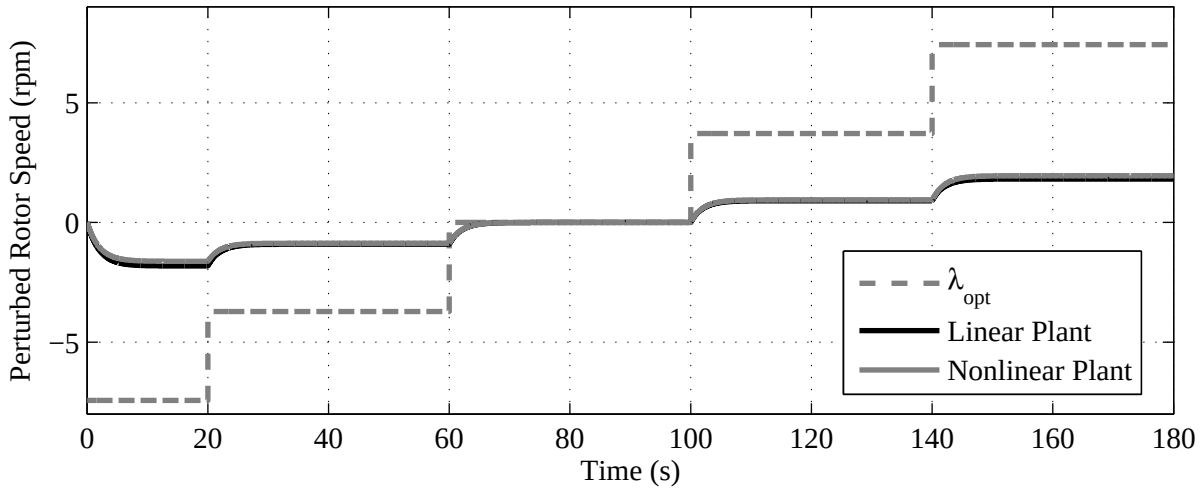

Figure 5.1: Rotor speed for 1-state feedback with multi-step wind input

associated with λ_{opt}. To correct this, DTC theory will be used.

DTC theory involves using an assumed disturbance waveform, estimating the disturbance, and tracking the disturbance. See Appendix D for details on DTC theory. The first step is to develop an assumed waveform, which is used to express the disturbance input vector, $u_d(t)$. The assumed waveform is written as,

$$\begin{aligned} u_d &= \Theta z_d \\ \dot{z}_d &= G z_d \end{aligned} \tag{5.6}$$

where $z_d \in \mathbb{R}^{n_d}$ is the disturbance state vector, and Θ and G matrices are chosen based on the assumed waveform. This research uses a step function as the assumed waveform for the wind speed disturbance present in the model, thus $\Theta = 1$ and $G = 0$. This is a good choice for sudden disturbances, like turbulent winds.

A new control feedback law is now formulated with the inclusion of the disturbance state vector. In it's general form, the ideal DTC feedback law is expressed as,

$$u = F_x x + F_d z_d \tag{5.7}$$

For the 1-state model considered here, this is written as,

$$\delta\tau_{load} = F_x \delta\omega_{rot} + F_d \delta v \tag{5.8}$$

which conveniently accounts for the disturbance input. The disturbance gain, $F_d \in \mathbb{R}^{m \times n_d}$, is computed such that the control input is commanded to make the perturbed rotor speed state track the disturbance state as desired. The proportionality of the plant states to the

disturbance states is set with variable Q, where $Q = \omega_{rot_o}/v_o = 0.389$ for this 1-state model which equates to λ_{opt}/r since the point of linearization is at $(C_p)_{max}$. Using this Q, the next step to finding F_d is solving the following for L,

$$Q\Theta = CL \tag{5.9}$$

The 1-state model is simple since $C = 1$ and $\Theta = 1$, thus $L = Q$. The disturbance gain matrix is then computed to satisfy,

$$(A + BF_x)L - LG + BF_d + \Gamma\Theta = 0 \tag{5.10}$$

This is simple to solve for the 1-state model since it's a scalar equation.

The value for F_x is still based on the desired transient response and the presence of F_d in the feedback law does not effect its tuning. If using the arbitrarily fast eigenvalue of -0.5 for $A + BF_x$, as was done previously and used for Figure 5.1, this leads to $F_d = -1237.6$. Reproducing the plots in Figure 5.1, but with ideal DTC, results in Figure 5.2. DTC with

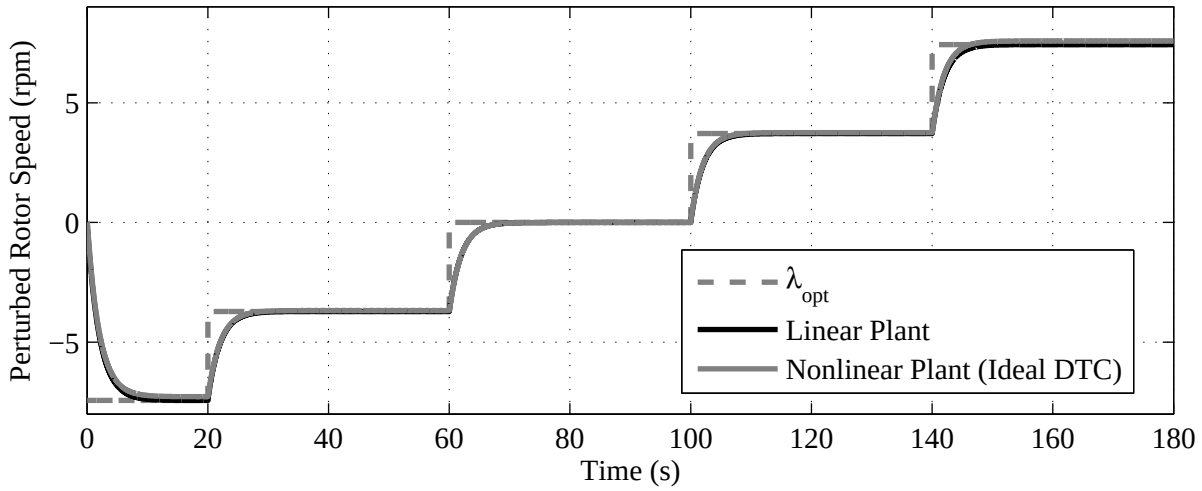

Figure 5.2: Rotor speed for 1-state ideal DTC with multi-step wind input

the nonlinear simulation tracks λ_{opt} closely. The benefit of DTC is now becoming clear, however, the ideal DTC feedback law is not so ideal for practical implementation. The controller still requires measurement of the disturbance, defeating a key purpose of using DTC theory. Therefore, a state observer is used to estimate the disturbance state, $z_d(t)$.

The general form of the DTC control law that eliminates the need to measure all states and disturbances is expressed as,

$$u = F_x\hat{x} + F_d\hat{z}_d \tag{5.11}$$

where the hat symbol indicates estimation. For the 1-state model, this is written as,

$$\delta\tau_{load} = F_x\hat{\delta\omega}_{rot} + F_d\hat{\delta v} \tag{5.12}$$

To formulate this law, observers are needed for both the plant states and disturbance states. See Appendix D for more complete details on deriving these. Using typical state space notation, the estimator is formulated as,

$$\begin{aligned} \dot{\hat{x}} &= A\hat{x} + Bu + \Gamma\hat{u}_d + K_x(y - \hat{y}) \\ \hat{y} &= C\hat{x} \end{aligned} \tag{5.13}$$

with

$$\begin{aligned} \hat{u}_d &= \Theta\hat{z}_d \\ \dot{\hat{z}}_d &= G\hat{z}_d + K_d(y - \hat{y}) \end{aligned} \tag{5.14}$$

where K_x is the state estimator gain and K_d is the disturbance estimator gain. Now consider the differential error equation,

$$\dot{e}(t) = \begin{bmatrix} \dot{e}_x^\top(t) \\ \dot{e}_d^\top(t) \end{bmatrix} = \begin{bmatrix} A - K_x C & \Gamma\Theta \\ -K_d C & G \end{bmatrix} \begin{bmatrix} e_x^\top(t) \\ e_d^\top(t) \end{bmatrix} = (\bar{A} - \bar{K}\bar{C})e(t) \tag{5.15}$$

$$\text{where} \quad \bar{A} = \begin{bmatrix} A & \Gamma\Theta \\ 0 & G \end{bmatrix}, \bar{C} = \begin{bmatrix} C & 0 \end{bmatrix}, \bar{K} = \begin{bmatrix} K_x \\ K_d \end{bmatrix}$$

If augmented pair $\{\bar{A}, \bar{C}\}$ is observable, K_x and K_d can be chosen such that error converges to zero. The eigenvalues of $(\bar{A} - \bar{K}\bar{C})$ determine the transient response of the error, or, in other words, how quickly the error converges. A useful form of the estimator for implementation into Simulink is,

$$\begin{bmatrix} \dot{\hat{x}} \\ \dot{\hat{z}}_d \end{bmatrix} = \begin{bmatrix} A - K_x C & \Gamma\Theta \\ -K_d C & G \end{bmatrix} \begin{bmatrix} \hat{x} \\ \hat{z}_d \end{bmatrix} + \begin{bmatrix} B & K_x \\ 0 & K_d \end{bmatrix} \begin{bmatrix} u \\ y \end{bmatrix} \tag{5.17}$$

which clearly shows how knowledge of the input, $u(t)$, and output, $y(t)$, along with an assumed waveform allows the disturbance state, $z_d(t)$, to be estimated.

The observability matrix for the pair $\{\bar{A}, \bar{C}\}$ is found to have a rank of 2, which equals the sum of plant and disturbance states. Therefore this system is observable, and estimator gains, K_x and K_d, should be chosen for fast convergence by selecting eigenvalues of $(\bar{A} - \bar{K}\bar{C})$ to the far left in the complex plane. For the 1-state model, estimating the disturbance state is of key interest since $\delta\omega_{rot}$ is measured anyway. The MATLAB place() command is used

to compute $\bar{K}$ for eigenvalues at -10 and -11 in the complex plane.

$$\bar{K} = \text{place}(\bar{A}^\top, \bar{C}^\top, [-10, -11]) = \begin{bmatrix} 20.96 \\ 2315.06 \end{bmatrix} \tag{5.18}$$

Notice the choice of $\bar{K}$ is independent of the feedback law. The plot of Figure 5.2 is reproduced using DTC with an observer. As expected, the results for tracking λ_{opt} are not as

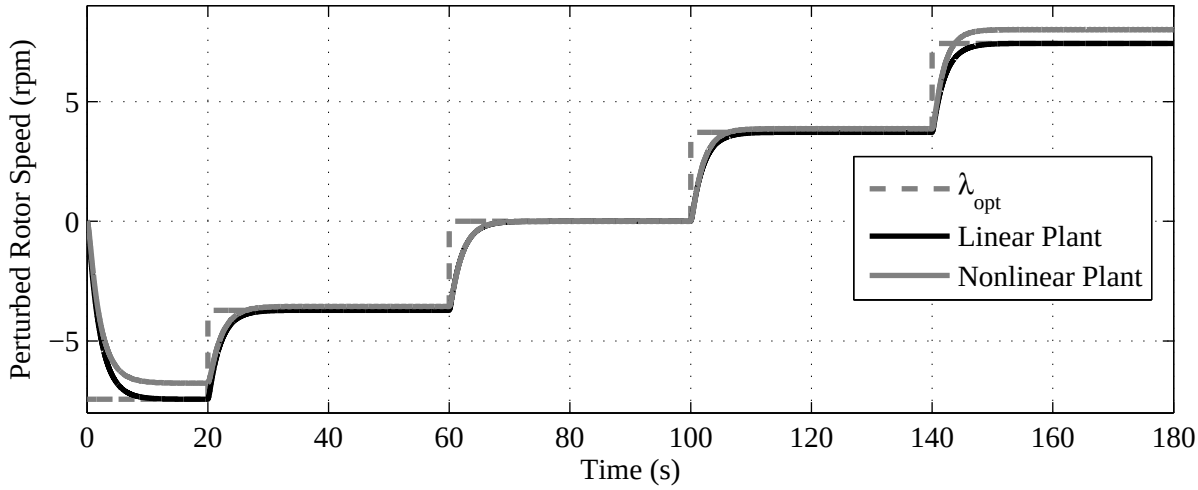

Figure 5.3: Rotor speed for 1-state DTC observer with multi-step wind input

good as ideal DTC, with the error being larger further from the operating point. This can be improved if observers are designed at multiple operating points in Region 2, but this is not considered here.

Now, the feedback gain, F_x, will be retuned to provide a rotor speed response similar to the typical torque law. This requires recalculating the disturbance feedback gain, F_d. The pole location of the linearized typical law transfer function between perturbed wind input and perturbed rotor speed output is -0.1232 for the Region 2 operating point of (4.5). Therefore, the eigenvalue of $(A+BF_x)$ will be assigned to -0.1232 with $F_x = 699.96$. Solving (5.10) for the disturbance gain gives $F_d = -3.479$. The estimator gains will be left the same

because they are independent of the feedback gains.

Prior to tuning the DTC controller to respond similar to the typical Region 2 law, the eigenvalue of $(A+BF_x)$ was assigned to be arbitrarily fast with a value at -0.5 in the complex plane. This would require very fast CVT actuation, likely resulting in reduced reliability and motoring to achieve net torques large enough to quickly accelerate the rotor However, the fast eigenvalue was helpful in illustrating the benefit of DTC, hence its usage.

In summary, DTC with a state estimator has been successfully designed for the Region 2 operating point of (4.5). The step inputs of wind speed perturbation to the linear and nonlinear plants show that DTC is capable of commanding the CVT such that rotor speed tracks λ_{opt}. For CVT control, the 1-state model is only used for Region 2. It's been verified that 1-state DTC is capable of operating in conjunction with the Region 2.5 TT controller.

5.2 2-State Model

The 1-state system can express $\delta\tau_{load}$ in terms of perturbations in rotor acceleration, rotor speed, CVT ratio, and CVT ratio rate. Taking the perturbed CVT ratio as a state variable and the perturbed ratio rate as a control input, the state space representation is,

$$\begin{aligned} \begin{bmatrix} \delta\dot{\omega}_{rot} \\ \delta\dot{c} \end{bmatrix} &= A \begin{bmatrix} \delta\omega_{rot} \\ \delta c \end{bmatrix} + B \begin{bmatrix} \delta\dot{c} \\ \delta\beta \end{bmatrix} + \Gamma\delta v \\ y &= C \begin{bmatrix} \delta\omega_{rot} \\ \delta c \end{bmatrix} \end{aligned} \tag{5.19}$$

where the state equation was previously given by (2.47), refer to it for A, B, and Γ. The output will again be rotor speed in units of rad/s, thus $C = 1$.

5.2.1 Region 2

This control method refers to C2 in Table 5.1. The numerical values for much of A, B, and Γ of the state equation at the Region 2 operating point were previously reported in Table 4.3, where the pitch input gain vector is not given since $\delta\beta = 0$ for Region 2. For convenience, the complete matrices are written here as,

$$A = \begin{bmatrix} -18.12 & -40.11 \\ 0 & 0 \end{bmatrix}, \quad B = \begin{bmatrix} -0.2402 \\ 1 \end{bmatrix}, \quad \Gamma = \begin{bmatrix} 0.04236 \\ 0 \end{bmatrix} \tag{5.20}$$

The controllability matrix for the pair $\{A, B\}$ has a rank of 2, thus the system controllable.

A different approach is used here compared to the previous section for the DTC controller. The state feedback law can be written as,

$$\delta\dot{c} = F_x \begin{bmatrix} \delta\omega_{rot} \\ \delta c \end{bmatrix} \tag{5.21}$$

where $F_x = \mathbb{R}^{1\times 2}$. Since $\delta\dot{c}$ is the time derivative of δc, an expression can be derived to correlate them. If $\delta\dot{c}$ is commanded as a function of $\delta\omega_{rot}$, then δc must have a relation to this. Start by writing,

$$\delta\dot{c} = F_x \delta\omega_{rot} \tag{5.22a}$$

$$\delta c = f_c \delta\omega_{rot} \tag{5.22b}$$

where (5.22a), with a scalar F_x, will be the feedback law instead of (5.21). This formulation is only done to relate the perturbed ratio and ratio rate for the purpose of developing the

feedback law for the ratio rate. The perturbed ratio still remains a state that is the integral of the commanded ratio rate perturbation. The new F_x must correlate to the gain in (5.22b), f_c. Taking the time derivative of (5.22b) and setting it equal to (5.22a) gives,

$$F_x \delta\omega_{rot} = f_c \delta\dot{\omega}_{rot} \tag{5.23}$$

Using the linearized rotor equation of motion, this can be written with index notation as,

$$F_x \delta\omega_{rot} = f_c(A_{11} + A_{12} f_c + B F_x)\delta\omega_{rot} \tag{5.24}$$

Solving this for F_x gives,

$$F_x = \frac{A_{11} f_c + A_{12} f_c^2}{1 - f_c B} \tag{5.25}$$

Currently there are two unknowns, F_x and f_c, with a single equation. A second equation can be formulated based on the desired eigenvalue placement for the $\delta\omega_{rot}$ state. This is formulated as,

$$\det(sI - (A_{11} + A_{12} f_c + B F_x)) = s - p_{des} \tag{5.26}$$

where p_{des} is the desired eigenvalue. Solving for f_c gives,

$$f_c = \frac{-A_{11} - B F_x + p_{des}}{A_{12}} \tag{5.27}$$

Together, (5.25) and (5.27) provide two equations with two unknowns. Using the resulting F_x will provide the desired transient response based on the eigenvalue placement. For a closed-loop rotor speed perturbation eigenvalue at -0.5, $F_x = 0.22031$, creating an arbitrarily fast rotor response like before.

To track λ_{opt}, the ideal DTC law is incorporated and can be written as,

$$\delta\dot{c} = F_x\delta\omega_{rot} + F_d\delta v \tag{5.28}$$

Computing the disturbance gain, F_d, can be done using the DTC equations used in the section before, but analyzing (5.28) for hypothetical operation provides an easier method. It's known that perturbed CVT ratio rate should always be zero at steady state. Assuming a wind speed perturbation of 1 m/s and knowing the desired rotor speed perturbation is λ_{opt}/r, the disturbance gain is solved as $F_d = -F_x\lambda_{opt}/r$. For the -0.5 rotor speed eigenvalue, this gives $F_d = -0.08570$ The same multi-step disturbance input used in Figures 5.1, 5.2, and 5.3 is simulated with this ideal DTC controller. The results are satisfactory with perfect

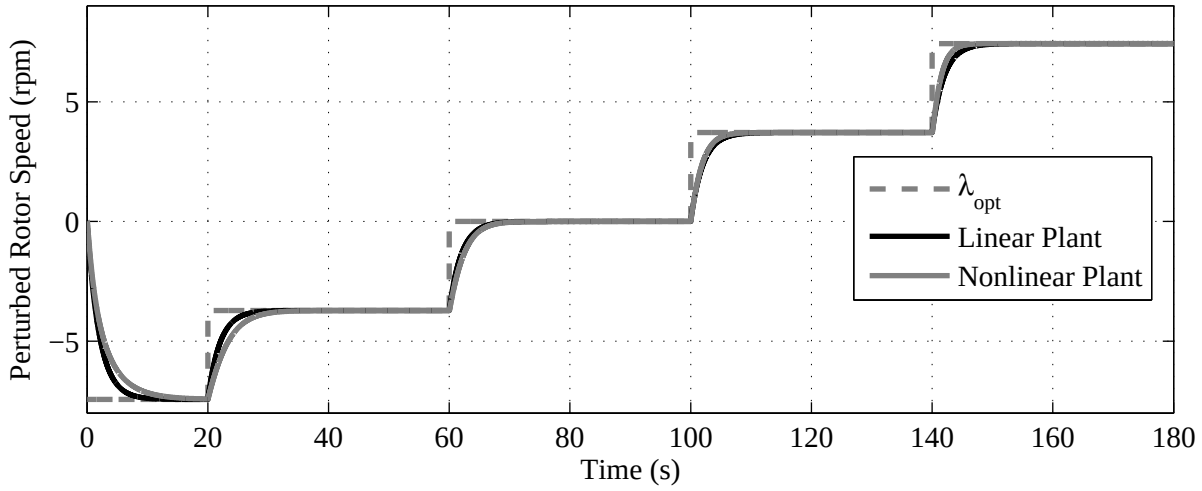

Figure 5.4: Rotor speed for 2-state ideal DTC with multi-step wind input

tracking of λ_{opt}, thanks to ideal DTC. The linear and nonlinear simulations are in close agreement, even far from the operating point. Now that ideal DTC has been demonstrated to work for the 2-state model, the rotor speed eigenvalue is retuned to respond like typical Region 2 control, i.e. $p_{des} = -0.1232$. This gives $F_x = 0.055321$ and $F_d = -0.0215204$.

Designing an LTI observer, for DTC, based on the 2-state model results in good disturbance estimation and λ_{opt} tracking when simulated with the LTI plant. However, simulation with the nonlinear model results in undesirable behavior due to poor disturbance estimation. Other methods should be considered for estimating the disturbance if it cannot be measured directly. One idea would be to use the observer based on $\delta\tau_{load}$ input, see previous section. This topic will not be considered further here and is suggested for future research. This thesis will use the ideal DTC law of this model for remaining simulations.

5.3 3-State Model

The same general procedures used to design 1-state DTC are used here, except now the model is 3-state. Also, typical torque realizable damper (TTRD) controllers will be designed for Region 2 and 3. The control objectives for this 3-state model now include adding drivetrain damping since a torsion mode exists with the LSS and MSS having finite stiffness. The state space representation for the 3-state system is written as,

$$\begin{aligned} \dot{x} &= A \begin{bmatrix} \delta\omega_{rot} \\ K_d\Big(\delta\theta_{rot} - \dfrac{\delta\theta_{cvt,i}}{N}\Big) \\ \delta\omega_{cvt,i} \end{bmatrix} + B \begin{bmatrix} \delta\tau_{load} \\ \delta\beta \end{bmatrix} + \Gamma\delta v \\ y &= C \begin{bmatrix} \delta\omega_{rot} \\ K_d\Big(\delta\theta_{rot} - \dfrac{\delta\theta_{cvt,i}}{N}\Big) \\ \delta\omega_{cvt,i} \end{bmatrix} \end{aligned} \tag{5.29}$$

where the state equation was previously given by (2.53), refer to it for A, B, and Γ. Rotor speed, in rad/s, will be the only output, thus $C = \begin{bmatrix} 1 & 0 & 0 \end{bmatrix}$.

5.3.1 Region 2

The FAST linearization at the usual operating point of (4.5) is used to obtain the linearized aerodynamic torque terms. The drivetrain equivalent torsional damping coefficient, C_d, is set to zero, while an equivalent stiffness of $K_d = 2.691 \times 10^7$ N-m/rad is used. This is the equivalent torsional stiffness determined for the normal, non-CVT, CART. Since the CVT CART of this research is only hypothetical and a model with geometrical and material properties is not considered, no estimation is available for the equivalent stiffness of the LSS and MSS components. Considering the normal CART gearbox and the CVT ratio range used in this research, and hence the torques experienced by the shafts, it's thought that the equivalent stiffness of such a system would closely compare to that of the normal CART. For practical implementation, higher fidelity models and modal analysis would be required. The result of evaluating the state matrix, control input matrix for $\delta\tau_{load}$ only (since $\delta\beta = 0$), and disturbance input matrix, is given as,

$$A = \begin{bmatrix} -0.04527 & -3.108 \times 10^{-6} & 0 \\ 2.691 \times 10^7 & 0 & -6.234 \times 10^5 \\ 0 & 1.035 \times 10^{-3} & 0 \end{bmatrix}, \quad B = \begin{bmatrix} 0 \\ 0 \\ -0.04466 \end{bmatrix}, \quad \Gamma = \begin{bmatrix} 0.05368 \\ 0 \\ 0 \end{bmatrix} \tag{5.30}$$

The controllability matrix is computed for the pair $\{A, B\}$ and found to have a rank of 3, which equals the number of states, hence the system is controllable. First consider the open-loop eigenvalues,

$$p_1 = -0.0401, \quad p_{2,3} = -0.0026 \pm 27\mathrm{i} \tag{5.31}$$

where the first eigenvalue corresponds to the transient response of the rotor speed state, like in the 1-state model, while the two complex values represent the drivetrain torsion mode. Since the pair $\{A, B\}$ is controllable, the feedback gain matrix, F_x, can be used to adjust the transient response of the system by assigning the eigenvalues of the closed-loop system to new locations in the complex plane.

Like the 1-state equation, this model is also tuned to have a rotor speed response similar to that of the typical control system of Region 2. Again, this is done by assigning the closed-loop eigenvalue to -0.1232. As for the drivetrain torsion mode, these closed-loop eigenvalues should be placed further to the left in the complex plane to add damping. Physically, this damping gets added by actuating the CVT to produce a load torque that counteracts the vibratory torque present due to the flexible shaft. Moving the real part of the complex eigenvalues to -1 quickly damps the drivetrain torsion mode. The feedback gain matrix is calculated using the MATLAB place() command, which gives $F_x = \begin{bmatrix} -1312.5 & 4.158 \times 10^{-5} & 46.64 \end{bmatrix}$.

5.3.1.1 Disturbance Tracking Control

This control method refers to T2 in Table 5.1. To implement the DTC feedback law of (5.11), equations (5.9) and (5.10) must be solved to determine the disturbance feedback gain. Rewriting (5.10) gives,

$$BF_d = -\Gamma\Theta + LG - (A + BF_x)L \tag{5.32}$$

where $L = Q$ if $C = I$, the identity matrix. For the 1-state system, the value of Q was chosen to proportionally relate the rotor speed to the wind speed. For the 3-state system, $Q \in \mathbb{R}^{3\times 1}$, and Q_1 is set to ω_{rot_o}/v_o like it was for the 1-state model. If the zero terms for

this 3-state model are set to zero, then (5.32) is written with matrix index notation as,

$$\begin{bmatrix} 0 \\ 0 \\ b_3 \end{bmatrix} F_d = \begin{bmatrix} -\gamma_1 - a_{11}Q_1 - a_{12}Q_2 \\ -a_{21}Q_1 - a_{23}Q_3 \\ -b_3 f_1 Q_1 - (a_{32} + b_3 f_2)Q_2 - b_3 f_3 Q_3 \end{bmatrix} \tag{5.33}$$

This gives three equations with three unknowns: Q_2, Q_3, and F_d. Solve for Q_2 and Q_3,

$$Q_2 = \frac{-a_{11}Q_1 - \gamma_1}{a_{12}}, \quad Q_3 = \frac{-a_{21}Q_1}{a_{23}} \tag{5.34}$$

Computing Q_1 and using the numerical matrices of (5.30), this results in $Q_2 = 1.1603 \times 10^4$ and $Q_3 = 16.792$. This leads to solving (5.33) for the disturbance gain, giving $F_d = -3.3177$.

Following the same steps used in the 1-state model, an observer is now designed for use with the DTC control law. The observability matrix is computed for the pair $\{\bar{A}, \bar{C}\}$ and found to have a rank of 4, which equals the sum of plant and disturbance states, thus the pair is observable. Now $\bar{K}$ must be chosen such that convergence of the estimator error is sufficiently fast. Using the MATLAB place() command to locate the poles of $(\bar{A} - \bar{K}\bar{C})$ at -10, -11, -15 $\pm$ 27i gives $\bar{K} = \begin{bmatrix} 50.955 & -2.5822 \times 10^8 & -4.9355 \times 10^3 & 3.0308 \times 10^3 \end{bmatrix}^\top$. This complete DTC controller with observer will actuate the CVT in nonlinear simulations.

5.3.1.2 Typical Torque with Realizable Damper

An alternative method for tracking λ_{opt} while also damping the drivetrain torsion mode is to use TT control for Region 2 with a realizable drivetrain damper designed at the Region 2 operating point, (4.5). This will command the CVT ratio rate to create load torque as a function of shaft speed squared while allowing perturbations about that for drivetrain

damping. This control method refers to R2 in Table 5.1. This is illustrated in Figure 5.5. The Region 2 TT controller was already designed and tested in section 3.1. The other aspect

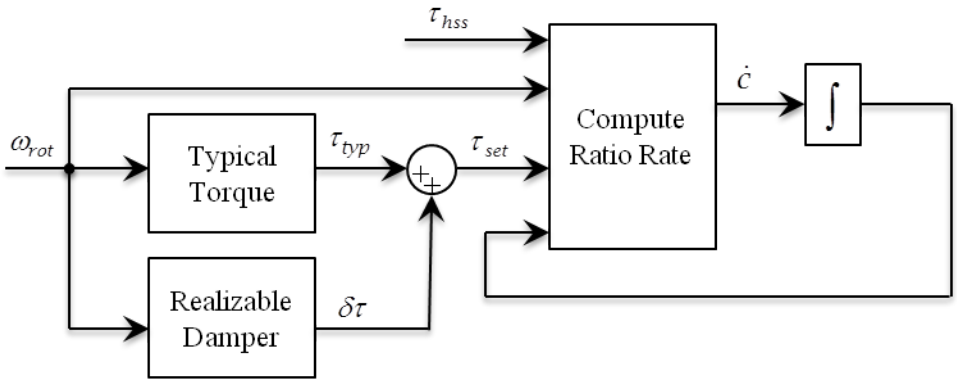

Figure 5.5: Block diagram illustration of implementing TTRD in the context of CVT

is to design a realizable drivetrain damper.

The objective of the realizable drivetrain damper is to add damping, not to track or accommodate disturbances. Therefore, the feedback law excludes any disturbances. Only the transient response of the drivetrain torsion mode is tuned via the feedback gain matrix, F_x, moving the corresponding closed-loop eigenvalues to the same location as the DTC controller above. This gives $F_x = \begin{bmatrix} -1933.0 & -3.573 \times 10^{-5} & 44.78 \end{bmatrix}$. To avoid measuring all states, an observer is used so that only rotor speed needs measured. The observer is different than the one used above for DTC since the disturbance state does not need estimated. Thus, only the estimator gain matrix, K_x, is used. This is tuned the same as the DTC controller above.

5.3.2 Region 2.5

The controller used here is like the one used for TT control. The main difference is the interpolation of Region 2 and 3 torque commands now includes torque perturbations, therefore active drivetrain damping is also expected for Region 2.5.

5.3.3 Region 3

The commanded CVT ratio rate for Region 3 is based on the setpoint torque of the typical law, τ_{rated}, except the setpoint will not be fixed for the 3-state model. The setpoint torque will consist of the usual rated torque summed with a torque perturbation computed by a realizable damping controller. In other words, the setpoint torque will be allowed to deviate from the rated torque in order to actively damp the drivetrain torsion mode in Region 3. This slightly variable setpoint torque is then achieved by commanding the CVT ratio rate like is done for TT control. This is similar to Region 2, except the typical torque is different and the realizable damper is based on a different operating point. Refer back to Figure 5.5 for an illustration of this control process.

The realizable drivetrain damper design is based on transient response characteristics only. There is no need to track or accommodate the disturbance, only to damp the drivetrain torsion mode. Therefore, DTC and DAC theory are not needed. However, an observer for the plant states is used to minimize measurements. The state equation matrices are evaluated at the same Region 3 operating point used for the PI pitch controller, see (C.5).

$$A = \begin{bmatrix} -0.1330 & -3.108 \times 10^{-6} & 0 \\ 2.691 \times 10^{7} & 0 & -6.234 \times 10^{5} \\ 0 & 1.035 \times 10^{-3} & 0 \end{bmatrix}, \quad B = \begin{bmatrix} 0 \\ 0 \\ -0.04466 \end{bmatrix}, \quad \Gamma = \begin{bmatrix} 0.08056 \\ 0 \\ 0 \end{bmatrix} \tag{5.35}$$

where B is the torque disturbance input gain matrix only. The pitch input is ignored since the pitch controller is designed to affect only rotor speed response.

The controllability matrix for the pair $\{A, B\}$ is found to have a rank of 3, thus the pair is controllable. The open-loop eigenvalues are $p_1 = -0.1177$ and $p_{2,3} = -0.0076 \pm 27\text{i}$,

where the realizable damper is tuned to have faster complex eigenvalues. The eigenvalue corresponding to rotor speed should be unaffected by the realizable damper. The eigenvalues of $(A+BF_x)$ are assigned in the complex plane using the MATLAB place() command, which gives $F_x = \begin{bmatrix} -1.295 \times 10^3 & -1.575 \times 10^{-5} & 30.00 \end{bmatrix}$. The state estimator must be tuned by selecting an estimator gain, K_x, to quickly converge estimates of the plant states. The eigenvalues of $(A - K_x C)$ are assigned to -10 and -15 $\pm$ 27i with the MATLAB place() command, giving $K_x = \begin{bmatrix} 40.87 & -1.787 \times 10^8 & -8.233 \times 10^3 \end{bmatrix}^\top$. Notice there is no need for an estimator disturbance gain, K_d, since the disturbance state does not need estimating for the realizable damper.

5.4 Simulations

Simulations will be run for both Region 2 controllers based on the rigid drivetrain model, 1- and 2-state DTC, as well as both based on the flexible drivetrain model, 3-state DTC and TTRD control. For Region 3, the rigid models will use TT control for the CVT, while flexible models will use TTRD control. Region 2.5 will only be tested for the flexible configuration since it involves the new objective of damping the drivetrain torsion mode.

5.4.1 Region 2

The simple Region 2 wind input is simulated with the nonlinear rigid drivetrain model using 1- and 2-state DTC. The rotor speed and CVT ratio rate are plotted with the ideal λ_{opt} rotor speed as reference, see Figure 5.6. Both 1- and 2-state DTC controllers track λ_{opt} with some discrepancies. Comparing Figure 5.6 to Figure 3.2 shows these state space controllers respond similar to typical torque control, as intended. However, the λ_{opt} error

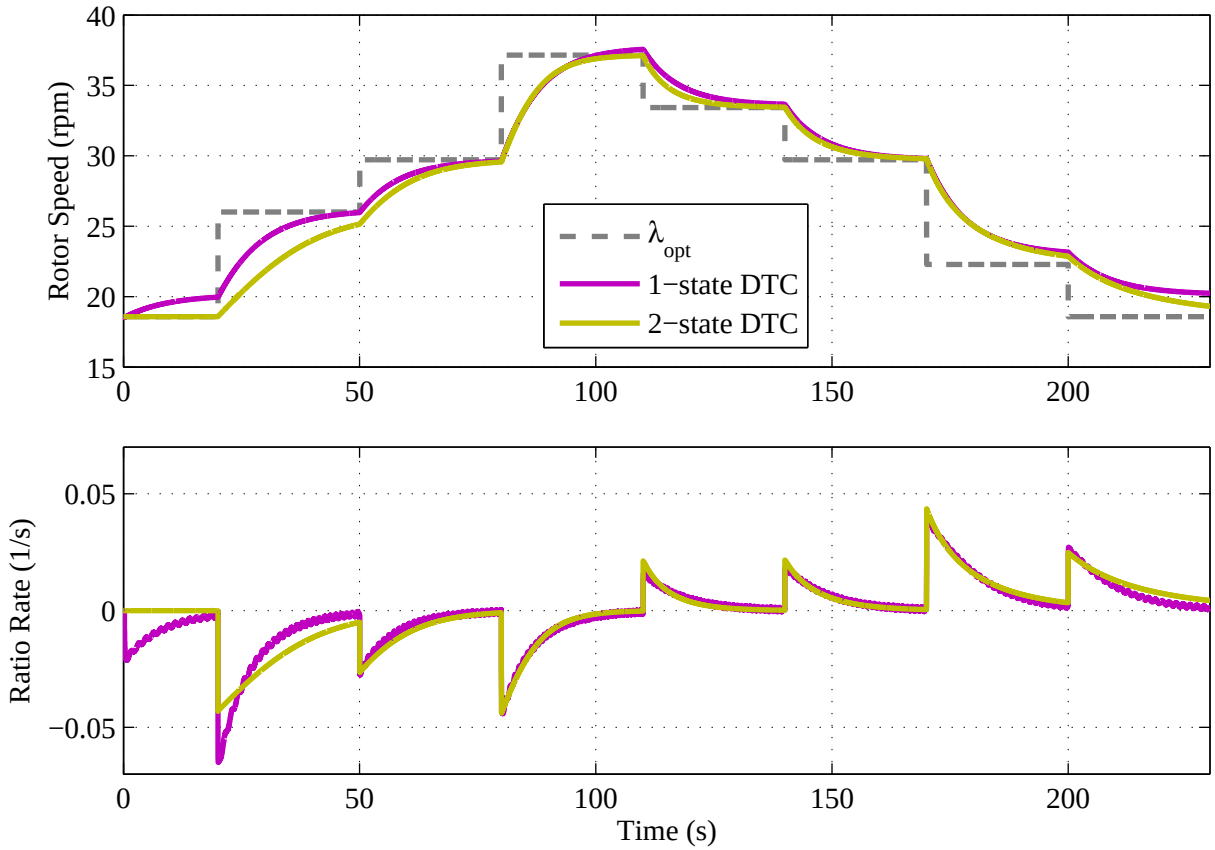

Figure 5.6: Rotor speed and ratio rate for 1- and 2-state DTC control with simple Region 2 wind input

is larger for 1-state DTC farther from the operating point of 8 m/s. For 2-state DTC, the rotor speed response is noticeably slow at wind speeds below the operating point.

The simple Region 2 wind input is now used to verify λ_{opt} tracking and damping abilities of 3-state DTC and TTRD control. The simulations are first run without enhancing drivetrain damping, i.e. the complex eigenvalues remain in their open-loop position. The rotor speed and CVT ratio rate are plotted with the ideal λ_{opt} rotor speed as reference, see Figure 5.7. Note, the initial conditions of the wind turbine are set to the operating point. Interestingly, the TT method has relatively good results even without a realizable damper. The DTC controller may seem acceptable when examining only rotor speed, however looking

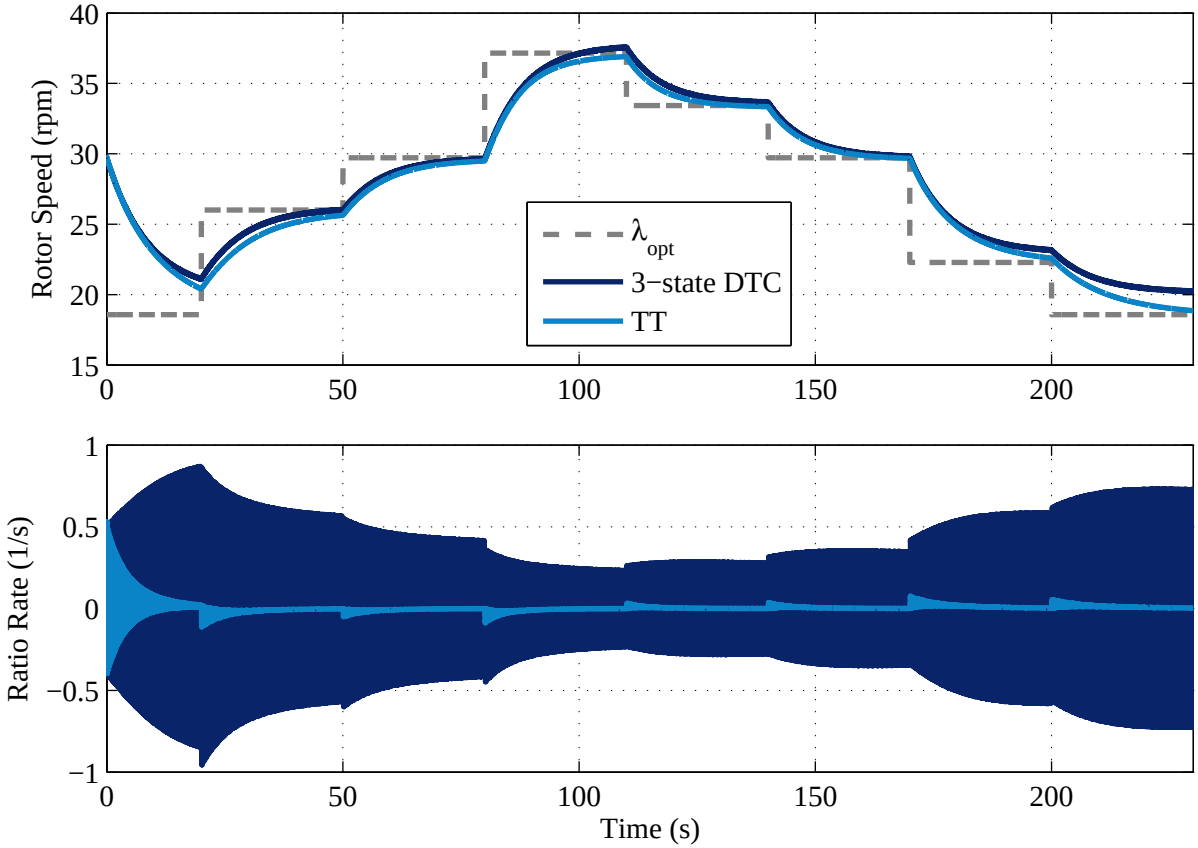

Figure 5.7: Rotor speed and ratio rate for 3-state DTC and TT without damping for simple Region 2 wind input

at the CVT ratio rate reveals a problem which results in high cyclic accelerations throughout the drivetrain. This would likely result in early fatigue failure, extreme loads, and unstable operation in a physical system.

The same 3-state controllers are now used with active drivetrain damping. The same multi-step simulation is run and results are in Figure 5.8. Again, the initial conditions of the wind turbine are set to the operating point. The results for both controllers are very similar. TTRD control tracks λ_{opt} better, but both provide good damping.

Lastly, all four Region 2 controllers tested above are simulated with the Region 2 turbulent input. For now, the drivetrain DOF is only turned on for simulations with controllers

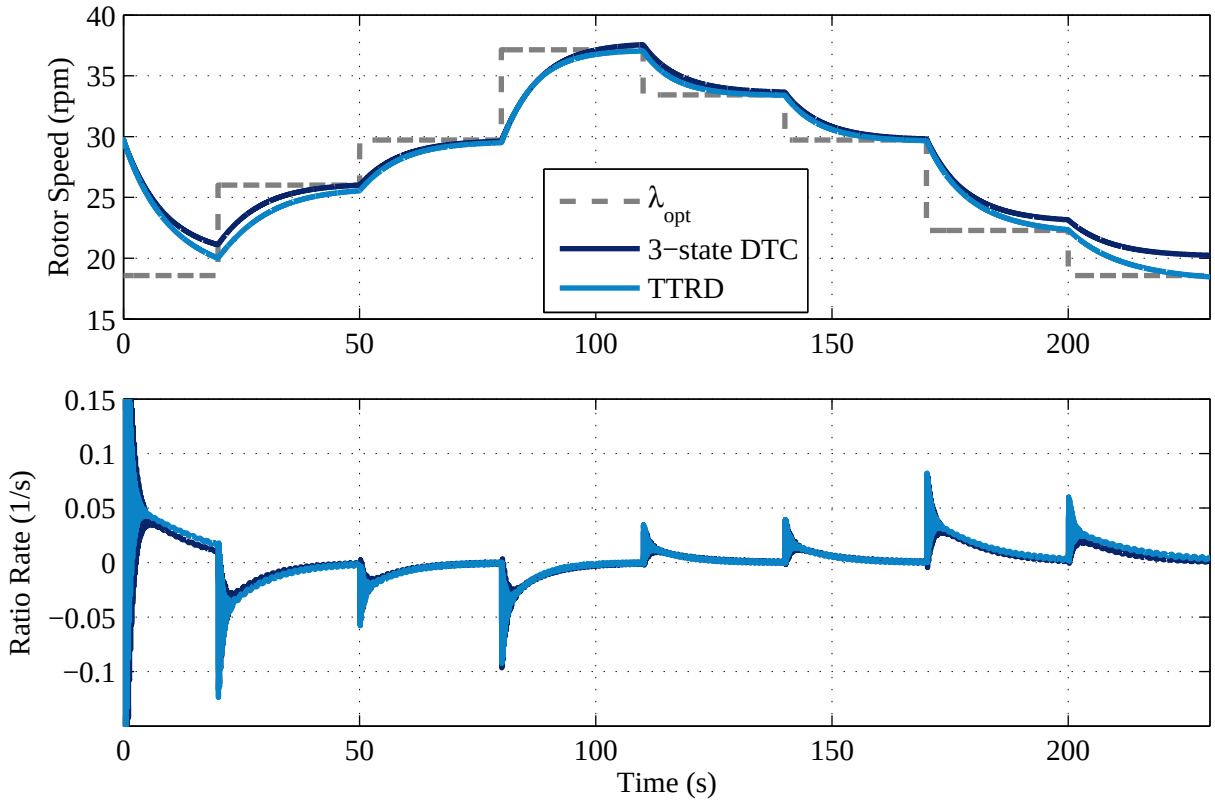

Figure 5.8: Rotor speed and ratio rate for 3-state DTC and TTRD for simple Region 2 wind input

that account for it, i.e. 3-state designs. Key results are presented in Table 5.2.

Parameter	**Units**	**1-s DTC**	**2-s DTC**	**3-s DTC**	**TTRD**
Max $\lvert\dot{\omega}_{rot}\rvert$	deg/s^2	6.038	7.578	5.835	6.024
RMS $\Delta\omega_{dr}$	rpm	n/a	n/a	1.036E-02	8.321E-03
Max $\lvert\dot{c}\rvert$	1/s	5.776E-02	8.604E-02	7.969E-02	7.063E-02
RMS $\dot{c}$	1/s	1.268E-02	1.517E-02	1.698E-02	1.670E-02
Max $\lvert\ddot{c}\rvert$	1/s^2	0.5251	18.93	1.278	1.129
Min ω_{gen}	rpm	1801.3	1800.1	1801.3	1801.4
Max $\lvert\dot{\omega}_{gen}\rvert$	deg/s^2	287.1	326.0	481.8	407.2
RMS $\Delta\lambda$	-	0.9162	0.8871	0.9182	0.9012
E_{cap}	kW-hr	25.93	25.84	25.93	25.90

Table 5.2: Data from state space controllers with Region 2 turbulent wind input

Looking at the rigid drivetrain models, 2-state DTC has less desirable statistics in almost every category, yet captures less energy. Its excessive control action results in highly variable drivetrain torque, a cause of fatigue. The CVT ratio rate and MSS torque for the two rigid drivetrain simulations are plotted in Figure 5.9.

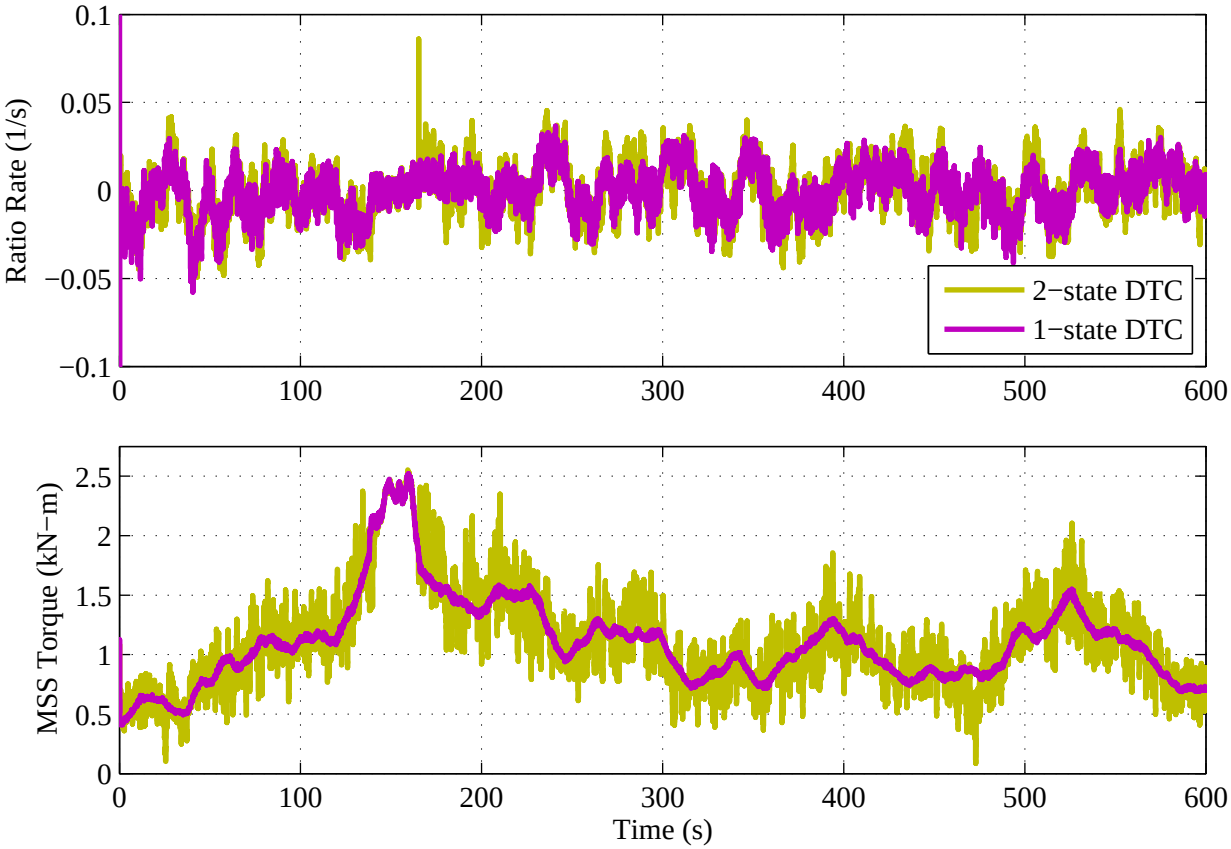

Figure 5.9: Ratio rate and MSS torque for 1- and 2-state DTC with full-field Region 2 wind input

Next, looking at the flexible drivetrain models, 3-state DTC and TTRD are very comparable in all categories. Plots of ratio rate and MSS torque are created to inspect for any noticeable differences, see Figure 5.10. From the figure, it appears 3-state DTC has slightly more aggressive control action, which agrees with Table 5.2. Both provide good drivetrain damping, with TTRD having the slight advantage, as indicated by the MSS torque plot.

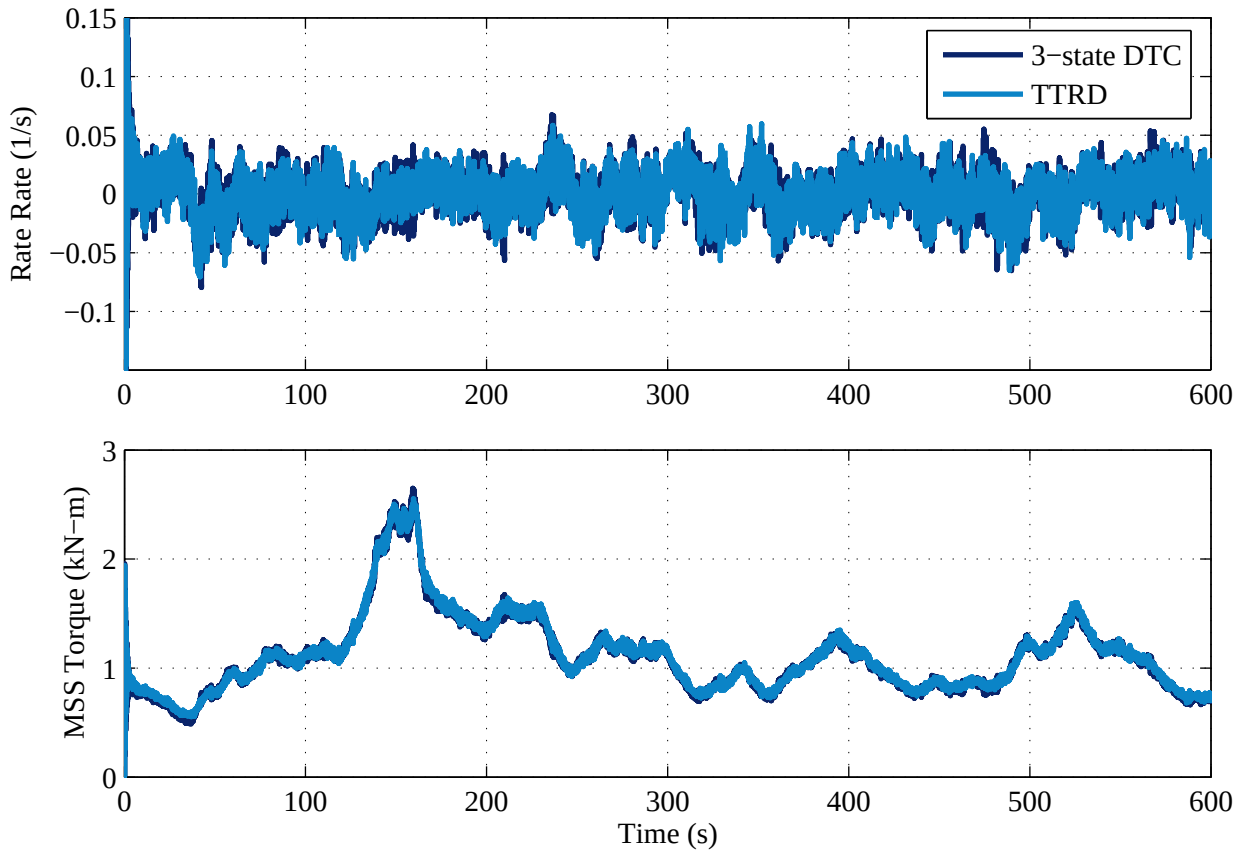

Figure 5.10: Ratio rate and MSS torque for 3-state DTC and TTRD with full-field Region 2 wind input

In summary, the 1- and 2-state DTC controllers proved to be stable and successful in tracking λ_{opt}, but 1-state DTC performed better. Tracking could be improved by designing multiple DTC observers at different operating points throughout Region 2, but this is left to future research. The 3-state DTC and TTRD controllers performed similarly for the rotationally-flexible drivetrain model, with TTRD having slightly less CVT control action.

5.4.2 Region 3

The flexible drivetrain model will be simulated using PI pitch control and TTRD CVT control. Remember, damping the drivetrain torsion mode was left entirely to the CVT

controller. To test its damping ability, the simple Region 3 wind input is simulated with the nonlinear model. The rotor speed and MSS torque are plotted in Figure 5.11 for both damping and no damping, i.e. TTRD and TT control, respectively. The difference made

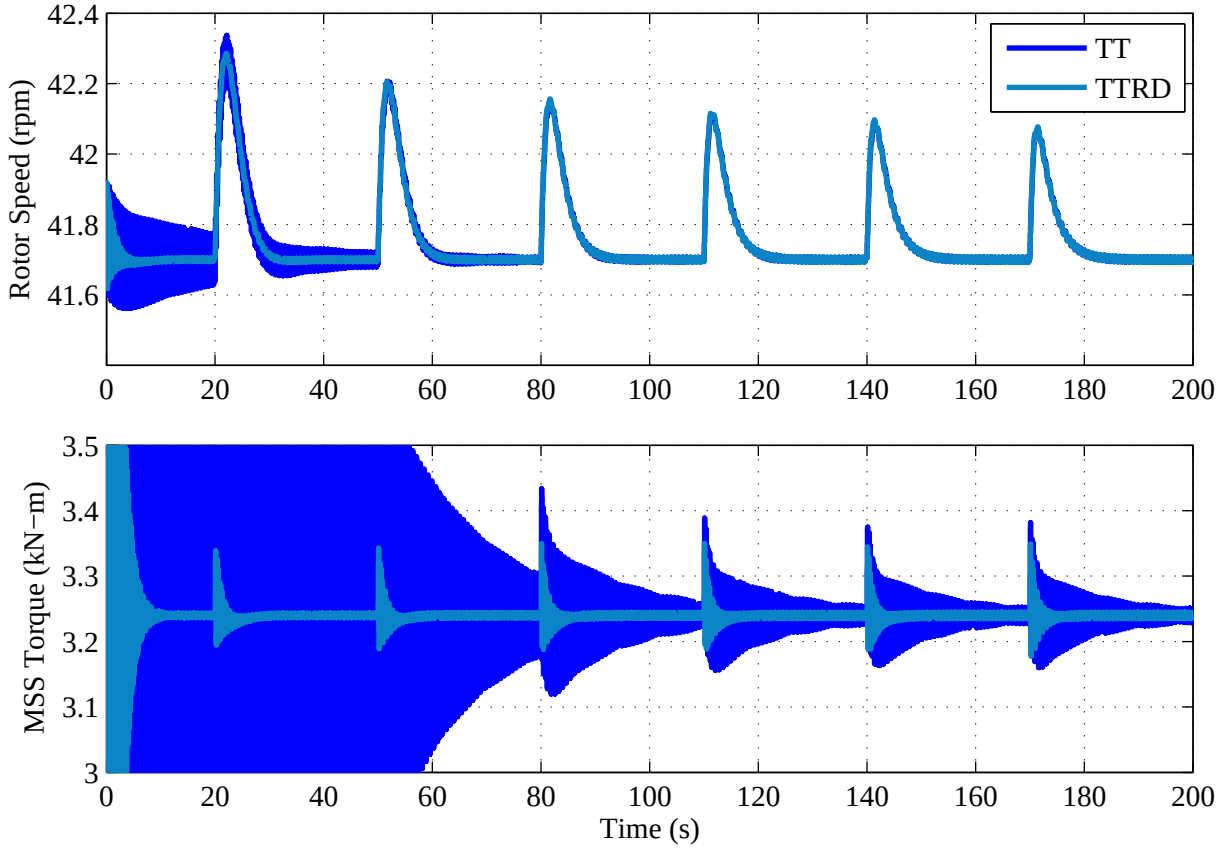

Figure 5.11: Rotor speed and MSS torque for TT and TTRD with simple Region 3 wind input

by adding damping becomes obvious when observing the MSS torque plot. The large and persistent oscillations encountered with TT control will lead to fatigue failure quicker than the small oscillations with TTRD control.

Lastly, both controller configurations used above for Region 3 are simulated with the Region 3 turbulent input. For now, the drivetrain DOF is only turned on for simulations with controllers that account for it, i.e. the 3-state designs. Key results are in Table 5.3.

Parameter	**Units**	**TT**	**TTRD**
Max $\lvert\dot{\beta}\rvert$	deg/s	4.234	4.445
RMS $\dot{\beta}$	deg/s	1.015	1.090
Max $\lvert\ddot{\beta}\rvert$	deg/s^2	74.29	88.60
Max ω_{rot}	rpm	43.37	43.39
RMS $\Delta\omega_{rot}$	rpm	0.4282	0.4332
Max $\lvert\dot{\omega}_{rot}\rvert$	deg/s^2	10.77	11.65
RMS $\Delta\omega_{dr}$	rpm	n/a	5.662E-02
Max $\lvert\dot{c}\rvert$	1/s	4.295E-02	1.308E-01
RMS $\dot{c}$	1/s	1.019E-02	3.472E-02
Max $\lvert\ddot{c}\rvert$	1/s^2	0.8078	3.207
Max ω_{gen}	rpm	1816.2	1816.5
RMS $\Delta\omega_{gen}$	rpm	0.5258	0.4991
Max $\lvert\dot{\omega}_{gen}\rvert$	deg/s^2	390.8	1202.8

Table 5.3: Data from state space controllers with Region 3 turbulent wind input

It's interesting to note that actuation of both the pitch system and CVT is more aggressive for the flexible drivetrain simulation. This was somewhat expected since the CVT is trying to damp the first drivetrain torsional mode.

5.4.3 Region 2 to 3

As with previous Region 2 to 3 simulations, smooth transitions between controllers is important. An additional objective for the flexible drivetrain model is to damp the first drivetrain torsion mode, like was done for Regions 2 and 3. Rather than designing a realizable damper in Region 2.5, the torque interpolation method is used but the interpolations are between the Region 2 damping controllers and the Region 3 TTRD controller.

Both 3-state Region 2 controllers are used with the Region 3 TTRD controller. To test their damping ability, the simple Region 2-3 wind input is simulated with the nonlinear

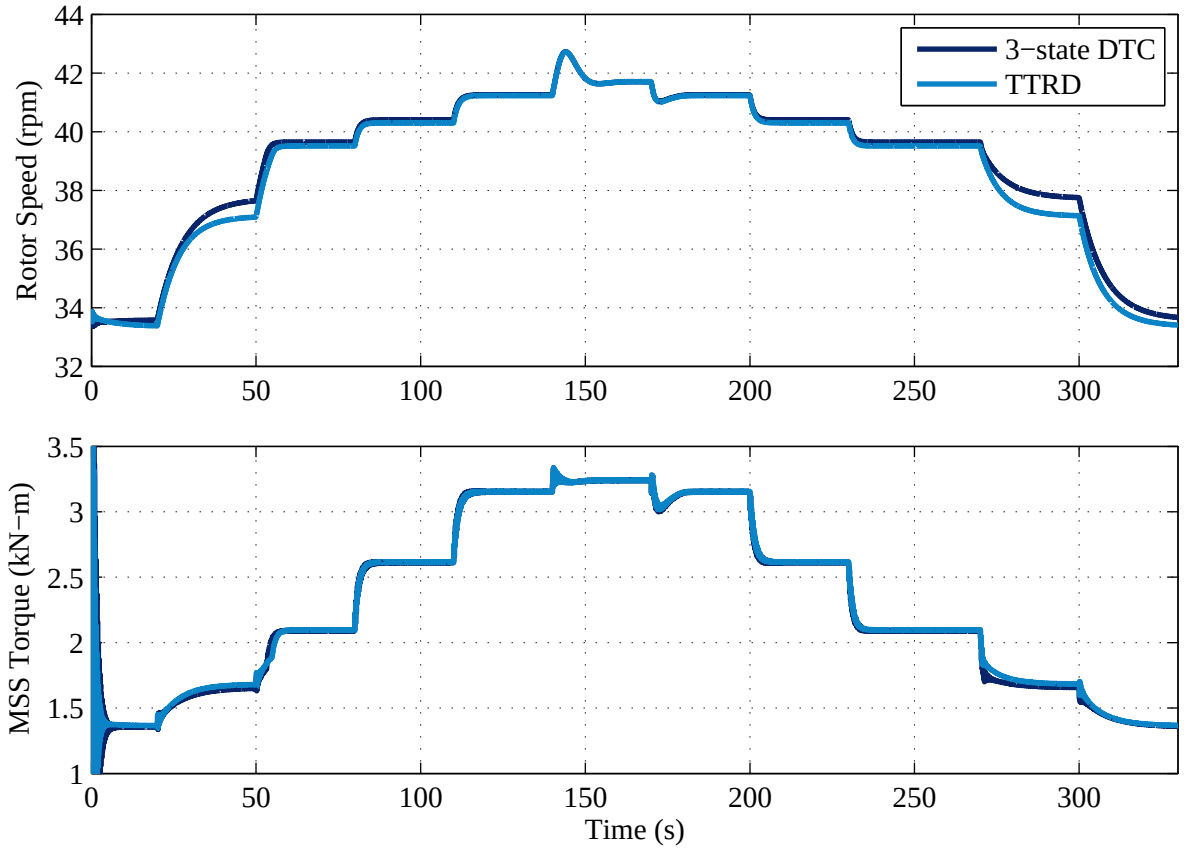

Figure 5.12: Rotor speed and MSS torque for 3-state DTC and TTRD with simple Region 2-3 wind input

model. The rotor speed and MSS torque are plotted in Figure 5.12. The results are satisfactory with smooth transitions and good damping overall.

Lastly, these controllers are used for the Region 2-3 turbulent input. Key results are in Table 5.4. Both controller setups perform similarly, with no clear advantages of one over the other. TTRD control has a lower RMS ratio rate, but higher peak ratio rate and acceleration. The CVT ratio rate and MSS torque are plotted in Figure 5.13 to better understand how these two setups compare. There is little to distinguish between the plots, much like Table 5.4. Using 3-state DTC for Region 2 appears to result in slightly more control action and oscillatory drivetrain behavior. The tabular results agree with this statement.

Parameter	Units	3-s DTC	TTRD
Max ω_{rot}	rpm	43.65	43.62
Max $\lvert\dot{\omega}_{rot}\rvert$	deg/s^2	10.20	9.482
RMS $\Delta\omega_{dr}$	rpm	4.029E-02	3.669E-02
Max $\lvert\dot{c}\rvert$	1/s	9.461E-02	1.035E-01
RMS $\dot{c}$	1/s	2.556E-02	2.359E-02
Max $\lvert\ddot{c}\rvert$	1/s^2	2.406	2.650
Max ω_{gen}	rpm	1816.4	1816.4
Max $\lvert\dot{\omega}_{gen}\rvert$	deg/s^2	862.7	946.1
E_{cap}	kW-hr	86.81	86.80

Table 5.4: Data from state space controllers with Region 2-3 turbulent wind input

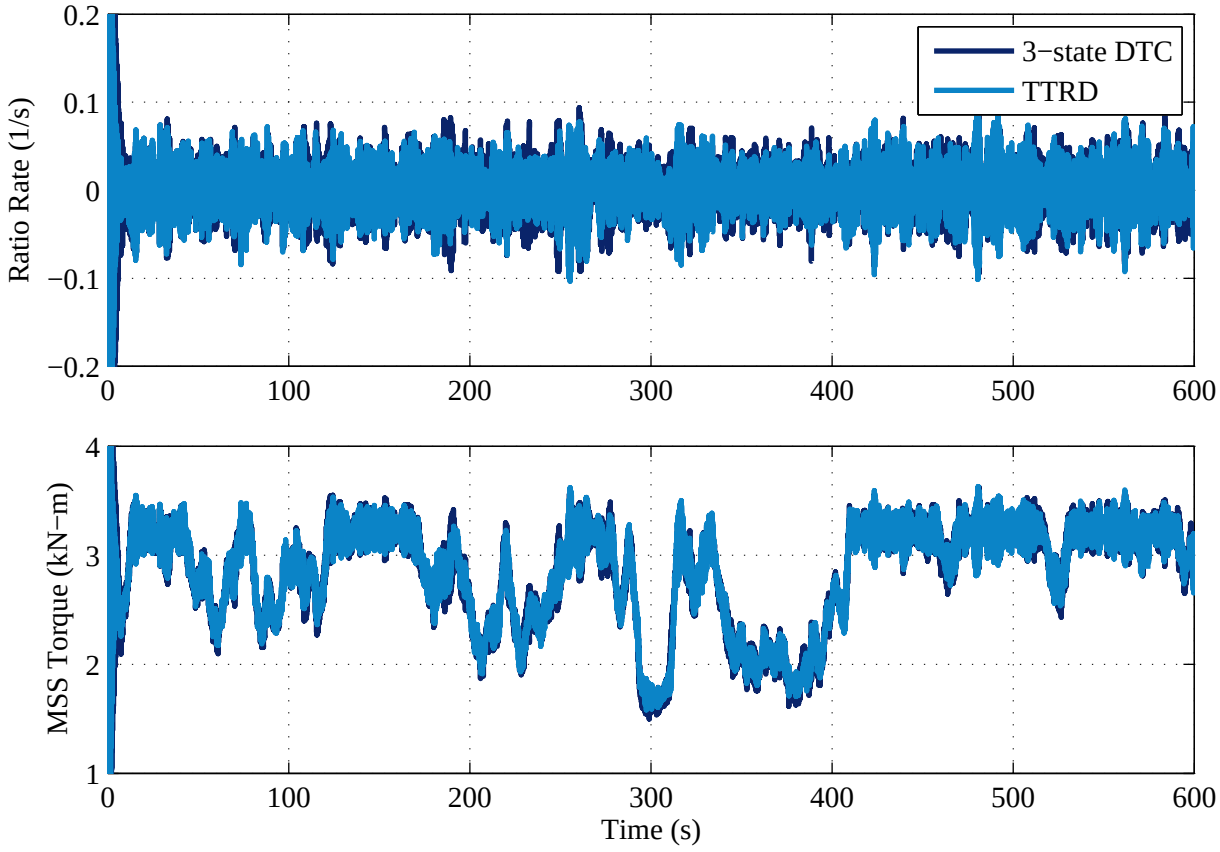

Figure 5.13: Ratio rate and MSS torque for 3-state DTC and TTRD with full-field Region 2-3 wind input

Chapter 6

Controller Comparisons

Many of controllers have been designed and tested for the CVT CART in this thesis, particularly for Region 2. Both rigid and flexible drivetrain linear control models were considered. To better understand the pros and cons of each, a systematic comparison will be done. To do this, the comparisons will be categorized by model fidelity as well as region of operation. Furthermore, only chosen controllers from previous chapters will be compared.

Region 2 comparisons will be narrowed down to the following controllers: TT, P-GS, 3-state DTC, and TTRD. The former two were designed from the rigid drivetrain linear model, and the latter two were designed from the torsional drivetrain linear model. This means the following controllers are excluded from the comparison: SSTT, OTR, PD, 1-state DTC, and 2-state DTC, which were all designed from the rigid drivetrain linear model.

Region 2.5 and 3 have little to compare. Region 2.5 always uses the interpolated torque method, but the resulting command adds drivetrain damping when Region 2 and 3 use CVT controllers that damp the first drivetrain torsion mode. For Region 3, TT and TTRD CVT control are compared, both accompanied by PI pitch control. The SSTT controller is ex-

cluded from the Region 3 comparisons.

The following table summarizes the comparisons to be performed. Notice, the comparisons are organized by DOF and region of operation. Only the controllers based on the linearized rigid drivetrain model are compared for the rigid drivetrain nonlinear simulations, but all controllers will be compared for higher fidelity simulation models.

	Region 2	**Region 2.5**	**Region 3**
Rigid Drivetrain	TT	TT	TT
	P-GS		
Additional DOF	TT	TT	TT
	P-GS		
	3-state DTC	TT	TTRD
	TTRD		

Table 6.1: Approach for CVT controller comparisons

6.1 Rigid Drivetrain

Simulations with only the rotor rotation DOF will be compared for the Region 2 turbulent input. For the rotor rotation model, the key objective is energy capture. Other interests are CVT actuator effort and drivetrain loading. Pertinent values from Tables 3.3 and 4.5 are compared in Table 6.2. The values from this table suggest TT control is less of a workload for the CVT but with better energy capture. The plot of CVT ratio rate, in Figure 6.1, compares the two simulations. It clearly illustrates that CVT control action is less demanding using the TT method. As a side note, recall SSTT results were also reported in Table 3.3 and found to be very similar to TT control. Therefore, TT and SSTT are the preferred methods of the rigid drivetrain models.

Parameter	Units	TT	P-GS
RMS $\dot{c}$	1/s	1.293E-02	1.723E-02
Max $\lvert\ddot{c}\rvert$	$1/s^2$	0.3315	1.481
RMS $\Delta\lambda$	-	0.9082	0.8648
E_{cap}	kW-hr	25.89	25.85

Table 6.2: Rigid drivetrain data comparison for full-field Region 2 wind input

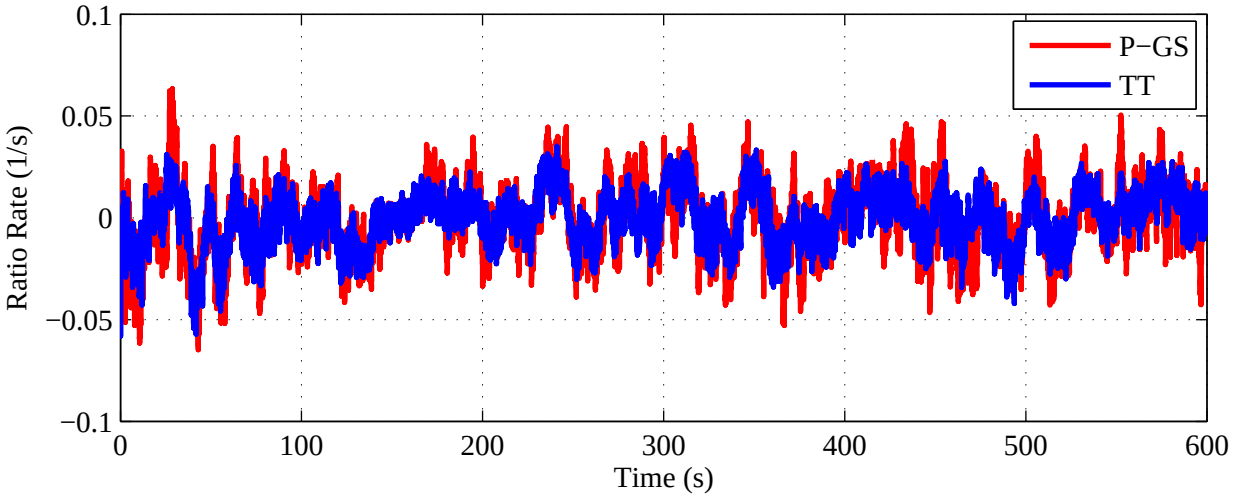

Figure 6.1: Ratio rate comparison for TT and P-GS with full-field Region 2 wind input

6.2 Flexible Drivetrain

Simulations with the drivetrain DOF active will be compared for all regions and controllers outlined in Table 6.1. Region 2.5 will only be compared with the TT versions of Region 2, i.e. TT and TTRD, one rigid and one flexible design. In summary, there will be four Region 2 comparisons, two Region 3 comparisons, and two Region 2.5 comparisons.

6.2.1 Region 2

The two main objectives in Region 2 are energy capture and drivetrain damping. Another interest is CVT actuator effort. Simulations, with the drivetrain DOF active, are

performed with the Region 2 turbulent input for TT and P-GS control. Pertinent values from these simulations and Table 5.2 are compared in Table 6.3.

Parameter	**Units**	**TT**	**P-GS**	**3-s DTC**	**TTRD**
RMS $\Delta\omega_{dr}$	rpm	1.314E-02	2.399E-02	1.036E-02	8.321E-03
RMS $\dot{c}$	1/s	2.008E-02	1.709E-02	1.698E-02	1.670E-02
Max $\lvert\ddot{c}\rvert$	$1/s^2$	1.697	3.021	1.278	1.129
RMS $\Delta\lambda$	-	0.9084	0.8682	0.9182	0.9012
E_{cap}	kW-hr	25.92	25.85	25.93	25.90

Table 6.3: Flexible drivetrain data comparison for Region 2 turbulent wind input

As expected, TT and P-GS control have the highest RMS of drivetrain twist rate, $\Delta\omega_{dr}$, suggesting they have the worst damping characteristics. Furthermore, TT and P-GS have the highest workload for the CVT according to the ratio rate and acceleration values reported. Similar energy capture is achieved with each controller, P-GS being the lowest.

To verify the results in Table 6.3, simulation plots are compared for the CVT ratio rate and MSS torque, see Figure 6.2. As both plots show, the conclusions drawn from the tabular results are correct, particularly with respect to drivetrain damping for P-GS control. The P-GS controller, as tuned and without filters, is not feasible for implementation into the physical system. Early fatigue failure, and perhaps instability, is likely to occur due to large cyclic torque loads. TT control provides a reasonable torque response but at the cost of slightly higher CVT ratio rates. As reviewed in the previous chapter, 3-state DTC and TTRD have similar results, with DTC having slightly more CVT control action and less drivetrain damping.

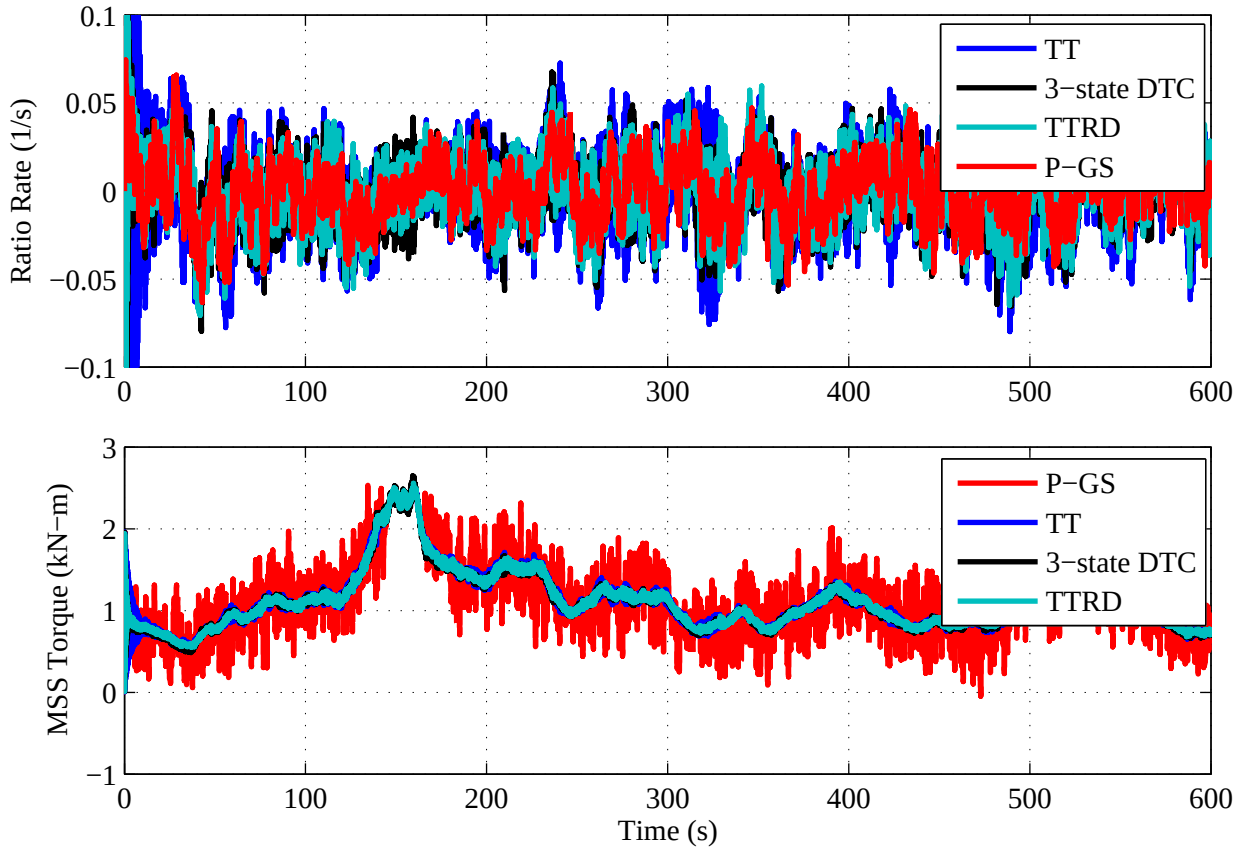

Figure 6.2: Ratio rate and MSS torque comparison for Region 2 controllers with flexible drivetrain and full-field wind input

6.2.2 Region 3

The two main objectives in Region 3 are power regulation and drivetrain damping. Another interest is CVT actuator effort. A simulation, with the drivetrain DOF active, is performed with the Region 3 turbulent input for TT CVT control and PI pitch control. Pertinent values from this simulation and Table 5.3 are compared in Table 6.4.

The values reported in Table 6.4 suggest TTRD performs better in nearly every category, as expected. To better understand the behavior of these controllers, simulation plots are generated. Generator power output is compared in Figure 6.3, since this is the primary objective for Region 3. The TT and TTRD Region 3 controllers regulate power output

Parameter	Units	TT	TTRD
Max $\|\dot{\beta}\|$	deg/s	5.122	4.445
RMS $\dot{\beta}$	deg/s	1.264	1.090
Max $\|\ddot{\beta}\|$	deg/s^2	111.7	88.60
Max ω_{rot}	rpm	43.36	43.39
RMS $\Delta\omega_{rot}$	rpm	0.4283	0.4332
RMS $\Delta\omega_{dr}$	rpm	1.133E-01	5.662E-02
RMS $\dot{c}$	1/s	6.522E-02	3.472E-02
Max $\|\ddot{c}\|$	1/s^2	24.06	3.207
Max ω_{gen}	rpm	1816.5	1816.5
RMS $\Delta\omega_{gen}$	rpm	0.5310	0.4991

Table 6.4: Flexible drivetrain data comparison for Region 3 turbulent wind input

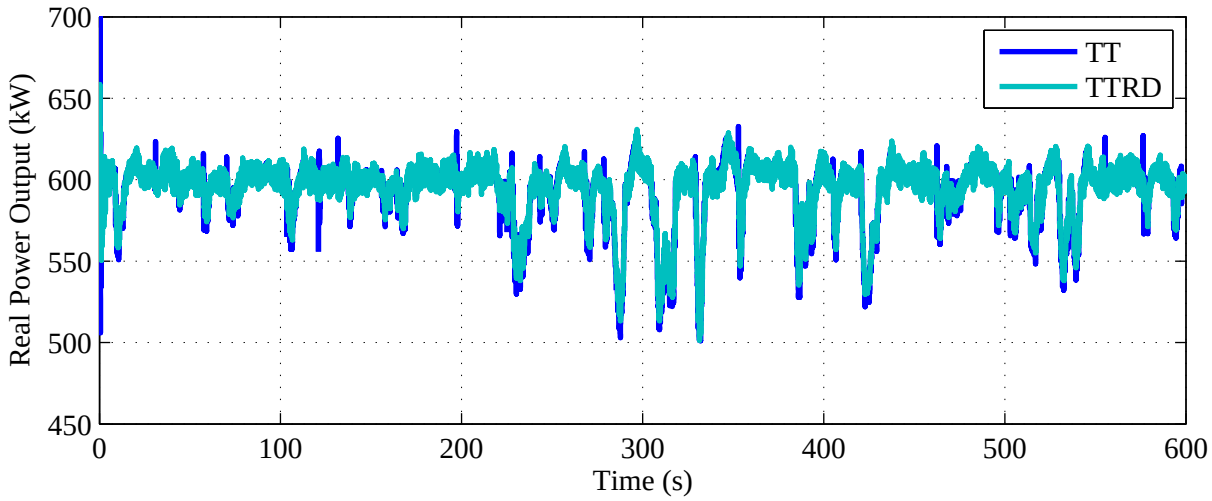

Figure 6.3: Generator power comparison for Region 3 controllers with flexible drivetrain and full-field wind input

similarly, but TTRD has fewer spikes, thus providing a smoother delivery of electrical power. To visualize drivetrain damping effectiveness, the MSS torque is compared in Figure 6.4. Not shown here, the CVT ratio rate plot looks similar, in shape, to the MSS torque plot. It's that using TTRD control is advantageous because the CVT workload is much less, energy capture is better, pitch rates are lower, and better drivetrain damping is achieved.

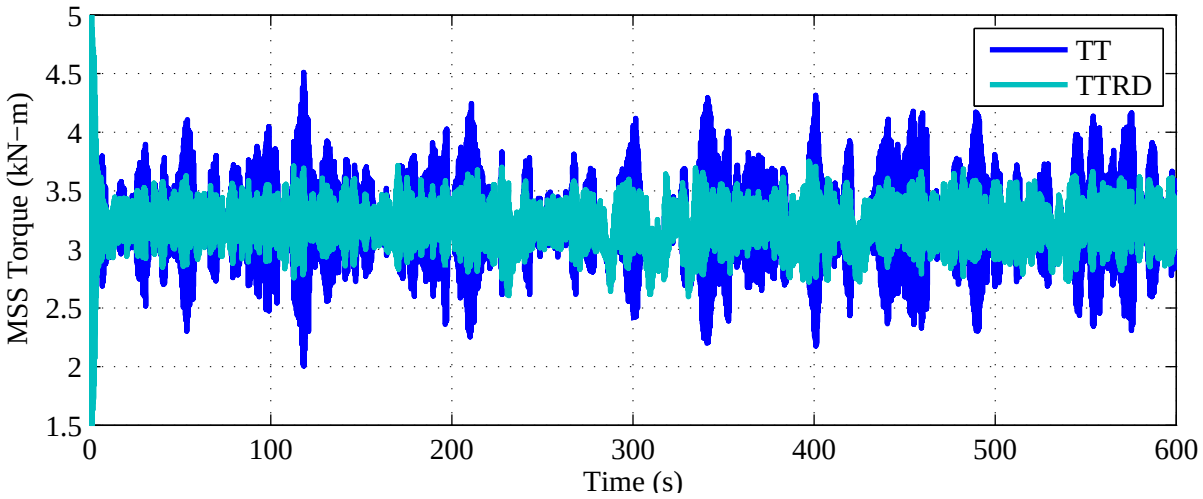

Figure 6.4: MSS torque comparison for Region 3 controllers with flexible drivetrain and full-field wind input

6.2.3 Region 2 to 3

The two main interests for transitions between Region 2 and 3 are smooth transitions and drivetrain damping. As always, CVT actuator effort is also a key interest. A simulation, with the drivetrain DOF active, is performed with the Region 2-3 turbulent input for TT control in Region 2, 2.5, and 3. PI pitch control is used to regulate rotor speed in Region 3. Pertinent values from this simulation and Table 5.4 are compared in Table 6.5.

Parameter	**Units**	**TT**	**TTRD**
Max ω_{rot}	rpm	43.62	43.62
RMS $\Delta\omega_{dr}$	rpm	7.168E-02	3.669E-02
Max $\lvert\dot{c}\rvert$	1/s	2.241E-01	1.035E-01
RMS $\dot{c}$	1/s	4.134E-02	2.359E-02
Max $\lvert\ddot{c}\rvert$	$1/s^2$	20.56	2.650
Max ω_{gen}	rpm	1816.4	1816.4

Table 6.5: Flexible drivetrain data comparison for Region 2-3 turbulent wind input

The results are analogous to the Region 3 comparison. TTRD control appears to have

the advantage again, particularly with better drivetrain damping and less CVT workload. To verify this, a plot of MSS torque is shown in Figure 6.5. Like above, the MSS torque is also a

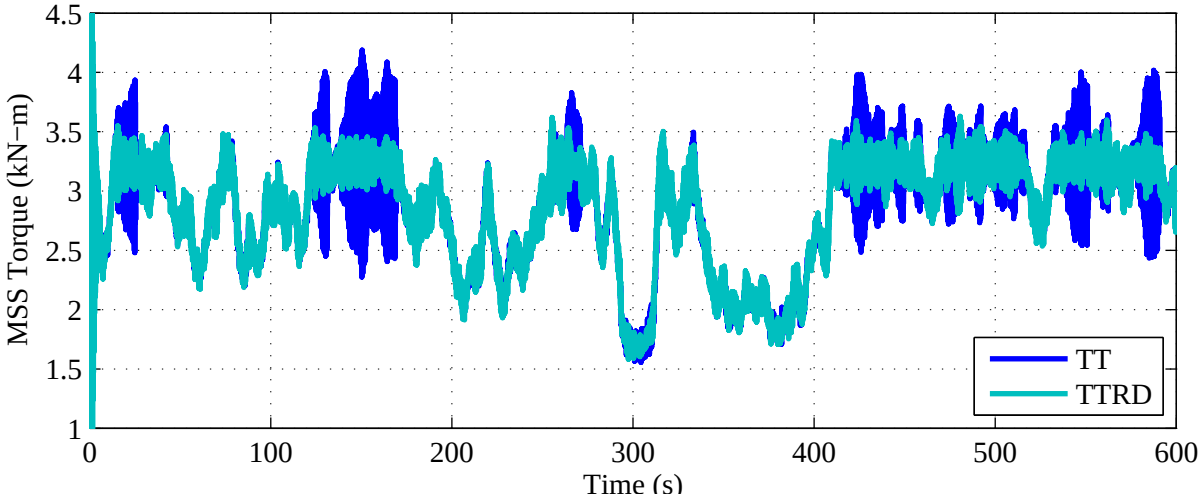

Figure 6.5: MSS torque comparison for Region 2-3 controllers with flexible drivetrain and full-field wind input

reflection of the CVT ratio rate, not shown here. It's concluded that drivetrain damping and CVT workload are much better for TTRD control, particularly when transitioning between Region 2 and 3.

6.3 Flexible System Load

As a final test, the controllers are now compared in simulations with the system load having rotational-flexibility, modeled as an equivalent torsional spring with no damping. The equivalent stiffness is subjectively chosen to result in torsional twist equal to that of the flexible drivetrain at rated load. This gives a stiffness of 6.181 $\times 10^5$ N-m/rad. Recall, the system load consists of the CVT, HSS, and generator connected to the electrical grid. None of the control models considered rotational-flexibility of these HSS components, therefore control is not exercised over the system load torsion mode. Since preliminary simulations,

not shown here, indicate problems with the Region 2.5 transitions, only Region 2 and 3 controllers will be tested with their respective turbulent inputs.

6.3.1 Region 2

Table 6.3 is reproduced by running simulations with the same wind turbine configurations, except now with the added DOF of a rotationally-flexible system load. The root mean square of system load twist rate, $\Delta\omega_{sl}$, is added to the table. Results are not reported

Parameter	**Units**	**TT**	**P-GS**	**3-s DTC**	**TTRD**
RMS $\Delta\omega_{dr}$	rpm	1.247E-02	n/a	9.663E-03	7.740E-03
RMS $\Delta\omega_{sl}$	rpm	5.985E-04	n/a	1.369E-03	1.212E-03
RMS $\dot{c}$	1/s	1.921E-02	n/a	1.647E-02	1.631E-02
Max $\lvert\ddot{c}\rvert$	$1/s^2$	1.864	n/a	1.146	1.066
RMS $\Delta\lambda$	-	0.9040	n/a	0.9170	0.9000
E_{cap}	kW-hr	25.83	n/a	25.92	25.90

Table 6.6: Flexible system load data comparison for Region 2 turbulent wind input

for P-GS control because simulations became unstable for this wind turbine setup. Interestingly, the results for TT control suggest it has the least damping of the drivetrain (LSS and MSS components), yet the best loading conditions for the system load (HSS components). TTRD control appears to have the best overall results with the best drivetrain damping, the smallest workload for CVT, and good energy capture.

To verify these results, graphical comparisons are now done with focus on drivetrain damping and HSS loading. Figure 6.6 shows plots of MSS torque and HSS torque as an indication of loading conditions. The HSS torque plot looks at only a small time frame of the simulation to help distinguish results. These plots agree with the conclusions reached

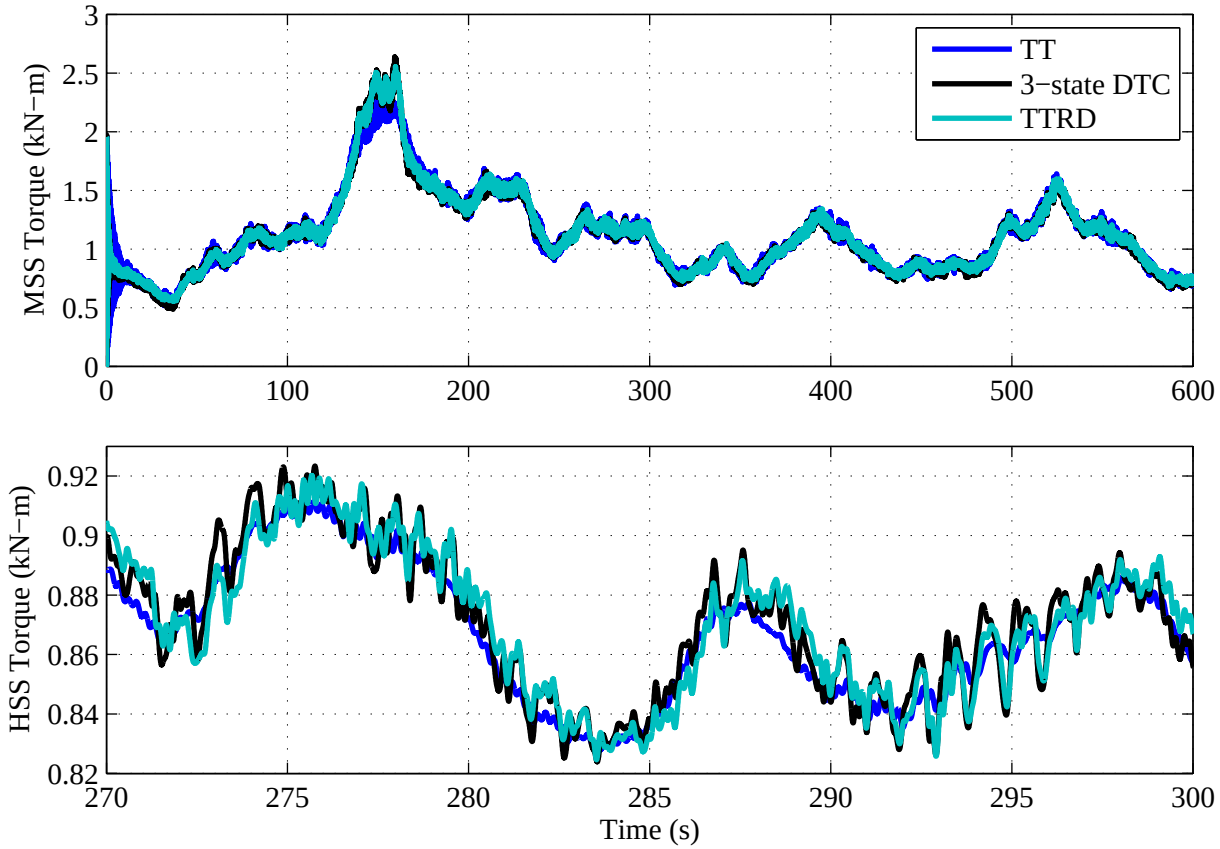

Figure 6.6: Shaft torque comparisons for Region 2 controllers with flexible drivetrain and system load for full-field wind input

from the values reported in Table 6.6. TT has the worst drivetrain damping but the best HSS loading conditions. TTRD control slightly outperforms 3-state DTC in both areas while having the smallest CVT workload.

6.3.2 Region 3

Table 6.4 is reproduced by running simulations with the same wind turbine configurations, only now with a rotationally-flexible system load, see Table 6.7. TTRD control outperforms TT control in nearly every parameter with the exception of HSS loading and power output regulation. TTRD control leads to reduced actuation for both pitch and CVT.

Parameter	**Units**	**TT**	**TTRD**
Max $\lvert\dot{\beta}\rvert$	deg/s	8.838	5.216
RMS $\dot{\beta}$	deg/s	1.525	1.113
Max ω_{rot}	rpm	43.69	43.69
RMS $\Delta\omega_{rot}$	rpm	0.5161	0.5242
RMS $\Delta\omega_{dr}$	rpm	1.637E-01	5.311E-02
RMS $\Delta\omega_{sl}$	rpm	4.992E-03	5.293E-03
RMS $\dot{c}$	1/s	9.469E-02	3.302E-02
Max $\lvert\ddot{c}\rvert$	$1/s^2$	15.73	3.128
Max ω_{gen}	rpm	1816.4	1816.5
RMS $\Delta\omega_{gen}$	rpm	0.2086	0.2181

Table 6.7: Flexible system load data comparison for Region 3 turbulent wind input

Graphical comparisons are now done to verify the conclusions of Table 6.7. The electrical power output and MSS torque are plotted in Figure 6.7. TT control regulates power with less amplitude in its oscillations, but it does result in higher frequencies (not noticeable on this time scale). The HSS torque response, not shown here, is a reflection of power output plot, as expected since rotor speed is regulated. This means TT control exhibits better HSS loading conditions, but at the cost of MSS loading conditions as the MSS torque plot shows. The CVT ratio rate, not shown here, is a reflection of MSS torque. Therefore, TTRD control not only provides better damping of the first drivetrain torsion mode, but does so with less CVT control action while sacrificing minor HSS loading conditions.

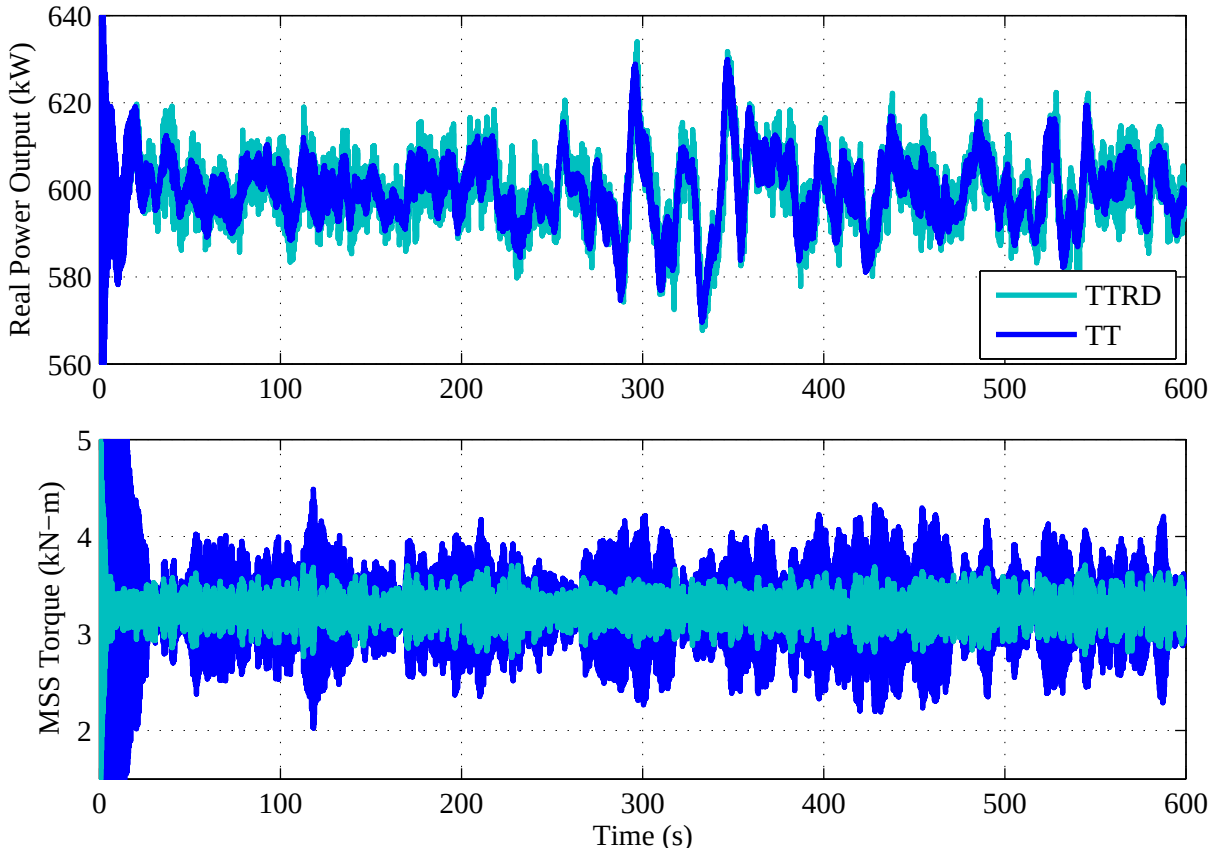

Figure 6.7: Generator power and MSS torque comparisons for Region 3 controllers with flexible drivetrain and system load for full-field wind input

Chapter 7

Conclusions and Future Work

The study of CVT control, for a grid-connected wind turbine, in this thesis moved beyond the usual proof-of-concept found in previous research by analytically and systematically designing and tuning controllers using various methods. The perspective of viewing the system load as the CVT coupled with the electrical generator was introduced as a means of understanding how a CVT is capable of controlling the torque at its input. Control of this torque is valuable for achieving control objectives in all regions considered here.

To study a wind turbine system using a CVT in its drivetrain, mathematical models were derived for the most relevant physical phenomena. Linearization of these models was required for linear control theory to be applied. Simulation codes, AeroDyn/FAST and MATLAB/Simulink, were used to model the complete system, including controllers for CVT and pitch, in an environment that uses numerical integration to solve equations of motion.

Three different approaches were used for controller design. First, typical torque control was shown how it can be implemented in the context of a CVT. This approach relied on the system load perspective mentioned above. The advantages of this approach are: 1) not based

on linearized models and 2) no knowledge of wind speed is needed. The key disadvantage is that knowledge of HSS torque is required. Next, classical control theory, often used in previous CVT research, was used with various tuning methods for proportional, PD, and PID controllers, including the use of gain scheduling. The key advantage of this approach it that little knowledge of the system is required, unless analytically tuning. The big disadvantage is that knowledge of hub-height wind speed is required. Lastly, modern control theory was used to design DTC and realizable drivetrain dampers for use with typical torque control. The key advantages of this approach are: 1) enhanced damping of the first drivetrain torsion mode, and 2) no knowledge of wind speed is needed. The key disadvantage, applying only to the typical torque approach is that knowledge of HSS torque is required. In summary, entire control systems ranging from start-up through rated conditions were designed, implemented, and simulated with nonlinear plant models using full-field turbulent wind inputs.

7.1 Conclusive Results

Various controller designs, based on rigid and flexible drivetrain models, were compared for turbulent flow simulations of the nonlinear model with rotor rotation, drivetrain twist, and system load twist degrees of freedom. For the rigid drivetrain model in Region 2, the TT controller outperformed the P-GS controller in terms of better energy capture and lower CVT workload. Given that P-GS uses a wind speed measurement, it becomes even less attractive. For the flexible drivetrain model, P-GS results suggest it's infeasible for practical implementation due to its excessive drivetrain torque fluctuations. The most attractive option, for all regions tested, was TTRD control. It proved to have the best damping characteristics, lowest CVT workload, good energy capture, lowest corresponding pitch rates,

and best power regulation. The 3-state DTC controller also performed well with slightly less favorable results than TTRD. For the flexible system load model, TTRD control again had the most favorable performance statistics in Region 2, except for HSS loading conditions where TT control had the smallest torque fluctuations. In Region 3, TTRD again has favorable results over TT control in nearly all areas of performance except the HSS loading conditions, which includes power output regulation. These results suggest damping the first drivetrain torsion mode leads to more HSS excitation. This is understandably the case since the CVT is utilizing the inertia and torque of its output side to create an input torque that counteracts vibrations of the first drivetrain torsion mode. The thorough comparison of CVT controllers led to the identification of which methods achieve the control objectives best.

This research has focused on the continued development of wind turbine technology as part of a global effort to reduce the COE for wind turbines. This thesis considered model development, controller design, and simulation for a wind turbine with a CVT in its drivetrain. The decoupling it provides between the aerodynamic rotor and generator dynamics allows their inherently mismatched torque characteristics to be manipulated such that desirable torque mappings can be used to achieve control objectives. This ability enables variable-speed operation, thus tracking optimal aerodynamic efficiency in Region 2, without the use of typical frequency-conversion PE. Drivetrain torque regulation was also achieved with CVT control, enabling power regulation in Region 3 when used in conjunction with an active pitch controller to regulate rotor speed. Lastly, drivetrain damping characteristics can be enhanced by including the associated physical phenomena in the CVT control model. Together, these various abilities of CVT could lead to a cost-effective drivetrain design with improved energy capture, power regulation, and reliability.

7.2 Suggestions

The progress made in this thesis towards advancing wind turbine technology is only a beginning for CVTs. One of the large steps forward is to design, implement, and test these controls on a drivetrain dynamometer or actual wind turbine system. Either setup would ideally allow drivetrain stiffness parameters to be adjusted for the purpose of completing parametric studies associated with active drivetrain damping. Before practical implementation is fully considered, many other suggestions are made for building onto the research found in this thesis.

Listed below are suggestions for future work in wind turbine CVT technology. Discussion of key items is found after the itemized list.

- Improve transitions between Region 2 and 3.
- Relationship between load torque and CVT parameters for high fidelity CVT models.
- Region 3 CVT controller design for variable-speed stall, eliminating the pitch system.
- Drivetrain fatigue analysis and gearbox reliability.
- Cost comparison of wind turbine designs with CVT, PE, and direct-drive generators.
- Adaptive control to accommodate modeling errors and improve performance.
- Analysis of the OTR law with CVT to understand the tradeoffs.
- Design of CVTs for large scale wind, requiring high operating torques.
- Operation with induction generator connected to a weak grid.
- Simulations using aerodynamic modeling based on generalized dynamic-wake theory.
- High fidelity simulations using multi-body dynamics codes such as ADAMS.

A suggestion for improving the Region 2 to 3 transitions is to use a single high-order polynomial curve fit to the ideal setpoint torque for Region 2, 2.5, and 3. This would avoid using

conditional statements to switch between controllers for each region. Due to its importance in controller design for any CVT controller involving a setpoint torque, the relationship between the CVT input torque, ratio, and ratio rate should be studied in detail for higher fidelity models. To further improve COE reductions, a variable-speed stall CVT controller could eliminate the need for a pitch system. The stall controller would work by varying rotor speed such that aerodynamic stall limits the power coefficient enough to regulate power output. Unfortunately, with current CVT technology, a gearbox would be required for any practical implementation due to the high LSS torques. Given the history of gearbox failures in industry, in-depth study of CVT drivetrain reliability is suggested. Lastly, a wind turbine cost comparison between a typical PE system, CVT, and direct-drive generator is suggested. The PE approach has been most common to date, but CVT and direct-drive are emerging. Direct-drive addresses the serious issue of gearbox failures by eliminating it entirely, but at the cost of a large, unique, expensive generator and PE for variable-speed. The many suggestions in the itemized list as well as others mentioned throughout this thesis, are ways of moving forward in the quest for advancements in wind turbine technology and ultimately reducing the COE.

APPENDICES

Appendix A

Simulation Files

A.1 FAST

Figures A.1 through A.6 illustrate a version of the FAST input file used to model the CART in this research. The blade and tower property files, not shown here, can be found at [32].

```
------------------------------------------------------------------------
------- FAST INPUT FILE -------------------------------------------------
Model of the 2-bladed Controls Advanced Research Turbine (CART) at NREL/NWTC.
Compatible with FAST v7.00.00.
---------------------- SIMULATION CONTROL --------------------------------
False       Echo            - Echo input data to "echo.out" (flag)
  1         ADAMSPrep       - ADAMS preprocessor mode {1: Run FAST, 2: use FAST as
  1         AnalMode        - Analysis mode {1: Run a time-marching simulation, 2: create a
  2         NumBl           - Number of blades (-)
 600.0      TMax            - Total run time (s)
 0.004      DT              - Integration time step (s)
---------------------- TURBINE CONTROL -----------------------------------
  0         YCMode          - Yaw control mode {0: none, 1: user-defined from routine User
9999.9      TYCOn           - Time to enable active yaw control (s) [unused when YCMode
  2         PCMode          - Pitch control mode {0: none, 1: user-defined from routine Pitc
```

Figure A.1: FAST input file for modeling the CART, part 1

```
  0.0      TPCOn          - Time to enable active pitch control (s) [unused when PCMode
  3        VSContrl       - Variable-speed control mode {0: none, 1: simple VS, 2: user-
1781.98    VS_RtGnSp      - Rated generator speed for simple variable-speed generator co
3524.36    VS_RtTq        - Rated generator torque/constant generator torque in Region 3
.0008992   VS_Rgn2K       - Generator torque constant in Region 2 for simple variable-spe
 23.05     VS_SlPc        - Rated generator slip percentage in Region 2 1/2 for simple var
  1        GenModel       - Generator model {1: simple, 2: Thevenin, 3: user-defined from
True       GenTiStr       - Method to start the generator {T: timed using TimGenOn, F: g
True       GenTiStp       - Method to stop the generator {T: timed using TimGenOf, F: w
  0.0      SpdGenOn       - Generator speed to turn on the generator for a startup (HSS s
  0.0      TimGenOn       - Time to turn on the generator for a startup (s) [used only when
9999.9     TimGenOf       - Time to turn off the generator (s) [used only when GenTiStp=T
  1        HSSBrMode      - HSS brake model {1: simple, 2: user-defined from routine Use
9999.9     THSSBrDp       - Time to initiate deployment of the HSS brake (s)
9999.9     TiDynBrk       - Time to initiate deployment of the dynamic generator brake [C
9999.9     TTpBrDp(1)     - Time to initiate deployment of tip brake 1 (s)
9999.9     TTpBrDp(2)     - Time to initiate deployment of tip brake 2 (s)
9999.9     TTpBrDp(3)     - Time to initiate deployment of tip brake 3 (s) [unused for 2 bla
9999.9     TBDepISp(1)    - Deployment-initiation speed for the tip brake on blade 1 (rpm)
9999.9     TBDepISp(2)    - Deployment-initiation speed for the tip brake on blade 2 (rpm)
9999.9     TBDepISp(3)    - Deployment-initiation speed for the tip brake on blade 3 (rpm)
9999.9     TYawManS       - Time to start override yaw maneuver and end standard yaw co
9999.9     TYawManE       - Time at which override yaw maneuver reaches final yaw angle
  0.0      NacYawF        - Final yaw angle for yaw maneuvers (degrees)
9999.9     TPitManS(1)    - Time to start override pitch maneuver for blade 1 and end star
9999.9     TPitManS(2)    - Time to start override pitch maneuver for blade 2 and end star
9999.9     TPitManS(3)    - Time to start override pitch maneuver for blade 3 and end star
9999.9     TPitManE(1)    - Time at which override pitch maneuver for blade 1 reaches fin
9999.9     TPitManE(2)    - Time at which override pitch maneuver for blade 2 reaches fin
9999.9     TPitManE(3)    - Time at which override pitch maneuver for blade 3 reaches fin
 -1.0      BlPitch(1)     - Blade 1 initial pitch (degrees)
 -1.0      BlPitch(2)     - Blade 2 initial pitch (degrees)
  0.0      BlPitch(3)     - Blade 3 initial pitch (degrees) [unused for 2 blades]
  0.0      BlPitchF(1)    - Blade 1 final pitch for pitch maneuvers (degrees)
  0.0      BlPitchF(2)    - Blade 2 final pitch for pitch maneuvers (degrees)
  0.0      BlPitchF(3)    - Blade 3 final pitch for pitch maneuvers (degrees) [unused for 2
---------------------- ENVIRONMENTAL CONDITIONS -------------------------------
 9.80665   Gravity        - Gravitational acceleration (m/s^2)
---------------------- FEATURE FLAGS ------------------------------------------
False      FlapDOF1       - First flapwise blade mode DOF (flag)
False      FlapDOF2       - Second flapwise blade mode DOF (flag)
```

Figure A.2: FAST input file for modeling the CART, part 2

```
False       EdgeDOF          - First edgewise blade mode DOF (flag)
False       TeetDOF          - Rotor-teeter DOF (flag) [unused for 3 blades]
True        DrTrDOF          - Drivetrain rotational-flexibility DOF (flag)
True        GenDOF           - Generator DOF (flag)
False       YawDOF           - Yaw DOF (flag)
False       TwFADOF1         - First fore-aft tower bending-mode DOF (flag)
False       TwFADOF2         - Second fore-aft tower bending-mode DOF (flag)
False       TwSSDOF1         - First side-to-side tower bending-mode DOF (flag)
False       TwSSDOF2         - Second side-to-side tower bending-mode DOF (flag)
True        CompAero         - Compute aerodynamic forces (flag)
False       CompNoise        - Compute aerodynamic noise (flag)
---------------------- INITIAL CONDITIONS ---------------------------------------
  0.0       OoPDefl          - Initial out-of-plane blade-tip displacement (meters)
  0.0       IPDefl           - Initial in-plane blade-tip deflection (meters)
  0.0       TeetDefl         - Initial or fixed teeter angle (degrees) [unused for 3 blades]
  0.0       Azimuth          - Initial azimuth angle for blade 1 (degrees)
 20.32      RotSpeed         - Initial or fixed rotor speed (rpm)
  0.0       NacYaw           - Initial or fixed nacelle-yaw angle (degrees)
  0.0       TTDspFA          - Initial fore-aft tower-top displacement (meters)
  0.0       TTDspSS          - Initial side-to-side tower-top displacement (meters)
---------------------- TURBINE CONFIGURATION ------------------------------------
 21.336     TipRad           - The distance from the rotor apex to the blade tip (meters)
  1.381     HubRad           - The distance from the rotor apex to the blade root (meters)
  1         PSpnElN          - Number of the innermost blade element which is still part of th
  0.000     UndSling         - Undersling length [distance from teeter pin to the rotor apex] (
  0.210     HubCM            - Distance from rotor apex to hub mass [positive downwind] (m
 -3.858     OverHang         - Distance from yaw axis to rotor apex [3 blades] or teeter pin [
 -1.098     NacCMxn          - Downwind distance from the tower-top to the nacelle CM (m
  0.0       NacCMyn          - Lateral  distance from the tower-top to the nacelle CM (meter
  1.734     NacCMzn          - Vertical distance from the tower-top to the nacelle CM (meter
 34.862     TowerHt          - Height of tower above ground level [onshore] or MSL [offsho
  1.734     Twr2Shft         - Vertical distance from the tower-top to the rotor shaft (meters)
  0.0       TwrRBHt          - Tower rigid base height (meters)
 -3.77      ShftTilt         - Rotor shaft tilt angle (degrees)
  0.0       Delta3           - Delta-3 angle for teetering rotors (degrees) [unused for 3 blad
  0.0       PreCone(1)       - Blade 1 cone angle (degrees)
  0.0       PreCone(2)       - Blade 2 cone angle (degrees)
  0.0       PreCone(3)       - Blade 3 cone angle (degrees) [unused for 2 blades]
  0.0       AzimB1Up         - Azimuth value to use for I/O when blade 1 points up (degrees)
---------------------- MASS AND INERTIA -----------------------------------------
  0.0       YawBrMass        - Yaw bearing mass (kg)
```

Figure A.3: FAST input file for modeling the CART, part 3

```
29113.0     NacMass             - Nacelle mass (kg)
5852.0      HubMass             - Hub mass (kg)
  0.0       TipMass(1)          - Tip-brake mass, blade 1 (kg)
  0.0       TipMass(2)          - Tip-brake mass, blade 2 (kg)
  0.0       TipMass(3)          - Tip-brake mass, blade 3 (kg) [unused for 2 blades]
71750.0     NacYIner            - Nacelle inertia about yaw axis (kg m^2)
 22.39  !34.4   GenIner          - Generator inertia about HSS (kg m^2) --- CVT: GenIner = Ils
15000.0     HubIner             - Hub inertia about rotor axis [3 blades] or teeter axis [2 blades
---------------------- DRIVETRAIN --------------------------------------------
 100.0      GBoxEff             - Gearbox efficiency (%)
 100.0      GenEff              - Generator efficiency [ignored by the Thevenin and user-define
 43.165     GBRatio             - Gearbox ratio (-)
False       GBRevers            - Gearbox reversal {T: if rotor and generator rotate in opposite
6000.0      HSSBrTqF            - Fully deployed HSS-brake torque (N-m)
  0.5       HSSBrDT             - Time for HSS-brake to reach full deployment once initiated (s
""          DynBrkFi            - File containing a mech-gen-torque vs HSS-speed curve for a
 2.691E7    DTTorSpr            - Drivetrain torsional spring (N-m/rad)
  0.0       DTTorDmp            - Drivetrain torsional damper (N-m/(rad/s))
---------------------- SIMPLE INDUCTION GENERATOR ----------------------------
  0.001     SIG_SlPc            - Rated generator slip percentage (%) [used only when VSCont
1799.98     SIG_SySp            - Synchronous (zero-torque) generator speed (rpm) [used only
1799.98     SIG_RtTq            - Rated torque (N-m) [used only when VSContrl=0 and GenM
  2.0       SIG_PORt            - Pull-out ratio (Tpullout/Trated) (-) [used only when VSContrl=
---------------------- THEVENIN-EQUIVALENT INDUCTION GENERATOR ---------------
 60.0       TEC_Freq            - Line frequency [50 or 60] (Hz) [used only when VSContrl=0
  4         TEC_NPol            - Number of poles [even integer > 0] (-) [used only when VSC
  0.0185    TEC_SRes            - Stator resistance (ohms) [used only when VSContrl=0 and Ge
  0.017     TEC_RRes            - Rotor resistance (ohms) [used only when VSContrl=0 and Ge
 480.0      TEC_VLL             - Line-to-line RMS voltage (volts) [used only when VSContrl=0
  0.0340    TEC_SLR             - Stator leakage reactance (ohms) [used only when VSContrl=0
  0.0050    TEC_RLR             - Rotor leakage reactance (ohms) [used only when VSContrl=0
  0.7750    TEC_MR              - Magnetizing reactance (ohms) [used only when VSContrl=0 a
---------------------- PLATFORM ----------------------------------------------
  0         PtfmModel           - Platform model {0: none, 1: onshore, 2: fixed bottom offshore,
""          PtfmFile            - Name of file containing platform properties (quoted string) [un
---------------------- TOWER -------------------------------------------------
 15         TwrNodes            - Number of tower nodes used for analysis (-)
"CART_Tower.dat" TwrFile        - Name of file containing tower properties (quoted string)
---------------------- NACELLE-YAW -------------------------------------------
  0.0       YawSpr              - Nacelle-yaw spring constant (N-m/rad)
  0.0       YawDamp             - Nacelle-yaw damping constant (N-m/(rad/s))
```

Figure A.4: FAST input file for modeling the CART, part 4

```
  0.0         YawNeut              - Neutral yaw position--yaw spring force is zero at this yaw (de
---------------------- FURLING ---------------------------------------------
False         Furling              - Read in additional model properties for furling turbine (flag)
""            FurlFile             - Name of file containing furling properties (quoted string) [unus
---------------------- ROTOR-TEETER ----------------------------------------
  1           TeetMod              - Rotor-teeter spring/damper model {0: none, 1: standard, 2: us
  0.0         TeetDmpP             - Rotor-teeter damper position (degrees) [used only for 2 blade
  4.0e4       TeetDmp              - Rotor-teeter damping constant (N-m/(rad/s)) [used only for 2
  0.0         TeetCDmp             - Rotor-teeter rate-independent Coulomb-damping moment (N
  0.0         TeetSStP             - Rotor-teeter soft-stop position (degrees) [used only for 2 blad
 180.0        TeetHStP             - Rotor-teeter hard-stop position (degrees) [used only for 2 bla
  1.0         TeetSSSp             - Rotor-teeter soft-stop linear-spring constant (N-m/rad) [used
  5.0e6       TeetHSSp             - Rotor-teeter hard-stop linear-spring constant (N-m/rad) [used
---------------------- TIP-BRAKE -------------------------------------------
  0.0         TBDrConN             - Tip-brake drag constant during normal operation, Cd*Area (m
  0.0         TBDrConD             - Tip-brake drag constant during fully-deployed operation, Cd*
  0.0         TpBrDT               - Time for tip-brake to reach full deployment once released (sec
---------------------- BLADE -----------------------------------------------
"CART_Blades.dat"      BldFile(1) - Name of file containing properties for blade 1 (quoted string)
"CART_Blades.dat"      BldFile(2) - Name of file containing properties for blade 2 (quoted string)
"CART_Blades.dat"      BldFile(3) - Name of file containing properties for blade 3 (quoted string)
---------------------- AERODYN ---------------------------------------------
"CART_AD01.ipt"  ADFile           - Name of file containing AeroDyn input parameters (quoted str
---------------------- NOISE -----------------------------------------------
""          NoiseFile             - Name of file containing aerodynamic noise input parameters (
---------------------- ADAMS -----------------------------------------------
""          ADAMSFile             - Name of file containing ADAMS-specific input parameters (qu
---------------------- LINEARIZATION CONTROL -------------------------------
""          LinFile               - Name of file containing FAST linearization parameters (quotec
---------------------- OUTPUT ----------------------------------------------
True          SumPrint            - Print summary data to "<RootName>.fsm" (flag)
True          TabDelim            - Generate a tab-delimited tabular output file. (flag)
"ES10.3E2"    OutFmt              - Format used for tabular output except time.  Resulting field sh
  0.0         TStart              - Time to begin tabular output (s)
 10           DecFact             - Decimation factor for tabular output {1: output every time step
  1.0         SttsTime            - Amount of time between screen status messages (sec)
  0.0         NcIMUxn             - Downwind distance from the tower-top to the nacelle IMU (m
  0.0         NcIMUyn             - Lateral  distance from the tower-top to the nacelle IMU (mete
  0.0         NcIMUzn             - Vertical distance from the tower-top to the nacelle IMU (mete
  0.0         ShftGagL            - Distance from rotor apex [3 blades] or teeter pin [2 blades] to
  0           NTwGages            - Number of tower nodes that have strain gages for output [0 to
```

Figure A.5: FAST input file for modeling the CART, part 5

```
  0          TwrGagNd        - List of tower nodes that have strain gages [1 to TwrNodes] (-
  3          NBlGages        - Number of blade nodes that have strain gages for output [0 to
 3,5,7       BldGagNd        - List of blade nodes that have strain gages [1 to BldNodes] (-)
             OutList         - The next line(s) contains a list of output parameters.  See OutL
"WindVxi"                    - Nominal downwind component of hub-height wind velocity (m
"WindVyi"                    - Cross-wind component of hub-height wind velocity (m/s)
"WindVzi"                    - Vertical component of hub-height wind velocity (m/s)
"HorWindV"                   - Horizontal (in the x-y plane) hub-height wind speed (m/s)
"TotWindV"                   - Total hub-height wind speed magnitude (m/s)
"HorWndDir"                  - Horizontal hub-height wind direction, about z-axis (deg)
"VerWndDir"                  - Vertical hub-height wind direction, about an axis orthogonal to
"Azimuth"                    - Rotor azimuth angle (deg)
"LSSGagPxa"                  - LSS strain-gage azimuth angle (on the GB side of the LSS) (d
"RotSpeed"                   - Rotor azimuth angular speed (rpm)
"LSSGagVxa"                  - LSS strain-gage angular speed (on the GB side of the LSS) (r
"RotAccel"                   - Rotor azimuth angular acceleration (deg/sec^2)
"GenSpeed"                   - Angular speed of the HSS and generator (rpm)
"GenAccel"                   - Angular accelerator of the HSS (deg/sec^2)
"TSR"                        - Rotor blade tip speed ratio
"RotTorq"                    - LSS torque (kN-m)
"RotPwr"                     - LSS power (kW)
"RotCq, RotCp"               - Rotor torque and power coefficients
"HSShftTq, HSShftPwr"        - HSS torque (kN-m) and power (kW)
"GenTq, GenPwr"              - Electrical generator torque (kN-m) and power (kW)
"GenCq, GenCp"               - Electrical generator torque and power coefficients
"BldPitch1, BldPitch2"       - Blade pitch angles (deg)
END of FAST input file (the word "END" must appear in the first 3 columns of this last line).
---------------------------------------------------------------------------
```

Figure A.6: FAST input file for modeling the CART, part 6

A.2 AeroDyn

Figures A.7 and A.8 illustrate a version of the AeroDyn input file used to model aerodynamics for the CART in this research. The blade data files, not shown here, can be found at [32]. Following the main AeroDyn input file is a sample of a hub-height wind input file in Figure A.9.

```
CART aerodynamics parameters for FAST.
SI                      SysUnits    - System of units for used for input and output [must be SI for F
STEADY                  StallMod    - Dynamic stall included [BEDDOES or STEADY] (unquoted
NO_CM                   UseCm       - Use aerodynamic pitching moment model? [USE_CM or NO
EQUIL                   InfModel    - Inflow model [DYNIN or EQUIL] (unquoted string)
WAKE                    IndModel    - Induction-factor model [NONE or WAKE or SWIRL] (unqu
  0.005                 AToler      - Induction-factor tolerance (convergence criteria) (-)
PRANDtl                 TLModel     - Tip-loss model (EQUIL only) [PRANDtl, GTECH, or NONE
NONE                    HLModel     - Hub-loss model (EQUIL only) [PRANDtl or NONE] (unquo
"Wind/cart_5to6.wnd"    WindFile    - Name of file containing wind data (quoted string)
 36.850                 HH          - Wind reference (hub) height [TowerHt+Twr2Shft+OverHang
  0.05                  TwrShad     - Tower-shadow velocity deficit (-)
  3.0                   ShadHWid    - Tower-shadow half width (m)
  4.0                   T_Shad_Refpt - Tower-shadow reference point (m)
  1.03  !1.225          AirDens     - Air density (kg/m^3)
  1.7e-5  !1.4639e-5    KinVisc     - Kinematic air viscosity (m^2/sec)
  0.01                  DTAero      - Time interval for aerodynamic calculations (sec)
 11                     NumFoil     - Number of airfoil files (-)
"AeroData/cart15.dat"   FoilNm      - Names of the airfoil files [NumFoil lines] (quoted strings)
"AeroData/cart25.dat"
"AeroData/cart35.dat"
"AeroData/cart45.dat"
"AeroData/cart55.dat"
"AeroData/cart65.dat"
"AeroData/cart75.dat"
"AeroData/cart75-5.dat"
"AeroData/cart85.dat"
"AeroData/cart85-5.dat"
"AeroData/cart95.dat"
 20                     BldNodes    - Number of blade nodes used for analysis (-)
RNodes  AeroTwst DRNodes Chord NFoil PrnElm
 1.8799  3.3740  0.998   1.1929  1   NOPRINT
 2.8777  3.1895  0.998   1.3286  1   NOPRINT
 3.8754  3.0569  0.998   1.4276  1   NOPRINT
 4.8731  2.8685  0.998   1.5637  1   NOPRINT
 5.8709  2.7371  0.998   1.6633  2   NOPRINT
 6.8686  2.5294  0.998   1.6575  2   NOPRINT
 7.8663  2.3700  0.998   1.6163  3   NOPRINT
 8.8641  2.1379  0.998   1.5555  3   NOPRINT
 9.8618  1.9386  0.998   1.5017  4   NOPRINT
 10.8595 1.6665  0.998   1.4274  4   NOPRINT
```

Figure A.7: AeroDyn input file for modeling the CART aerodynamics, part 1

```
11.8573  1.4339  0.998   1.3735  5   NOPRINT
12.8550  1.0945  0.998   1.3000  5   NOPRINT
13.8528  0.8374  0.998   1.2461  6   NOPRINT
14.8506  0.4020  0.998   1.1718  6   NOPRINT
15.8483  0.0770  0.998   1.1179  7   NOPRINT
16.8460 -0.4568  0.998   1.0444  7   NOPRINT
17.8438 -0.8951  0.998   0.9906  8   NOPRINT
18.8416 -1.5209  0.998   0.9171  9   NOPRINT
19.8393 -2.1452  0.998   0.8626  10  NOPRINT
20.8371 -2.9979  0.998   0.7889  11  NOPRINT
```

Figure A.8: AeroDyn input file for modeling the CART aerodynamics, part 2

```
! Hub-height wind file used for CART simulations
! Time    Wind     Wind    Vert.    Horiz.   Vert.    LinV     Gust
!         Speed    Dir     Speed    Shear    Shear    Shear    Speed
  0.0     5.0      0.0     0.0      0.0      0.147    0.0      0.0
  0.1     5.0      0.0     0.0      0.0      0.147    0.0      0.0
 10.0     5.0      0.0     0.0      0.0      0.147    0.0      0.0
 15.05    5.0      0.0     0.0      0.0      0.147    0.0      0.0
 15.1     5.0      0.0     0.0      0.0      0.147    0.0      0.0
 19.99    5.0      0.0     0.0      0.0      0.147    0.0      0.0
 20.0     6.0      0.0     0.0      0.0      0.147    0.0      0.0
 25.05    6.0      0.0     0.0      0.0      0.147    0.0      0.0
 25.1     6.0      0.0     0.0      0.0      0.147    0.0      0.0
 30.05    6.0      0.0     0.0      0.0      0.147    0.0      0.0
 30.1     6.0      0.0     0.0      0.0      0.147    0.0      0.0
 35.05    6.0      0.0     0.0      0.0      0.147    0.0      0.0
 35.1     6.0      0.0     0.0      0.0      0.147    0.0      0.0
 40.00    6.0      0.0     0.0      0.0      0.147    0.0      0.0
999.9     6.0      0.0     0.0      0.0      0.147    0.0      0.0
```

Figure A.9: Sample of AeroDyn hub-height wind input file

Appendix B

Induction Generator

This appendix is included to explain how the equivalent circuit analysis is done for the induction generator modeled in this research. Recall the equivalent circuit illustrated in Figure 2.18 with parameter values given in Table 2.7. A simplified circuit can be formed by combining the appropriate resistances and reactances in series and parallel. Doing so results in the equivalent circuit shown Figure B.1 [3].

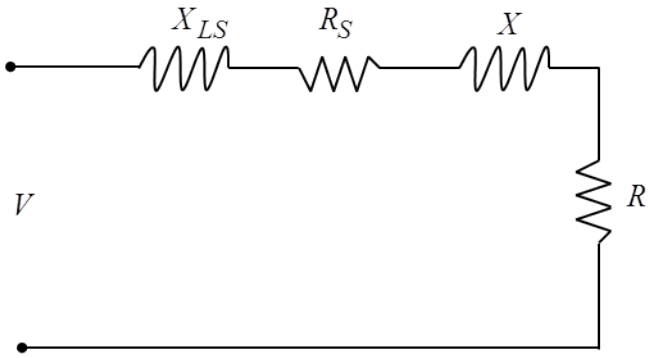

Figure B.1: Simplified equivalent circuit used for analysis of induction generator

The resistance, R, and reactance, X, of Figure B.1 can be computed as a function of the elements in the detailed circuit of Figure 2.18, where R_M is ignored. The impedance of

the combined resistance and reactance is written as,

$$R + jX = jX_M\left(jX'_{LR} + \frac{R'_R}{s}\right) \Big/ \left[\frac{R'_R}{s} + j\big(X_M + X'_{LR}\big)\right] \tag{B.1}$$

where s is slip, as defined by (2.25). The resistance and reactance are then computed as,

$$R = X_M^2 \frac{R'_R}{s} \Big/ \left[\left(\frac{R'_R}{s}\right)^2 + \big(X'_{LR} + X_M\big)^2\right] \tag{B.2}$$

$$X = X_M\left[\left(\frac{R'_R}{s}\right)^2 + X'_{LR}\big(X'_{LR} + X_M\big)\right] \Big/ \left[\left(\frac{R'_R}{s}\right)^2 + \big(X'_{LR} + X_M\big)^2\right] \tag{B.3}$$

The equivalent impedance of the circuit is easily calculated as a series of impedances,

$$\hat{\boldsymbol{Z}} = \big(R + R_S\big) + j\big(X + X_{LS}\big) \tag{B.4}$$

The stator current, a phasor, is computed as the division of stator voltage by total impedance,

$$\hat{\boldsymbol{I}}_S = \hat{\boldsymbol{V}}/\hat{\boldsymbol{Z}} \tag{B.5}$$

The mechanical power converted per phase is computed as a function of slip according to,

$$P_m = (1 - s)I_S^2 R \tag{B.6}$$

The real power output per phase is computed based on the total resistance as,

$$P_{out} = I_S^2\big(R_S + R\big) \tag{B.7}$$

whereas the reactive power per phase is computed from the total reactance as,

$$Q = I_S^2\big(X_{LS} + X\big) \tag{B.8}$$

Together, these results are used to compute the torque and real power characteristics as a function of slip for the induction machine used in this research. Figure 2.19 and Table 2.8 are results of this mathematical modeling.

Appendix C

Classical Pitch Control

The pitch controller used in this research is based on the one designed in [38]. It's purpose is to regulate rotor speed in Region 3 while remaining in the run position in Region 2. The pitch angle will be commanded with a PI controller using a rated rotor speed setpoint, ω_{rated}. This is illustrated in Figure C.1.

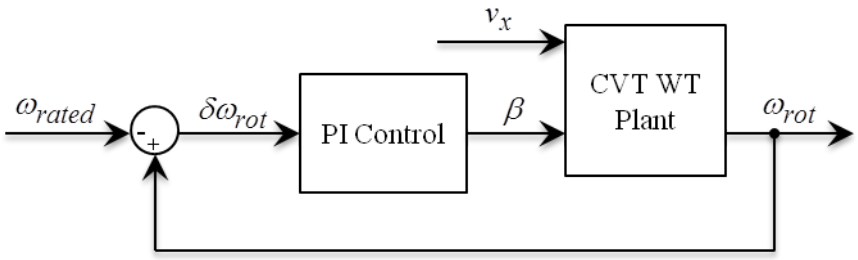

Figure C.1: Block diagram of pitch controller

The PI control law is written in the Laplace domain as,

$$\begin{aligned}\Delta\boldsymbol{\beta}(s) &= \Big(K_p + \frac{K_i}{s}\Big)E(s) \\ &= \Big(K_p + \frac{K_i}{s}\Big)(\Omega_{rot} - \Omega_{rated}) \\ &= \Big(K_p + \frac{K_i}{s}\Big)\Delta\Omega_{rot}\end{aligned} \tag{C.1}$$

where Ω_{rot} is measured rotor speed and $\Delta\Omega_{rot}$ is perturbed rotor speed since the point of linearization will be at rated rotor speed. Inserting this into (2.34) in the Laplace domain and assuming perfect torque regulation in Region 3, i.e. $\delta\tau_{lss} = 0$, results in,

$$I_{dr}s\Delta\Omega_{rot} = \frac{\partial\tau_{aero}}{\partial\omega_{rot}}\Delta\Omega_{rot} + \frac{\partial\tau_{aero}}{\partial\beta}\Big(K_p + \frac{K_i}{s}\Big)\Delta\Omega_{rot} + \frac{\partial\tau_{aero}}{\partial v}\Delta V \tag{C.2}$$

This is notated the same as (2.45) by dividing I_{dr} on both sides,

$$s\Delta\Omega_{rot} = A\Delta\Omega_{rot} + B\Big(K_p + \frac{K_i}{s}\Big)\Delta\Omega_{rot} + \Gamma\Delta V \tag{C.3}$$

The rotor speed transfer function can easily be solved as,

$$\frac{\Delta\Omega_{rot}}{\Delta V} = \frac{\Gamma s}{s^2 + \Big(-A - BK_p\Big)s + \Big(-BK_i\Big)} \tag{C.4}$$

The poles of this transfer function are dependent on the proportional and integral gains, therefore they can be tuned for desirable rotor speed response. This response directly correlates to how well power output is regulated since power is a product of torque and angular velocity.

Before tuning can be done, an operating point must be chosen. Upon doing so, the linearized terms will be evaluated at that point. Fortunately, FAST is capable of computing the periodic matrices for a first-order system. These matrices can then be averaged to estimate an LTI first-order representation of the system at the chosen operating point. To perform a Region 3 linearization of this model with FAST, the hub-height wind speed, vertical shear

exponent, rotor speed, and load torque, at equilibrium are specified as,

$$\begin{aligned} v_o &= 18 \text{ m/s} \\ \alpha_o &= 0.147 \\ (\omega_{rot})_o &= 41.7 \text{ rpm} \\ (\tau_{load})_o &= 3240 \text{ N-m} \end{aligned} \tag{C.5}$$

where the blade collective-pitch is trimmed (by FAST) to 11.55° to satisfy these conditions. Since FAST does not account for the CVT, what has been specified here as load torque is notated as generator torque in FAST, but for the CVT model it's the torque at the CVT input shaft. The equilibrium load torque is determined by knowing the rated rotor torque for Region 3 and simply mapping it to the CVT input. The rated generator torque can be used to compute the equilibrium CVT ratio that satisfies the torque condition. The equilibrium CVT ratio for Region 3 is 1.0087.

Performing a FAST linearization, the first-order equations of the linearized system can be determined in the form of,

$$\dot{x} = Ax + Bu + \Gamma u_d \tag{C.6}$$

For a FAST linearization of the rigid drivetrain wind turbine, the terms in (C.4) can be determined. The results for the Region 3 operating point of (C.5) are summarized as,

$\boldsymbol{A}$	$\boldsymbol{B}$	$\boldsymbol{\Gamma}$
-0.1177	-2.905	0.07131

Table C.1: Region 3 linearization of 1-state with pitch input

The PI pitch controller can now be tuned. The method of tuning is based on considering the characteristic equation of (C.4) in the light of a standard form second-order differential

equation written in the Laplace domain as,

$$s^2 + 2\zeta\omega_n s + \omega_n^2 = 0 \tag{C.7}$$

where ζ is the damping ratio and ω_n is the natural frequency. Comparing the characteristic equation of (C.4) to this standard form, it can be written that,

$$K_p = -\frac{2\zeta\omega_n + A}{B}, \qquad K_i = -\frac{\omega_n^2}{B} \tag{C.8}$$

Therefore, all that's left is to decide on the damping ratio and undamped natural frequency to use for tuning these gains. Since this pitch controller is nearly the same as the one used by [38], the same values used for tuning will be used, $\zeta = 1.0$ and $\omega_n = 0.6$ rad/s. This results in $K_p = 0.3726$ and $K_i = 0.1240$ for the CART's PI pitch controller.

C.1 Anti-Windup

Anti-windup for the PI pitch controller was also designed in [38], and will be used with here to avoid an accumulating error signal due to integral control below Region 3. The integrator error signal is modified when pitch is saturated, e.g. in the run position for Region 2. This is done by taking the difference between the pitch command before and after saturation is imposed, and multiplying this difference by an integrator anti-windup gain. The resulting signal is then subtracted from the error signal normally sent to the integrator. A properly tuned anti-windup gain is designed to minimize this error signal during saturation such that build up of an integrated error signal is avoided. An anti-windup gain of 10 is used for the CVT CART in this research.

Appendix D

Modern Control Theory

Modern control models use state space representation, known as an internal description, whereas transfer functions from classical theory are an input-output model, known as an external description. The state and output equations for a continuous linear time-invariant state space representation is given by a system of first-order ordinary differential equations,

$$\dot{x} = Ax + Bu \tag{D.1a}$$

$$y = Cx + Du \tag{D.1b}$$

If a disturbance input vector is included, as in the case of a wind turbine experiencing disturbances from the wind, the state space representation then becomes,

$$\dot{x} = Ax + Bu + \Gamma u_d \tag{D.2a}$$

$$y = Cx + Du \tag{D.2b}$$

$x =$ state vector
$u =$ control input vector
$u_d =$ disturbance input vector
$y =$ output vector
$A =$ state matrix
$B =$ control gain matrix
$\Gamma =$ disturbance gain matrix
$C =$ output matrix
$D =$ feedthrough matrix

where $A \in \mathbb{R}^{n\times n}$, $B \in \mathbb{R}^{n\times m}$, $\Gamma \in \mathbb{R}^{n\times q}$, $C \in \mathbb{R}^{p\times n}$, and $D \in \mathbb{R}^{p\times m}$ with $x \in \mathbb{R}^n$, $u \in \mathbb{R}^m$, $u_d \in \mathbb{R}^q$, and $y \in \mathbb{R}^p$. For the physical system modeled in this research, the CVT CART, the feedthrough, D, will always be a zero matrix (this will be used from here forward). Section 2.5, on linearization, shows how the equations of motion for the drivetrain dynamics are put into state space form.

Once the state space model has been formulated for the wind turbine drivetrain dynamics, controllability and observability of the system must be checked. This is easily done by computing the rank of controllability and observability matrices. The respective matrices are computed as,

$$\mathcal{C} = \begin{bmatrix} B & AB & A^2B & \cdots & A^{n-1}B \end{bmatrix} \tag{D.3}$$

$$\mathcal{O} = \begin{bmatrix} C \\ CA \\ CA^2 \\ \vdots \\ CA^{n-1} \end{bmatrix} \tag{D.4}$$

The state space system is controllable and observable if and only if the rank($\mathcal{C}$) = n and rank($\mathcal{O}$) = n, respectively.

Once the controllability of the state space model is verified, full state feedback control will be used to command the CVT. The state vector, $x \in \mathbb{R}^n$, is fed to the state feedback gain matrix, $F_x \in \mathbb{R}^{m \times n}$, which is summed with a reference input vector, $r \in \mathbb{R}^m$, to formulate the control input vector of the closed-loop system. State feedback is used to assign closed-loop eigenvalues of the system such that desirable transient response is achieved. The control law is written as,

$$u = F_x x + r \tag{D.5}$$

However, this control law is of limited use for a wind turbine experiencing highly variable disturbance inputs, i.e. the wind. The upcoming paragraphs show how the control law of (D.5) can be modified such that wind turbine control, CVT and pitch actuation in this research, accounts for wind disturbances.

Moving forward with the control law of (D.5), the compensated closed-loop system of (D.1a) and (D.1b) is then written as,

$$\dot{x} = (A + BF_x)x + Br \tag{D.6a}$$

$$y = Cx \tag{D.6b}$$

Notice the eigenvalues of $A+BF_x$ can be chosen by choosing appropriate values for the state feedback matrix. This ability will be used to adjust the rotor speed response, torque regulation response, and add damping to the drivetrain torsion mode. Notice if the disturbance input were included in (D.6a), the state feedback gain matrix is not influenced by it. This

issue will be addressed soon.

Once the observability of the state space model is verified, a linear state observer will be designed to avoid requiring measurements of all states since that would be impractical if not impossible. Using knowledge of the control input and system output, the state observer estimates the state vector. Still assuming a zero matrix for the feedthrough matrix, the state estimates are formulated as,

$$\dot{\hat{x}} = A\hat{x} + Bu + K_x(y - \hat{y}) \tag{D.7a}$$

$$\hat{y} = C\hat{x} \tag{D.7b}$$

where $\hat{x}$ and $\hat{y}$ are the estimated plant states and outputs, respectively, and $K_x \in \mathbb{R}^{n \times p}$ is the estimator gain matrix. Note however, this representation still neglects disturbance inputs. Equation (D.7a) can also be written as,

$$\dot{\hat{x}} = (A - K_x C)\hat{x} + \begin{bmatrix} B & K_x \end{bmatrix} \begin{bmatrix} u \\ \\ y \end{bmatrix} \tag{D.8}$$

which is a useful form for implementation into Simulink. The error between the estimated and actual state is given by,

$$e_x(t) = x(t) - \hat{x}(t) \tag{D.9}$$

Taking (D.1a) and (D.7a), this leads to,

$$\dot{e}_x(t) = (A - K_x C)e_x(t) \tag{D.10}$$

where estimator gain, K_x, is chosen such that eigenvalues of $A - K_x C$ are fast. Eigenvalues with large real negative parts are fast, whereas eigenvalues close to the imaginary axis are slow and will dominate the transient response. Fast eigenvalues of $A - K_x C$ cause the error, $e(t)$, to converge to zero quickly. Practical consideration of noise, limits the gain K_x from making the observer eigenvalues arbitrarily fast.

Combining the function of state feedback and state observer, an output feedback controller is developed. In this case, the estimated states are fed to the feedback gain matrix, F_x. The new control law becomes,

$$u = F_x \hat{x} + r \tag{D.11}$$

The augmented system can be formulated as,

$$\begin{bmatrix} \dot{x} \\ \dot{e} \end{bmatrix} = \begin{bmatrix} A + BF_x & -BF_x \\ 0 & A - K_x C \end{bmatrix} \begin{bmatrix} x \\ e \end{bmatrix} + \begin{bmatrix} B \\ 0 \end{bmatrix} r \tag{D.12}$$

where the eigenvalues of $A + BF_x$ influence the control action and eigenvalues of $A - K_x C$ influence the estimation of states. This independent influence is known as the separation property [41]. An internally stable closed-loop system is ensured by choosing F_x and K_x such that eigenvalues for control action and state estimation have negative real parts.

D.1 Disturbance Tracking Control

Modern control of the CVT in Region 2 will be done with Disturbance Tracking Control (DTC) theory. To see the study of DTC theory in the context of wind turbines, consult [36, 37]. The purpose of DTC is to track input disturbances without measuring them.

The key fundamental to DTC theory is that it uses an assumed disturbance waveform. Knowledge of the input and output along with an assumed waveform allows the disturbance to be estimated, and tracked in the case of DTC. This is valuable for Region 2 control since the primary objective is to track λ_{opt}.

An assumed disturbance waveform is represented as,

$$u_d = \Theta z_d \tag{D.13a}$$

$$\dot{z}_d = G z_d; \quad z_d(0) = (z_d)_o \tag{D.13b}$$

where $u_d \in \mathbb{R}^{m_d}$ is the disturbance input vector and $z_d \in \mathbb{R}^{n_d}$ is the disturbance state vector. The matrices, $\Theta \in \mathbb{R}^{m_d \times n_d}$ and $G \in \mathbb{R}^{n_d \times n_d}$, define the assumed waveform, but the initial condition, $z_d(0)$, is unknown. A step waveform, a good representation of sudden disturbances, is used for this research and is defined by $\Theta \equiv 1$ and $G \equiv 0$. The single disturbance state is therefore a representation of the hub-height wind speed since it should be tracked in accordance with λ_{opt} for Region 2.

The typical state feedback law of (D.5) did not account for disturbance inputs. To correct this, the ideal DTC feedback law is formulated as,

$$u_* = F_x x + F_d z_d \tag{D.14}$$

where $F_d \in \mathbb{R}^{m_d \times n_d}$ is the disturbance feedback gain. Plugging (D.13a) and (D.14) into the state equation with disturbance input, (D.2a), gives,

$$\dot{x} = (A + BF_x)x + (\Gamma\Theta + BF_d)z_d \tag{D.15}$$

However, there is still the issue of estimating the disturbance state. If it were simply measured, a key purpose of DTC theory would be defeated. Incorporating the disturbance state into the state estimator gives,

$$\dot{\hat{x}} = A\hat{x} + Bu + \Gamma\hat{u}_d + K_x(y - \hat{y}) \tag{D.16a}$$

$$\hat{y} = C\hat{x} \tag{D.16b}$$

with,

$$\hat{u}_d = \Theta\hat{z}_d \tag{D.17a}$$

$$\dot{\hat{z}}_d = G\hat{z}_d + K_d(y - \hat{y}) \tag{D.17b}$$

where $K_d \in \mathbb{R}^{n_d \times p}$ is the disturbance estimator gain. Now, there are error equations for both the plant states, $x(t)$, as written in (D.9), and the disturbance states, $z_d(t)$, written as,

$$e_d(t) = z_d(t) - \hat{z}_d(t) \tag{D.18}$$

This leads to,

$$\begin{aligned} \dot{e}_x &= \dot{x} - \dot{\hat{x}} \\ &= (Ax + Bu + \Gamma u_d) - (A\hat{x} + Bu + \Gamma\hat{u}_d + K_x(y - \hat{y})) \\ &= (A - K_xC)e_x + \Gamma\Theta e_d \end{aligned} \tag{D.19}$$

$$\dot{e}_x = \begin{bmatrix} A - K_xC & \Gamma\Theta \end{bmatrix} \begin{bmatrix} e_x \\ \\ e_d \end{bmatrix} \tag{D.20}$$

The differential disturbance error is formulated similarly,

$$\begin{aligned}\dot{e}_d &= \dot{z}_d - \dot{\hat{z}}_d \\ &= Gz_d - (G\hat{z}_d + K_d(y - \hat{y})) \\ &= -K_d C e_x + G e_d\end{aligned} \tag{D.21}$$

$$\dot{e}_d = \begin{bmatrix} -K_d C & G \end{bmatrix} \begin{bmatrix} e_x \\ \\ e_d \end{bmatrix} \tag{D.22}$$

Together, the differential errors can be written as,

$$\dot{e}(t) = \begin{bmatrix} \dot{e}_x^\top(t) \\ \\ \dot{e}_d^\top(t) \end{bmatrix} = \begin{bmatrix} A - K_x C & \Gamma\Theta \\ \\ -K_d C & G \end{bmatrix} \begin{bmatrix} e_x^\top(t) \\ \\ e_d^\top(t) \end{bmatrix} = (\bar{A} - \bar{K}\bar{C})e(t) \tag{D.23}$$

$$\text{where} \quad \bar{A} = \begin{bmatrix} A & \Gamma\Theta \\ \\ 0 & G \end{bmatrix}, \quad \bar{C} = \begin{bmatrix} C & 0 \end{bmatrix}, \quad \bar{K} = \begin{bmatrix} K_x \\ \\ K_d \end{bmatrix}$$

If the pair $\{\bar{A}, \bar{C}\}$ is observable, the estimator gains, K_x and K_d, can be chosen such that the eigenvalues of $(\bar{A} - \bar{K}\bar{C})$ cause the errors to converge quickly.

A useful form of the estimator for implementation into Simulink is developed through augmentation of (D.16a) and (D.17b),

$$\begin{bmatrix} \dot{\hat{x}} \\ \\ \dot{\hat{z}}_d \end{bmatrix} = \begin{bmatrix} A - K_x C & \Gamma\Theta \\ \\ -K_d C & G \end{bmatrix} \begin{bmatrix} \hat{x} \\ \\ \hat{z}_d \end{bmatrix} + \begin{bmatrix} B & K_x \\ \\ 0 & K_d \end{bmatrix} \begin{bmatrix} u \\ \\ y \end{bmatrix} \tag{D.24}$$

which clearly shows how knowledge of the input, $u(t)$, and output, $y(t)$, along with an assumed waveform allows the disturbance state, $z_d(t)$, to be estimated. Using this new state

estimator that includes the disturbance states, the ideal DTC feedback law written in (D.14) is now rewritten as a realizable law,

$$u = F_x\hat{x} + F_d\hat{z}_d \tag{D.25}$$

Choosing values of F_x is done to adjust the transient response as desired. In the case of DTC for CVT, F_x directly impacts the CVT actuation with eigenvalues of $A + BF_x$ dictating the response. Choosing values of F_d is done to adjust the steady state response. In the case of DTC, F_d is used to relate the states to the disturbances such that tracking is achieved.

The final piece to applying DTC theory is the computation of the disturbance feedback gain matrix. The first step is relating the outputs to the assumed disturbances. This is done by solving the following equation for L,

$$Q\Theta = CL \tag{D.26}$$

where desired proportionality is assigned using Q. In the case of a wind turbine in Region 2, the proportionality should correlate to tracking λ_{opt}. This proportionality along with the disturbance feedback gain is then related to the closed-loop system as,

$$(A + BF_x)L - LG + BF_d + \Gamma\Theta = 0 \tag{D.27}$$

where F_d is computed to satisfy the equation. The realizable DTC law of (D.25) can then be used to manipulate the control signal such that disturbance tracking is achieved with a desirable transient response.

REFERENCES

REFERENCES

[1] website. http://www.pickensplan.com. Accessed 13-October-2011.

[2] website. http://www.japantimes.co.jp. Accessed 13-October-2011.

[3] J. F. Manwell, J. G. McGowan, and A. L. Rogers. *Wind Energy Explained: Theory, Design and Application*. John Wiley & Sons, 2009.

[4] L. Mangialardi and G. Mantriota. Dynamics behaviour of wind power systems equipped with automatically regulated continuously variable transmission. *Renewable Energy*, 7(2):185–203, 1996.

[5] A. H. J. A. Martens and P. H. W. M Albers. Investigation into cvt application in wind turbines. Wind Turbine Study DCT 2003.90, Technische Universiteit Eindhoven, October 2003.

[6] J. Cotrell. Assessing the potential of a mechanical continuously variable transmission for wind turbines. Conference Paper CP-500-38212, National Renewable Energy Laboratory, August 2005.

[7] Andrew Rex. Model development of a wind turbine system with a continuously variable transmission for design of region 2 speed control. Master's thesis, Colorado School of Mines, 2007.

[8] Nathaniel Haro. Active drive train control to improve energy capture of wind turbines. Master's thesis, Boise State University, 2007.

[9] Andrew H. Rex and Kathryn E. Johnson. Methods for controlling a wind turbine system with a continuously variable transmission in region 2. *Journal of Solar Energy Engineering*, 131(031012), August 2009.

[10] M. J. Verdonschot. Modeling and control of wind turbines using a continuously variable transmission. Master's thesis, Eindhoven University of Technology, April 2009.

[11] Tony Burton, David Sharpe, Nick Jenkins, and Ervin Bossanyi. *Wind Energy Handbook*. John Wiley & Sons, 2001.

[12] Vaughn Nelson. *Wind Energy: Renewable Energy and the Environment*. CRC Press, second edition, 2009.

[13] website. http://awea.org. Accessed 13-October-2011.

[14] Ben McGarry. *Durnin Transmission on Stage 1 - Engineering Assessment of IVT Concept*, August 2008.

[15] website. http://cvt.com.sapo.pt. Last modified 19-September-2008; accessed 6-July-2011.

[16] website. http://www.wikov.com/wind/index_en.php. Accessed 24-August-2011.

[17] website. http://www.orbital2.com. Accessed 24-August-2011.

[18] H. Muller, M. Poller, A. Basteck, J. Tilscher, and J. Pfister. Grid compatibility of variable speed turbines with directly coupled synchronous generator and hydro-dynamically controlled gearbox, October 2006.

[19] website. http://www.dewindco.com/eng. Accessed 24-August-2011.

[20] website. http://www.fallbrooktech.com/home.asp. Accessed 6-July-2011.

[21] website. http://www.viryd.com. Accessed 6-July-2011.

[22] website. http://www.magnomatics.com. Accessed 6-July-2011.

[23] K. A. Stol. Geometry and structural properties for the controls advanced research turbine (cart) from model tuning. Subcontractor Report SR-500-32087, National Renewable Energy Laboratory, September 2004.

[24] Alan D. Wright. Modern control design for flexible wind turbines. Technical Report TP-500-35816, National Renewable Energy Laboratory, July 2004.

[25] Kathryn E. Johnson. Adaptive torque control of variable speed wind turbines. Technical Report TP-500-36265, National Renewable Energy Laboratory, August 2004.

[26] NWTC Design Codes (FAST by Jason Jonkman Ph.D.). http://wind.nrel.gov/designcodes/simulators/fast/. Last modified 05-November-2010; accessed 27-January-2011.

[27] J. M. Jonkman and M. L. Buhl Jr. Fast user's guide. Technical Report EL-500-38230, National Renewable Energy Laboratory, August 2005.

[28] P. J. Moriarty and A. C. Hansen. Aerodyn theory manual. Technical Report EL-500-36881, National Renewable Energy Laboratory, December 2005.

[29] D. J. Laino and A. C. Hansen. *AeroDyn User's Guide*. Windward Engineering, December 2002.

[30] B. J. Jonkman. Turbsim user's guide. Technical Report TP-500-46198, National Renewable Energy Laboratory, September 2009.

[31] The MathWorks, Inc. *Simulink 7 User's Guide, Version 7.6*, September 2010.

[32] website. http://wind.nrel.gov/public. Accessed 12-March-2011.

[33] J. Pyrhonen, T. Jokinen, and V. Hrabovcova. *Design of Rotating Electrical Machines*. John Wiley & Sons, 2009.

[34] Ion Boldea. *The Electric Generators Handbook - 2 Volume Set*. CRC Press, 2005.

[35] Katsuhiko Ogata. *Modern Control Engineering*. Prentice Hall, fifth edition, 2010.

[36] K. A. Stol. Disturbance tracking and blade load control of wind turbines in variable-speed operation. Conference Paper CP-500-33011, National Renewable Energy Laboratory, January 2003.

[37] M. J. Balas, Y. J. Lee, and J. Kendall. Disturbance tracking control theory with application to horizontal axis wind turbines. In *17th ASME Wind Energy Conference*, Reno, NV, 12-15 January 1998.

[38] A. D. Wright and L. J. Fingersh. Advanced control design for wind turbines part i: Control design, implementation, and initial tests. Technical Report TP-500-42437, National Renewable Energy Laboratory, March 2008.

[39] K. E. Johnson, L. J. Fingersh, M. J. Balas, and L. Y. Pao. Methods for increasing region 2 power capture on a variable speed hawt. Conference Paper CP-500-34979, National Renewable Energy Laboratory, November 2003.

[40] A. D. Wright and M. J. Balas. Design of state-space-based control algorithms for wind turbine speed regulation. Conference Paper CP-500-31164, National Renewable Energy Laboratory, January 2002.

[41] Panos J. Antsaklis and Anthony N. Michel. *A Linear Systems Primer*. Birkhäuser, 2007.

[42] Paul Gipe. *Wind Energy Basics, A Guide to Home- and Community-Scale Wind Energy Systems*. Chelsea Green Publishing Company, second edition, 2009.

[43] Charles L. Phillips and Royce D. Harbor. *Feedback Control Systems*. Prentice Hall, fourth edition.

[44] R. C. Hibbeler. *Engineering Mechanics: Dynamics*. Prentice Hall, twelfth edition, 2010.

[45] Ramin S. Esfandiari and Bei Lu. *Modeling and Analysis of Dynamic Systems*. CRC Press, 2010.

[46] Jason H. Laks, Lucy Y. Pao, and Alan D. Wright. Control of wind turbines: Past, present, and future. Supported in part by the University of Colorado, the National Renewable Energy Laboratory, the National Science Foundation, and the Miller Institute for Basic Research in Science.

[47] Kirk G. Pierce and Paul G. Migliore. Maximizing energy capture of fixed-pitch variable-speed wind turbines. Conference Paper CP-500-27551, National Renewable Energy Laboratory, July 2000.

[48] M. M. Hand and M. J. Balas. Systematic controller design methodology for variable-speed wind turbines. Technical Report TP-500-29415, National Renewable Energy Laboratory, February 2002.

[49] M. M. Hand. Variable-speed wind turbine controller systematic design methodology: A comparison of non-linear and linear model-based designs. Technical Report TP-500-25540, National Renewable Energy Laboratory, July.

[50] R. Poore and T. Lettenmaier. Alternative design study report: Windpact advanced wind turbine drive train designs study. Subcontractor Report SR-500-33196, National Renewable Energy Laboratory, August 2003.

[51] K. A. Stol and L. J. Fingersh. Wind turbine field testing of state-space control designs. Subcontractor Report SR-500-35061, National Renewable Energy Laboratory, September 2004.

[52] A. D. Wright and M. J. Balas. Design of controls to attenuate loads in the controls advanced research turbine. Conference Paper CP-500-35084, National Renewable Energy Laboratory, November 2003.

[53] A. D. Wright, L. J. Fingersh, and Balas M. J. Testing state-space controls for the controls advanced research turbine. Conference Paper CP-500-39123, National Renewable Energy Laboratory, January 2006.

[54] A. D. Wright, L. J. Fingersh, and K. A. Stol. Designing and testing controls to mitigate tower dynamic loads in the controls advanced research turbine. Conference Paper CP-500-40932, National Renewable Energy Laboratory, January 2007.

[55] A. D. Wright and K. A. Stol. Designing and testing controls to mitigate dynamic loads in the controls advanced research turbine. Conference Paper CP-500-42490, National Renewable Energy Laboratory, January 2008.

[56] L. J. Fingersh and K. E. Johnson. Baseline results and future plans for the nrel controls advanced research turbine. Conference Paper CP-500-35058, National Renewable Energy Laboratory, November 2003.

[57] L. J. Fingersh and K. E. Johnson. Controls advanced research turbine (cart) commissioning and baseline data collection. Technical Report TP-500-32879, National Renewable Energy Laboratory, October 2002.

[58] K. Pierce. Control method for improved energy capture below rated power. Conference Paper CP-500-26322, National Renewable Energy Laboratory, July 1999.

[59] R. Jacobson and B. Gregory. Wind power quality test for comparison of power quality standards. Conference Paper CP-500-26760, National Renewable Energy Laboratory, August 1999.

[60] NWTC Design Codes (AeroDyn by Dr. David J. Laino). http://wind.nrel.gov/designcodes/simulators/aerodyn/. Last modified 31-March-2010; accessed 27-January-2011.

[61] NWTC Design Codes (IECWind by Dr. David J. Laino). http://wind.nrel.gov/designcodes/preprocessors/iecwind/. Last modified 18-March-2010; accessed 27-January-2011.

[62] NWTC Design Codes (TurbSim by Neil Kelley and Bonnie Jonkman). http://wind.nrel.gov/designcodes/preprocessors/turbsim/. Last modified 25-September-2009; accessed 27-January-2011.

[63] The MathWorks, Inc. *MATLAB User's Manual, Version 7.9*, 2010.